Wakefield Acceleration in the Universe

(Submitted to International Journal of Modern Physics D)

Toshikazu Ebisuzaki[1], Toshiki Tajima[2], and Barry C. Barish[3]

[1] RIKEN, Cluster for Pioneering Research, 2-1 Hirosawa, Wako 351-1198, Japan
[2] Depart. of Physics and Astronomy, University of California, Irvine, CA 92679, USA
[3] LIGO, California Institute of Technology, Pasadena, CA 91125, USA

Abstract

The important role of magnetic fields in the phenomena in and evolution of the Universe is well appreciated. A salient example of this is to make (often episodic) large magnetic fields in AGN accretion disks and their emanation of well collimated and longitudinally extended astrophysical jets. Such typical cases or related astrophysical processes, we find, provide a fertile ground for exciting large amplitude oscillations in the magnetic fields that constitute the spine of the jets. The energy sources of these oscillations can be traced originally to the gravitational energy of the central object. During their long propagation along the jet, because of the gradual changes of the density and magnetic fields, these large magnetic pulsations turn into relativistic amplitude electromagnetic (EM) pulses, which in turn induce intense wakefields that are capable of acceleration of electrons, positrons, and ions to high energies. In this review we survey a variety of astrophysical objects ranging from as large as the cosmic AGN accretion disks and their jets to as small as microquasars, to find or predict that there exist common astrophysical processes of emission of high energy particles and gamma (and other EM) emissions. A variety of these objects will be ideally observed and studied in the multi-messenger astrophysical observations. One example that already sticked out was the case of the simultaneous observations of gravitational wave emission and gamma ray pulse from the collision of the two neutron stars and their subsequent structure formation (such as a disk) around them.

Keywords: blackholes, accretion disks, jets, particle acceleration, stellar core collapse AGN, microquasars, multi-messenger astronomy

1. Introduction

The importance of magnetic field and plasma in cosmic plasma has been pointed out by H. Alfven.[1] He showed and demonstrated that magnetic fields and plasma play an importance role in astrophysical structure and dynamics. Some of the large structures observed (as shown in Figs. II.9 and II.10 of Alfven's book[1]) in cosmos are essential to be influenced or reflect the magnetic field influence. Lovelace[2] and Blandford[3], and Uchida and Shibata[4-7] showed that the presence of an axial magnetic field in accretion disk can generate coherent, elongated, stable jets. As we will analyze below, the global dynamics of the magnetic fields plays the essential role in this remarkable simulation. Perhaps, in anticipation of such importance of the global magnetic field dynamics Kennel and his group started efforts to develop a numerical global magnetohydrodynamics of cosmical plasma.[8,9] These works introduced and opened up the exploration of the essential role of magnetic fields in plasma in their determining topological, global, and collective influence on the structure and dynamics, while not denying magnetic field effects also in microscopic properties of astrophysical plasmas. Alfven mentioned the filamentary nature of cosmic plasma, whereas Uchida and Shibata showed the jets formation from an accretion disk, while Leboeuf et al. observed a shock cone.[8,9]

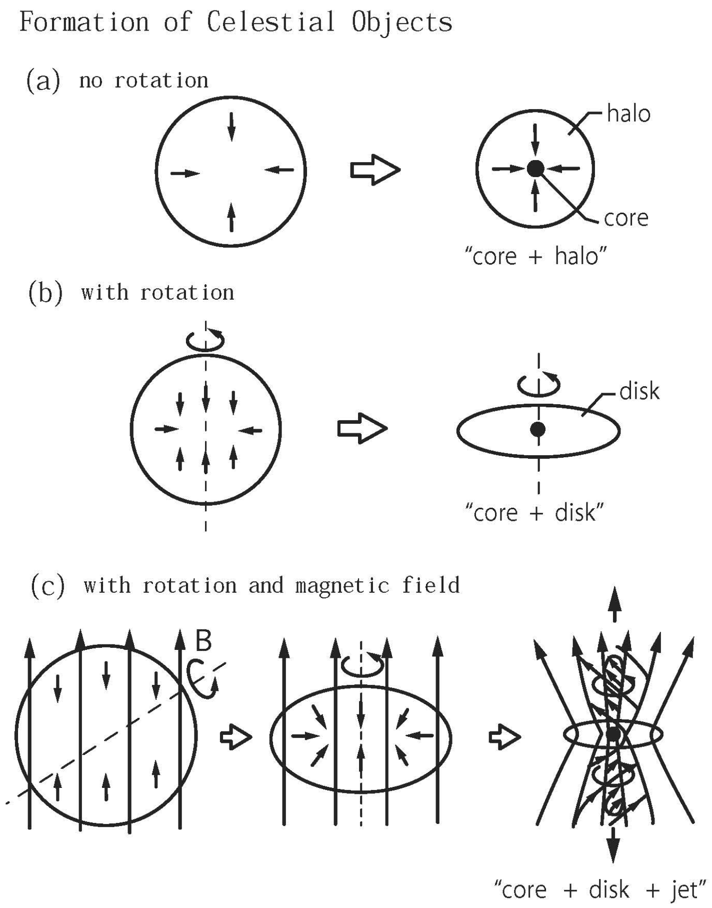

Figure 1. Astrophysical objects with gravitational center, its rotation, and magnetic fields (after TS97 p. 12 Fig. 1.5).[10] While the gravitational system does not have a rotation, it evolves a simple spherical collapse (scenario (a)), with rotation the system can evolve into a disk, which resembles accretion disk)scenario (b)). Finally if the primordial plasma in addition has magnetic fields embedded (scenario (c)), the system evolves into a accretion disk that emanates a pair of focused jets of plasma flow (and spiraling magnetic fields; after TS97).[10]

In the present review article, Uchida and Shibata's jet formation from an accretion disk lies in the heart of our understanding of the high energy astrophysical observations and corresponding physical mechanisms. (Here we note that global magnetic effects are primarily represented by magnetohydrodynamic (MHD) effects. It is possible that kinetic effects could give rise to the dynamo effects that spontaneously produce magnetic fields out of non-magnetized plasma (see e.g., Mima et al.[11]). However, barring such microscopic kinetic effects, the nonmagnetic dynamics in its equivalent gravitational accretion disk setup would produce no jets. It shows the fundamental importance of the presence of magnetic fields in the jet formation. We compare three cases of evolution of astrophysical objects (Tajima and Shibata 1997[10] hereafter TS97): (a) a gravitational object without rotation; (b) a gravitational object with rotation; (c) a gravitational object with rotation and magnetic fields (see Figure 1. (out of TS97 Fig. 1.5). The rotation gives rise to the formation of the central disk formation (the accretion disk). Only in case (c) we see the evolution of a large extended structure (jets formation) emanating out of the central region of the formed accretion disk that may appear from cases (b) or (c).

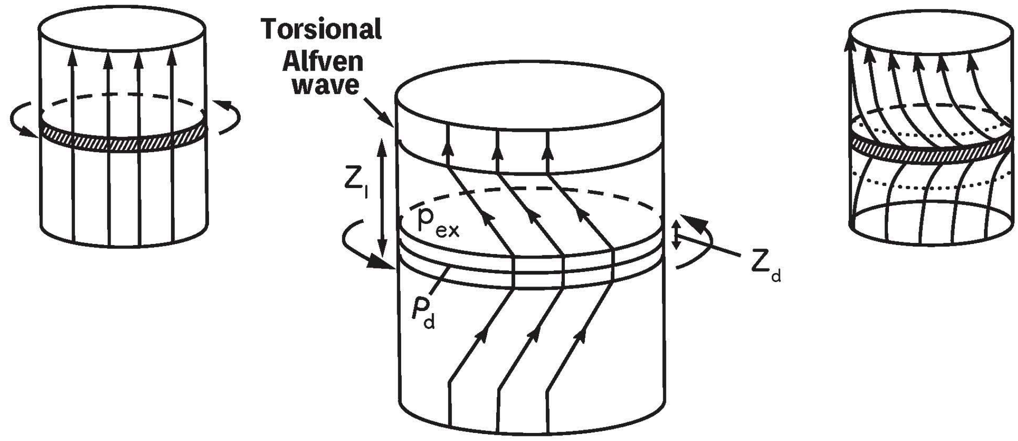

Figure 2. The magnetic evolution under the rotational motion of the astrophysical object, emanation of the torsional twist of magnetic fields and emission of the torsional Alfven wave. (after TS97 Fig. 4.17 p. 310).[10] As shown in the scenario (c) in Figure 1, the plasma embedded with magnetic fields rotates, its magnetohydrodynamic force *f* (shown in Eq. (2)) causes the uplifting force that resulting in the emanating plasma flows, which are the origin of the jets from the central part of the disk (After TS97).[10]

When there is a static constant axial magnetic field (call it B_z) originally penetrating the accretion disk plasma, the rotational motion of the accretion disk twists the magnetic field, which yields the azimuthal magnetic field (call it B_θ). See Figure 2 (from TS97 Fig. 4.17). Such bending/twisting of the originally uniform B_z field gives rise to the radial inward current J_r through the Ampere's law:

$$\frac{4\pi}{c}\boldsymbol{J} = \nabla \times \boldsymbol{B}. \tag{1}$$

The plasma induces the magnetohydrodynamic (MHD) force density:

$$\boldsymbol{f} = \frac{1}{c}(\boldsymbol{J} \times \boldsymbol{B}), \tag{2}$$

which points toward the axial (z) direction. This force is the very agent that generates the jet out of the edge of the accretion disk (Figure 3; TS97, Fig. 1.9), as already differentiated in Figure 1. Toward the axial z direction, as shown in the first self-consistent magnetohydrodynamic demonstration by Uchida-Shibata.[4-7] Once such sheared magnetic fields and flows are generated, these also shear the plasma flows and further magnetic fields. The shear magnetic fields and shear plasma plows are interwoven. These interrelations between the magnetic fields and plasma flows continuously generate collimated spiral magnetic fields and flows that we now come to know as the (astrophysical) jets. See Shibata, Tajima and Matsumoto (1990)[12] and Matsumoto et al. (1996)[13], also seen in the textbook (TS97[10], pp. 346-387). This outcome is one of the most beautiful, largest-scaled, and most robust self-organized structure of nature in the Universe. Such jet structure could stretch almost as far out as Mpc in the large AGN jets. It is important to also notice that because of the differential rotation of the accretion disk that is formed (see in Figure 1 (c), Figure 3, and also see Figure 4 (from Shibata and Uchida 1986)[5], the longitudinal B_z and the induced toroidal field form a spiraling emanating magnetic fields that wrap around the jets that we mention to be formed. Many subsequent numerical computations have verified and reinforced the above pictures.[13-15] Furthermore, its wrapping pitch is greater in the more inside of the spiraling magnetic flux (Figure 5). These intricate combination gives rise to a superbly well-collimated and long stretching mammoth jet structure that we witness in the Universe often. Astrophysical jets (in terms of the linear dimension) must be the largest self-organized structures in the Universe. The structure is mutually supported by the engine of the gravitational center, its rotating disk, and its emanating and intricately woven fabric of large-scale magnetic fields that wrap around the jets which int urn push the jets forward with collimation. A beautiful photograph of Cygnus A jets is shown in Figure 6. The structure shows such a succinct highly organized form, only because the jet forming forces of the plasma and magnetic field under the gravitational driven rotation mutually reinforce each other. The jets eventually slow down its velocity from relativistic dynamics so that their interaction with the intergalactic tenuous plasma eventually begins to kick in. This transition from ultra-relativistic jets to less than the relativistic dynamics induces the beam-plasma instabilities that slows the jets considerably and also forms a couple of turbulent plasma lobes that can emit copious microwaves. Thus, we see the long straight and narrow jets ending with the double humped lobes.

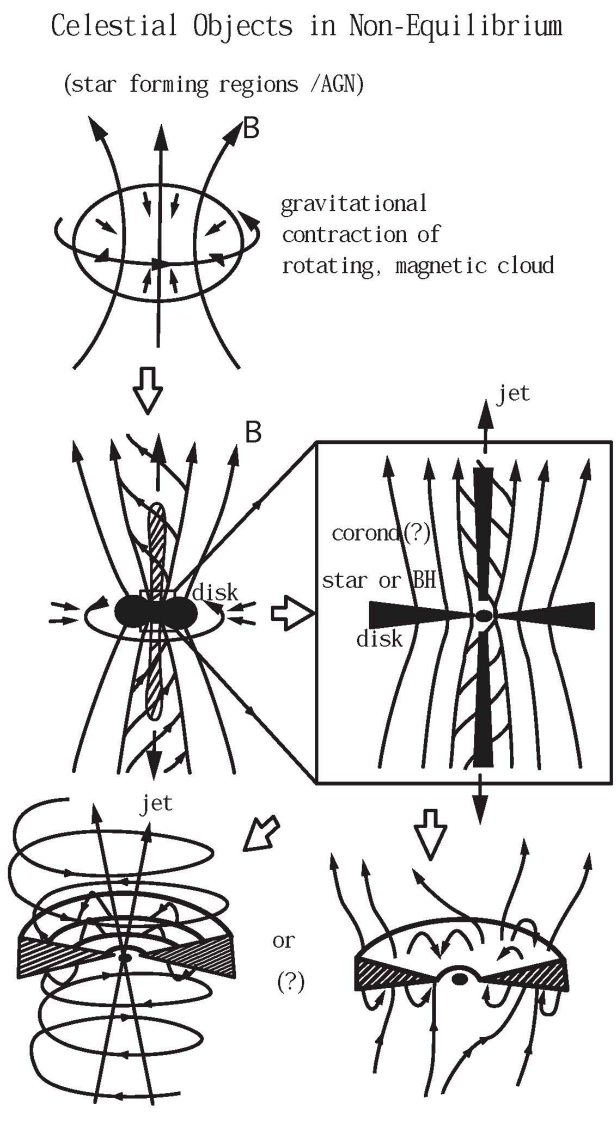

Figure 3. The evolutionary sequences of an astrophysical object with gravitational center, its rotation, and magnetic fields. (after TS97 Fig. 1.9, p. 17).[10] The compact gravitational object (such as a black hole (or merged neutron starts) tends to evolve an accretion disk, due to their rotational dynamics. With its presence of magnetic fields such dynamic evolution now accompanies collimated jet formation with magnetic fields wrapping around these jets. Meanwhile, the accretion disk embeds magnetic fields in it, which trigger the magneto-rotational instability and its associated evolutions of the disk and its jets (After TS97).[10]

It is important to notice that the more the central gravitational object is strongly localized, the more intensified toroidal rotation of the accretion disk is realized that has stronger differential rotation. Thus, it is natural that we find that a large-scale jet formation emanating from the center of accretion disk is often from a compact gravitation object of a black hole (e.g. Wheeler 1990[16]). See a conceptual black hole and its emanating magnetic fields in Figure 7 (b) (TS97 4.60). The recent observational revelation (Figure 7 (a)) not only showed the resemblance to those shown by Matsumoto Figure 7 (b), but also it exhibits a sure sign of the imprints of magnetic fields through its fibril stripes (Figure 7 (b)).

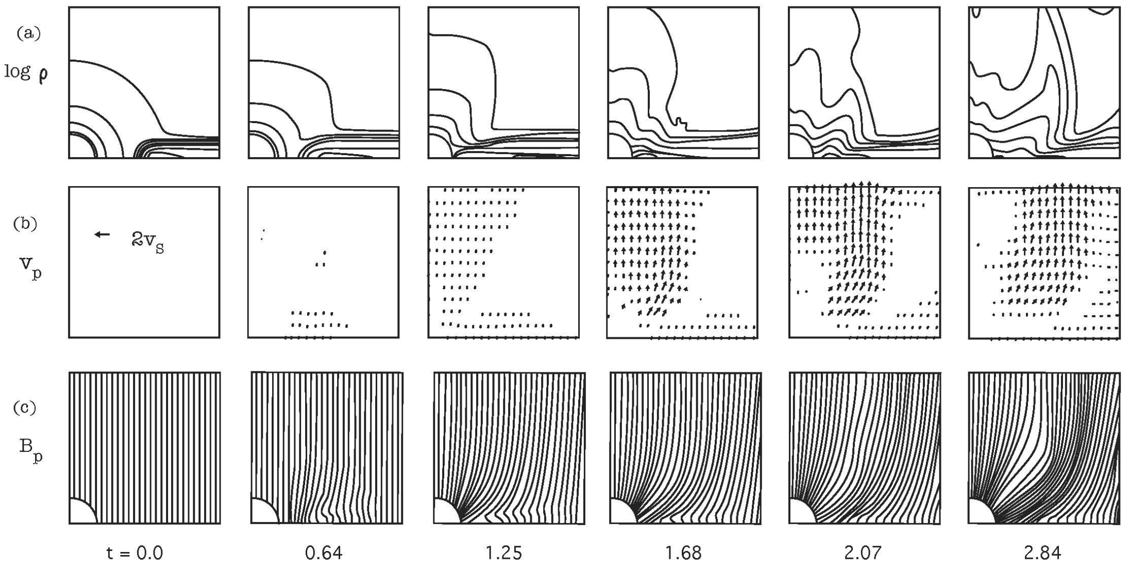

Figure 4. The shear flow of the accretion disk plasma and its embedded magnetic field dynamics as shown in Figure 2 give rise to a helical winding and axially extended magnetic fields. This jet magnetic fields accompany the plasma thrust emanating from the J x B force mentioned in Eq. (2) in Introduction. After Shibata and Uchida 1986,[7] also from TS97, p. 382-383).[10] Jets are launched from the accretion disk by the shearing magnetic fields driven by the rotating accretion disk via the Uchida-

Shibata mechanism.

As we see above, only relatively recent when the confluence of the gravitational objects of black hole (EHT)[17] and neutron stars[18,19] with the global structure formation that is initiated or stimulated by the presence of magnetic fields has happened. However, we reflect the brief history of research of these objects briefly here.

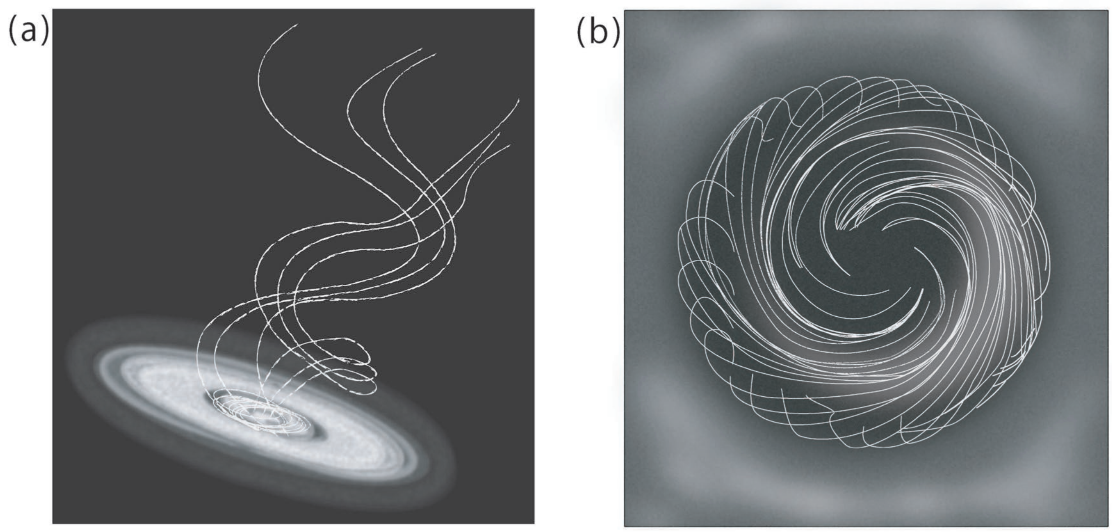

Figure 5. In the accretion disk the presence of magnetic fields is amplified magneto rotational instability due to its differential rotation. It has its characteristics spatial structure and temporal growth time scale, which impact the evolution of the disk and its jets. Schematic drawings inspired by the figure of Matsumoto 1996.[20]

Additional magnetic-plasma interactions of importance are seen in the accretion disk plasma. As has been suggested by Balbus and Hawley, it is known that even tiny seed magnetic fields may be amplified to grow to a large twisted and sheared magnetic fields inside of the accretion disk plasma.[21,22] For example, a tiny magnetic field seed of $\boldsymbol{B}$ in the disk plasma encounter the sheared rotational flows in the accretion disk, as the matter (in this case plasma) differentially rotates due to the gravitational rotation (such as the Keplerian motion). Balbus-Hawley[21,22] and Matsumoto et al.[20] showed that magnetic fields in the rotationally sheared accretion disk give rise to the instability to amplify its seed magnetic fields and flows in the disk (not just the Keplerian azimuthal systematic gravitational motion, but also multidimensional flows of plasma). Matsumoto et al.[20] showed a large magnetic field may be generated as a result of this instability, while there remains a possible flux escape and/or saturation via a variety of mechanisms such as the Parker instability[23] to make the generated flux tubes to become buoyant out of the accretion disk. There can be high β (β being the ratio of plasma matter pressure to the magnetic pressure) disks and low β disks[24,12]. Both show some similarity of the growth of magnetic fields, in the low β disks tend to show more explosively large magnetic fields that may become comparable to the plasma kinetic pressure. If the disk shows such high growth (or high level of) saturated magnetic fields in the disk, the plasma with such high magnetic fields would give rise to significant deviation of the disk's gravitational rotational motion (such as the Keplerian motion). Such state of large magnetic fields in the disk (see Matsumoto and Tajima 1995)[24] could give rise to the formation of the plasma clumps that may be no longer in the Keplerian motion in its orbital motion in the disk. This would lead to the disruption of such clumps of matter to fall out of the equilibrium Kepler motion in the disk. This leads to the disk disruption. (In some astrophysical objects such as microquasars shows such episodic transitions in its brightness).[25] If and when such disk disruption occurs due to the Balbus-Hawley (B-H) instability, we expect that a clump of mass falls toward the central gravitational object (such as the black hole). This would trigger a large perturbation, otherwise a steady emanation of the above described jet formation. This would be an episodic disruption of the jets whose root area is severely bombarded by the infalling accreting matter disrupted by this outgrowth of the B-H instability.[21,22] The episodic disruptions tend to occur, because after the matter infall due to the disk disruption, the magnetic fields have been erupted and released so that its power and pressure are pumped out. Thus, this B-H instability has to start from all over again from the minuscule stage. Because this above exponentiation of magnetic fields would take some dozens of exponentiation time of the B-H instability growth time, the episodic time would be on the order of several (or dozens) of times the B-H growth time.

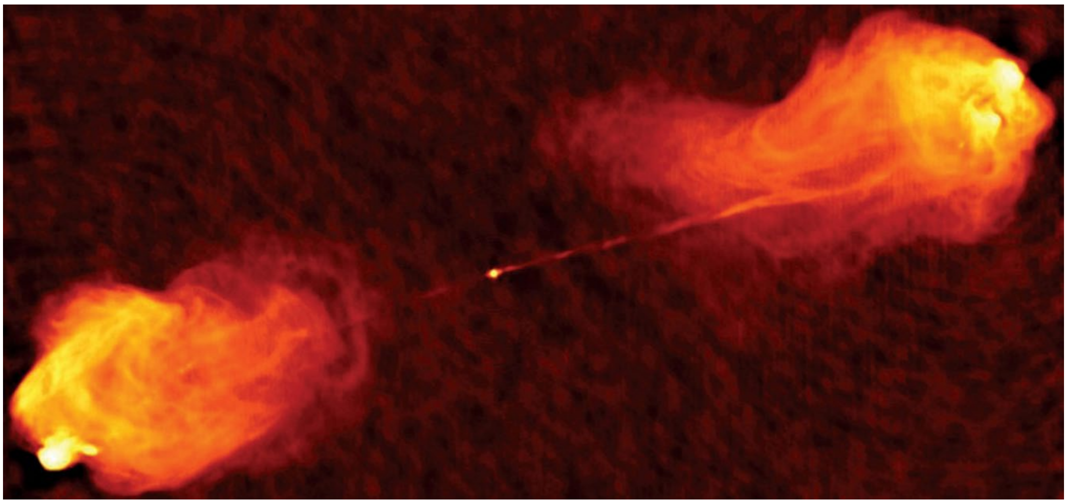

Figure 6. Narrow and long gigantic structure of jets (emanating to upper right and lower left directions, in white nearly staright lines) from the core (a central white spot, showing the AGN), which ends up in a pair of plasma cocoons (at the ends of the jets, shown in orange clouds) of the galaxy Cygnus A. (Credit: NRAO/AUI). The astrophysical high energy particle creation have been incubated in this structure and dynamics, not only at jets' bases but also along their long jet structures. After [26]

In short, we have learned that the B-H instability of the accretion disk (that contains magnetic fields) gives rise to the episodes of the fast magnetic field amplification in the disk, accompanied by episodic disruption of the Keplerian (otherwise steady rotational) motion of the disk, which accompanies a large-scale mass accretion of the non-Keplerian rotating matter in the disk toward its center. This also should accompany torsional shaking disturbance of the emanating jet magnetic fields that we have discussed above. We may call it a large disruptive shear Alfven shock. Once this release of a large flux of magnetic flux that was pent up by the B-H instability happens, the disk mass rotation resumes the more normal Keplerian rotation by the gravitational force nearly now unhindered by the magnetic forces. This however can still build up toward the next episode of the B-H instability buildup and repeats of the above disruptive emission of the Alfven shocks from the bottom of the jets' magnetic flux tubes.

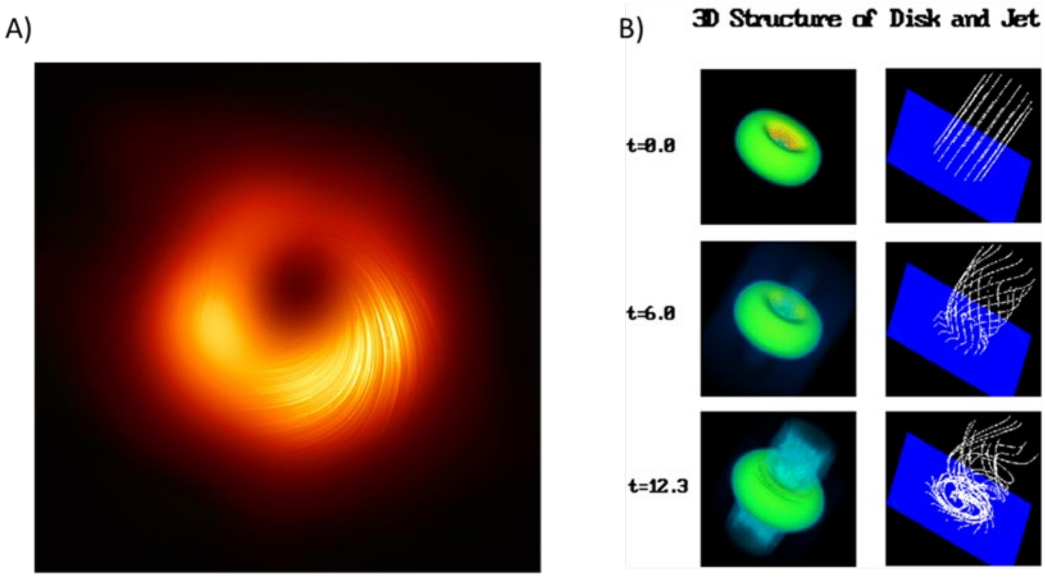

Event Horizon Telescope Collaboration

T. Tajima and K. Shibata, Plasma Astrophysics (Perseus Publishing, Cambridge Masachusetts 1997).

Figure 7. Comparison of the observation of the structure surrounding a blackhole and its (theoretically expected) evolution with the presence of surrounding magnetic fields. A) The shadow of the event horizon of supermassive blackhole at the center of M87 (Credit: Event Horizon Telescope).[27] The stripes may reflect an influence of the magnetic fields. B) The numerical simulation of accretion disk around a blackhole. The shear rotation and resultant magnetic shear (see Figure 2) give rise to the jet formation (After TS97).[10]

Ebisuzaki and Tajima[28-29] suggested that such accretion disruption at the root of the jet formation region would give rise to the strong excitation of the otherwise steady emanation of the jet flow, which leads to the formation of the large collective plasma wave excitations of the electromagnetic pulses (starting from the above-mentioned Alfven shocks) and their further collective behavior in the jet plasma. As discussed above, as the jet flows accompany the woven fabric of twisted magnetic fields, such episodic disruptions end up with episodic large excitation of Alfven waves (or shocks) starting at the root of the jets, which would propagate along the jet flows, as their phase velocity being the Alfven speed in that jet plasma. As we discovered, these Alfven shocks also give rise to another spectacular collective and robust display of intense celestial display of large intensity new structure formation, called wakefields. (We will discuss this in more detail in Sec. 2.) As we will discuss in Sec. 2, these Alfven waves (or shocks) phase velocity often is very close to the speed of light. Even if it is not, we will consider that these Alfven waves tend to mode convert into eventually high intensity electromagnetic pulse (as the density and magnetic field that sustains the Alfven waves decrease as the jets propagate over the long distance). We will see the implications of this as a spectacularly self-organized nature's development. The reason why the spectacularly self-organized motion and structure formation happen (we will find and show) is due largely to the relativistically strong wave excitation and their high speed (close to speed of light). We find that such relativistic entities tend to show robust structural and dynamical stability and resilience. This is why it can propagate sometimes to the end of its jets.

In the above, we have learned that there is a fundamental principle of the large structure formation by the presence of magnetic fields in astrophysical plasma such as near a compact gravitational object such as blackhole (neutron star) etc. This is a part of the broader structure formation enabled by the presence of magnetic fields in plasma that act as the agent of the coherent largely organized structure formation that Tajima and Shibata (1997: TS97)[10] found in their voluminous treatise of "Plasma Astrophysics". In that they state: "….The presence of magnetic fields and plasmas in the Universe …. (is) thus fundamental ……(in) enriching the astrophysical processes. …..(They) tend (i) to initiate, enhance or maintain the structure formation of the Universe; (ii) to provide efficient and sometimes violent paths to convert gravitational energies into flows, radiation, or kinetic energies; (iii) to facilitate or accelerate the evolution of the Universe….."

We will study the physical implications of these phenomena and their characteristics. Why they tend to be so robust and thus we can often be likely able to observe their imparted implications of its phenomena as observable far away to our Earth. This is the main reason why we believe and we try to show to the current extent that the phenomena we describe tend to show up in a multiple of observational channels such as multi-messenger astronomy observations. These could include optical lights, X-rays, Gamma-rays, microwaves, high energy cosmic rays, neutrinos, and even gravitational waves.

In recent years we further accumulated evidence that in addition to the large-scale structure formation such as the jets associated with an accretion disk around a compact gravitational object, there is an additional important principle in operation that facilitates the structural formation and evolution of the Universe in addition to the above we discussed. That is, the principle of the robustness of the wave structure that has a large phase velocity.[30] Once the magnetic fields in the Universe could set up such a robust structure as jets out of the accretion disk, when excited perturbations such as waves on the jets have the high phase velocity (such as the speed of light), we find that such waves stay robust and can propagate nearly un-disorganized over a huge propagation distance.

We call such a structure as wakefields. When wakefields excited by the large disturbances such as the B-H disruption by the large magnetic bulge, they remain as a coherent wave-like entity without decaying quickly in a turbulent mess. The reason they do not quickly turn into turbulence is its high phase velocity v_{p} of the wake waves. When the phase velocity is far removed from the bulk plasma (as characterized by its thermal velocity v_{t}), i.e. $v_{\mathrm{p}} \gg v_{\mathrm{t},}$ the wakefields remain to be highly organized and collectively interacting robust waves. We will see details of this process and its emergence in astrophysical plasmas such as in the astrophysical jets emanating from a compact gravitational object. In astrophysics, this high phase velocity often is in fact the speed of light. This means that wakefields are relativistic encasement of collectively organized plasma whose interaction is characterized by collective rather than single particle dynamics.[31] Here the single particle interaction strength is linearly proportional to the charge Ne, the collective interaction goes up with a much faster rate such as $(Ne)^2$. This means that even if the cosmic plasma density may be low, the reach of the collective fields such as the wavelength of the wakefields is so huge that the collective fields can become quite enormous. This is because the collective interaction reach is coherent and global in the plasma. We will see in the following that this combination of the magnetic field generated large scale magnetic robust structure like jets combined with the wakefields that have been excited by the accretion disk magnetic disruptions leads to the highly efficient energy converter of gravitational energy into kinetic and other energies over a truly cosmic distance.

In summary, the wakefield acceleration (WFA) theory in the jets of the accreting blackholes is considered as the backbone theory to explain signals through multi-messengers, including cosmic rays (charged particles), gravitational waves, neutrinos, and high-energy gammas as well as conventional electro-magnetic waves (radio, infrared, optical ultraviolet, and gammas).

In the rest of the paper, we will review how the observational results of multi messenger astronomy can be compared with the prediction of the WFA theory of accreting blackhole/jet system. The paper is organized as follows. In section 2, we describe how the WFA theory works in the accreting blackhole system. The production of the intense Alfvenic puleses, their propagation and mode conversion in the jets, and acceleration of the charged particles are described. In section 3, observational results are compared with the prediction of the WFA theory in the individual astronomical objects, which harbor accreting blackhole/jet systems. Those are blasars, radio galaxies, Seyfert galaxies, intermediate mass blackholes in the starburst galaxies, and galactic microquasars. In section 4, we will discuss short and long gamma-ray bursts in terms of NDAF disk produced in the NS-NS merging and the core-collapse of the rapidly rotating massive stars. Section 5 is for the discussions. We will discuss the comparison of WFA theory with other theories such as the Fermi acceleration mechanism. We also will present the prospects and implications for the future missions/projects.

2. Astrophysical Wakefield Acceleration in the jets of the Accreting blackholes

The violent time variabilities are produced by the magnetic eruption of the disk as described in section 1. In its strongly magnetized state, the plasma β, the ratio of thermal pressure to the magnetic pressure, decreases down to unity. In such a situation, magnetic field cannot be confined by matter. Violent eruptions take place to emit strong pulses of Alfvenic perturbations. This magnetic eruption can be considered as the cause of the violent time variabilities, which are frequently observed accretion disk systems. The pulses can propagate along the jets for long distance and accelerate charged particles (electrons, protons, and ions) by wakefiled acceleration up to high energies (above 10^{15} eV for electrons and above 10^{20} eV for protons and ions) to contribute various non-thermal phenomena.[28-30]

In turn, the pointing luminosity of the Alfvenic pulses, even if averaged over the time, is estimated as large as radiation luminosity and can sustain jets.[28-30,32] In this sense, two important features of accretion blackhole systems, those are 1) non-thermal emissions produced via collective processes (rather than single particle effects such as the Fermi acceleration) and 2) strong variabilities can be directly explained by a united collective interaction theory of accretion disk instabilities and wakefield accelerations.

In the subsection 2.1, we first describe the structure of the steady state accretion disk, according to Shakra and Sunyaev.[33] The desk instability and amplification of magnetic field are discussed in subsection 2.2 and the propagation of the Alfvenic pulse along the jets in subsection 2.3. In subsection 2.4, we present how charged particles are accelerated in the wakefield excited in the jets.

2.1. Disk structure

As we discussed in Figure 1 (b), accreting gas forms a disk around a blackhole.[33] In the accretion disk, gas move slowly inward while orbiting in a circular orbit with the Keplerian velocity around the blackhole without magnetic fields. If a viscosity works among the material (plasma) orbiting different radius, they can dissipate (slowly) its angular momentum resulting in the steady accretion of materials onto the central compact objects, such a BH. Here, in the disk, gravitational (potential) energy by the material accretion is converted into rotational (kinetic) energy, which is further converted into thermal energy by the friction and then eventually released in the form of various radiations (such as optical, UV, X-rays and gamma radiation, and perhaps cosmic rays depending on the situation).

Shakura and Sunyaev first obtained the structure of such an accretion disk around a compact object.[33] They estimated the physical quantities (densities, temperatures, and internal energies) in the disk, assuming 1) the steady state and 2) the minor importance of magnetic field in the disk dynamics, using the three equations of mass, angular momentum, and energy conservation. In this sense they are in the world of Figure 1(b).

In order to close the system of equations, they further assumed the proportionality of the viscosity coefficient to the gas pressure and introduced the parameter, α, as the proportionality constant. They, however, found that α must be as large as 0.01-0.1 to be compatible to the observations of the compact objects and is by far (many orders of magnitude) large compared with the viscosity coefficient estimated by the atomic diffusion of gas (plasma). They speculated that magnetic field may be responsible to this anomalously large α. The work by Balbus-Hawley[21,22] shows that the instability due to the shearing plasma flow velocity of the accretion disk (such as the Keplerian velocity) can give rise to exponential growth of the seed magnetic fields in the disk. Seed magnetic fields may be generated, for example, by such a mechanism by another plasma motion.[11] Matsumoto et al.[24] showed that the B-H instability makes the saturated magnetic fields either by the steady state formation of the enhanced magnetic viscosity or resistivity and the break of the accretion disk equilibrium motion by the presence of large enough grown magnetic fields. The self-consistently obtained magnetized plasma resistivity, η, may be calculated using

$$\eta = \frac{c^2}{4\pi\sigma_{\mathrm{e}}} = \left(\frac{\pi}{2}\right)^{\frac{1}{2}} \frac{1}{4\pi\rho C_{\mathrm{s}}} \sum_k \int d\omega \, \frac{{k_{\mathrm{J}}}^2}{k^3} \langle |b^2|(\mathbf{k},\omega)\rangle, \tag{3}$$

where σ_{e} is the electrical conductivity, ρ the density of plasma, C_{s} the sound velocity. Here, $\langle |b^2|(\mathbf{k},\omega)\rangle$ the time-averaged spectral intensity of magnetic fluctuations, and k_{J} the component of wavevector parallel to the mean electric current. By adopting the magnetic fluctuations that are produced in the disk by the BH instability, the magnitude of such fields may be evaluated as

$$\frac{\langle \delta B^2\rangle}{4\pi\rho C_S^2} = \chi_e \left(\frac{\pi}{2}\right)\left(\frac{k^2 {k_{\mathrm{z}}}^2}{{k_{\mathrm{J}}}^2}\right)\left(\frac{{k_{\parallel}}^2}{k^2}\right) f(q), \tag{4}$$

where $\langle \delta B^2 \rangle$ is the time-averaged magnetic fluctuations and χ_e the ionization rate. Here, the factor ${k_\parallel}^2/k^2$ is unity for the case of purely poloidal case and ${k_y}^2/{k_z}^2$ for purely toroidal case. By using this level of magnetic fields, we can estimate the enhancement fact of the accretion viscosity alpha as

$$\alpha_B = \chi_\mathrm{e} \frac{\langle \delta B^2 \rangle}{4\pi\rho C_s^2} \frac{-\langle \frac{\delta B_y}{\delta B_z} \rangle}{\langle \left(\frac{\delta B_y}{\delta B_z}\right)^2 \rangle + \langle \left(\frac{\delta B_z}{\delta B_z}\right)^2 \rangle + 1}, \tag{5}$$

$$\langle \frac{\delta B_y}{\delta B_x} \rangle = \frac{-2\Omega\gamma + (\gamma^2 + {\omega_A}^2 - 4A\Omega)(k_y/k_x)}{\gamma^2 + {\omega_A}^2 + 2\Omega\gamma(k_y/k_x)}, \tag{6}$$

$$\langle \frac{\delta B_z}{\delta B_x} \rangle = -q^{\frac{1}{2}} \frac{(\gamma^2 + {\omega_A}^2)(k_x/k_y + k_y/k_x + 2A/\gamma)}{\gamma^2 + {\omega_A}^2 + 2\Omega\gamma(k_y/k_x)}. \tag{7}$$

were δB_x, δB_y, and δB_z and k_x, k_y and k_z are three components of turbulent magnetic field, and wave vector, respectively, Ω the rotational frequency, A the Oort constant of the disk, ω_A the Alfven frequency, and γ the growth rate of the magnetorotational instability. Here $\langle x \rangle$ denotes time average of the quantity x.

This leads to an evaluation that α is a third of the ratio of the magnetic energy to the thermal energy,

$$\alpha = \frac{1}{3} \frac{\langle \delta B^2 \rangle}{4\pi\rho C_s^2} = \frac{1}{3\langle \beta \rangle}, \tag{8}$$

where $\langle \delta B^2 \rangle / 4\pi$ is the turbulent magnetic energy averaged over the time and place, ρ the gas density, C_s the sound velocity, and $\langle \beta \rangle$ the averaged ratio of the gas pressure to the magnetic pressure.

As can be seen in the next section, magnetic field can grow until their pressure is comparable to the thermal pressure (in other words, $\beta \sim 1$) in the accretion disk by magnetorotational instability, so that α could be as large as 0.1. In this sense, an accretion disk actually evolves under the overall scenario of Figure 1 (c).

After we have shown its magnitude of α may be in fact obtainable via self-consistent calculation of the magnitude fields that evolves under the overall scenario of Figure 1 (c).

The orbital angular velocity is given by:

$$\Omega = \left(\frac{GM_{\mathrm{BH}}}{R^3}\right)^{1/2} = \frac{c}{\sqrt{6}R_0}\frac{1}{mr^{3/2}}. \tag{9}$$

where c is the light velocity, M_{BH} the blackhole mass, R the distance from the center of the blackhole, G the gravitational constant, m the blackhole mass normalized by solar mass ($M_{\odot}$), and r the distance from the center of the blackhole normalized by the radius, R_{ISCO}, of the innermost stable circular orbit (ISCO):

$$R_{\mathrm{ISCO}} = 3R_g = \frac{6GmM_{\odot}}{c^2} = R_0 m, \tag{10}$$

where,

$$R_0 = \frac{6GM_{\odot}}{c^2}, \tag{11}$$

In other words,

$$R = R_0 mr. \tag{12}$$

Inside the ISCO, the circular orbits are unstable due to the relativistic effects, and the gas falls down at approximately the speed of light and are sucked into the blackholes. In other words, ISCO ($r = 1$) is the innermost radius of the gas disk.

According to Shakura and Sunyaev,[33] the steady state solutions of the disk can be calculated as follows. First, the disk is assumed to be axisymmetric and geometrically thin. The physical quantities in the disk are represented by the disk half thickness, z_{disk}, the density, ρ_{disk}, and internal energy, $\varepsilon_{\mathrm{disk}}$ averaged over the vertical direction of the disk (z-direction). Second, we assume the hydrostatic equilibrium in z-direction:

$$z_{\rm disk} = \frac{1}{\Omega}\left(\frac{\varepsilon_{\rm disk}}{3\rho_{\rm disk}}\right). \tag{13}$$

Third, the mass conservation equation turns out to be:

$$\dot{M} = -4\pi R \rho_{\rm disk} z_{\rm disk} v_r = const., \tag{14}$$

in steady-state assumption, where $\dot{M}$ is the mass accretion rate and v_r the radial velocity of the gas. Fourth, the angular moment conservation equation:

$$\dot{M}\Omega = 4\pi\alpha(\rho_{\rm disk} z_{\rm disk})\left(\frac{\varepsilon_{\rm disk}}{3\rho_{\rm disk}}\right), \tag{15}$$

where α the phenomenologically introduced parameter reflecting on the nature of of viscosity of the accretion disk. If all gravitational energy is released in the disk via the viscous heating of the disk plasma and that is released into the observable radiation emissions, we can relate the viscous evolution of the disk with the kinetic energy and potential energy of the disk, neglecting any magnetic energies (in the below shown through the parameter α.) Finally, when the gravitational energy release in the disk is assumed to be equal to the radiation flux from the disk, we obtain

$$\frac{3}{8\pi}\dot{M}\Omega^2 = \frac{4\varepsilon_{\rm disk}}{6\kappa_{\rm T}\rho_{\rm disk} z_{\rm disk}}. \tag{16}$$

Now, we can obtain three quantities $z_{\rm disk}$, $\varepsilon_{\rm disk}$, and $\rho_{\rm disk}$, solving three equations 13, 15, and 16 for a given parameter of $\dot{M}$ as the function r with the phenomenological parameter α.[26-28] Expressing these three quantities, we obtain

$$z_{\rm disk} = \frac{R_0}{8\epsilon}\dot{m}m,$$

where $\epsilon = 0.06$ the radiation efficiency of the accretion disk. (17)

$$\varepsilon_{\rm disk} = \frac{4c\Omega}{\kappa_{\rm T}\alpha} = \frac{4c^2}{\sqrt{6}\kappa_{\rm T}R_0}\frac{1}{\alpha m r^{3/2}}, \tag{18}$$

and

$$\rho_{\rm disk} = \frac{1024\pi^2 c^3}{27{\kappa_{\rm T}}^3 \alpha\Omega \dot{M}^2} = \frac{256\sqrt{6}\epsilon^2}{3\kappa_{\rm T} R_0} \frac{r^{3/2}}{\alpha \dot{m}^2\, m}, \tag{19}$$

where $\kappa_{\rm T} = 0.2$ [cm^2 g^{-1}]$(1 + X)$ is the opacity for the Thomson electron scattering, X the hydrogen concentration of gas, $\dot{m}$ the mass accretion rate normalized by the critical accretion rate, $\dot{M}_{\rm c}$,

$$\dot{M}_{\rm c} = \frac{L_{\rm Edd}}{\epsilon c^2} = \frac{4\pi G M_\odot}{c\epsilon\kappa_{\rm T}} m = \frac{2\pi c R_0}{3\epsilon\kappa_{\rm T}} m. \tag{20}$$

We note that the disk properties such as its thickness and diameter are expressed in terms of α.
In other words,

$$\dot{M} = \dot{m}\dot{M}_{\rm c} = \frac{2\pi c R_0}{3\epsilon\kappa_{\rm T}} \dot{m} m, \tag{21}$$

The radiation luminosity, $L_{\rm rad}$, is calculated as:

$$L_{\rm rad} = \frac{4\pi c G M_\odot}{\kappa_{\rm T}} \dot{m}\, m = \frac{2\pi c^3 R_0}{3\kappa_{\rm T}} \dot{m}\, m = \epsilon \dot{M} c^2, \tag{22}$$

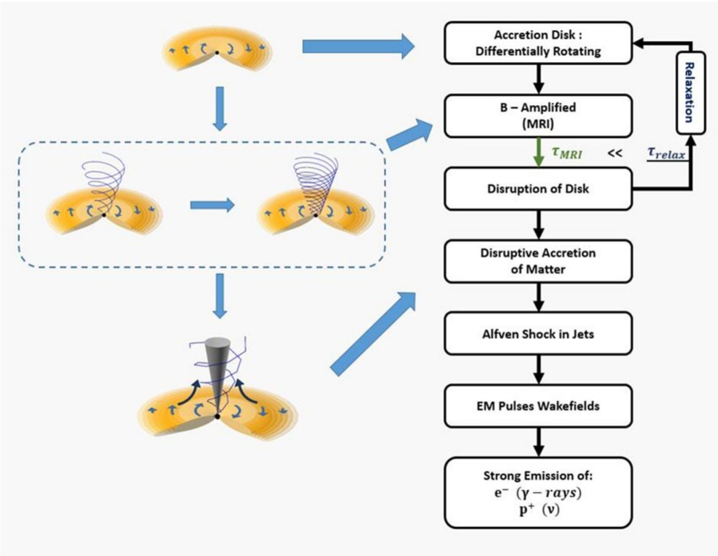

Figure 8. An accretion disk shows transitions between the strongly magnetized states to the weakly magnetized states, quasi-periodically, as suggested by Shibata et al.[12] Its theoretical framework is shown schematically.

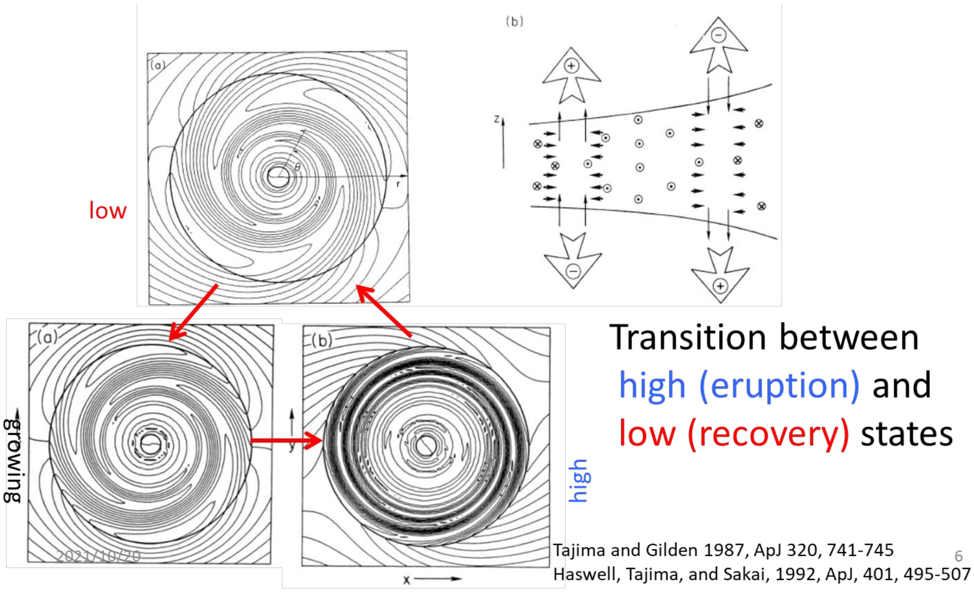

Figure 9. Magneto-rotational instability is developed in in an accretion disk to build up its magnetic fields in the disk and then leads to eruptions of magnetic field. And after its eruption, it relaxes back to a quiet stage, and repeat this episodic cycle. After the works by Tajima and Gilden[34] and Haswell et al.[35]

2.2. Alfvenic pulses emitted by the magnetic eruptions of the disk

As discussed in the rest of the section, the accretion disks are by no means in the steady state and rather unstable against magnet-rotational instability to become strongly fluctuated, if we take into account of magnetic field. The physical quantities obtained here must be understood as the average values integrated over a long period.

Many of astrophysical theoretical frameworks, as we reviewed above, are based on the steady state and purely gravitational objects without temporal, explosive, and extensive behaviors. However, as more observational evidence accumulates, we begin to learn the structured and behaviors that are beyond such models and descriptions. In these phenomena additionally magnetic fields have been found to play an important role. An example may be seen in Figure 6, in which central objects of AGN (seen as a tiny dot) emanates a pair of long (many kpc in the longest cases) jets, which form a pair of large lobes. Such objects, structure, and its emanating signals may not be explainable by gravitation alone. In fact, their strong active dynamics and high energy phenomena are considered to be mediated by magnetic activities.

The understanding of the production of the global magnetic field in the accretion disk was advanced step-by-step, as follows. First, Uchida and Shibata[4-7] pointed out that the magnetic field is amplified due to the winding by the differential rotation of the accretion disk and a pair of jets (both sides of the accretion disk) is launched along the rotation axis with the driving force of pinching and $\boldsymbol{j} \times \boldsymbol{B}$ force in the unwinding of the twisted magnetic field. Secondly, Balbus and Hawley[21,22] reveals that the accretion disk is unstable against magneto-rotational instability to develop magnetic turbulence in the disk. Although one usually may think that the turbulence would destroy the global structure, it is actually not in the case for an accretion disk around a blackhole. Thirdly, Tout and Pringle[36], who solved a set of simplified dynamo equations, showed that magnetic field is alternatively produced by the dynamo mechanism in the presence of the turbulence and the differential rotation in the disk. The magnetic field is transported by buoyancy from the disk along the rotation axis. This is consistent that the Uchida-Shibata's view that magnetic field twisted in the accretion disk drives the jets (Figure 8). In practice, Shibata et al.[12] performed a numerical simulation and revealed that the disk repeats transitions between strongly magnetized and weekly magnetized states as shown in Figure 8.

When we introduce β, the ratio of gas pressure to the magnetic pressure, the magnetic field is estimated as:

$$B_{\mathrm{disk}} = \left(\frac{8\pi}{3\beta}\varepsilon_{\mathrm{disk}}\right)^{1/2} = \left(\frac{32\pi c^2}{3\sqrt{6}\kappa_{\mathrm{T}} R_0}\right)^{\frac{1}{2}} \frac{1}{\alpha^{1/2}\beta^{1/2} m^{1/2} r^{3/4}}. \tag{23}$$

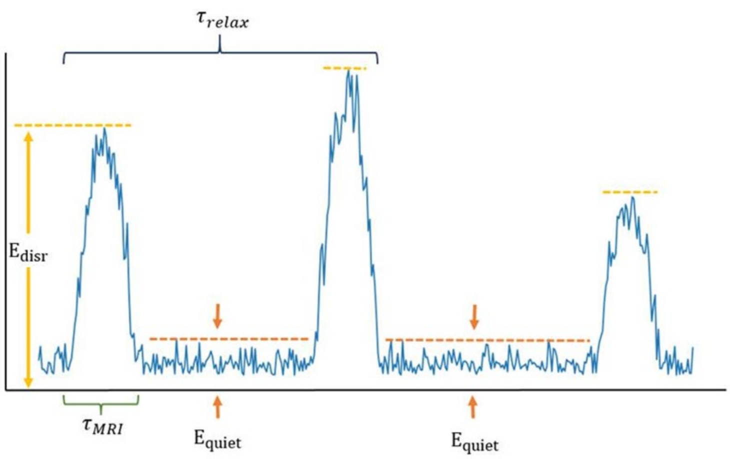

Figure 10. This episodic eruption of the disk and jets shown in Fig. 9 can lead to the generation of large perturbations of the jets and their magnetic fields. Such perturbations in the jets give rise to bursts of the Alfvenic perturbations, which are emitted in the transitions of the disk. An example is from Canac, et al., 2020.[37]

At the quasi-periodical transitions from the strongly magnetized states to the weakly magnetized states are magnetic eruptions and emit pulses of Alfvenic perturbations (Figure 9), which propagate along the jets perpendicular to the disk (along the rotational axis; Figure 10). The wavelengths of the emitted electro-magnetic disturbances are of the order of the size of the density clamps made in the disk. These are at the wavelength of the most unstable in magneto-rotational (B-H) instability;[21,22] in other words

$$\lambda = \left(\frac{V_{\mathrm{A,disk}}}{v_{\mathrm{s}}}\right)\left(\frac{\Omega}{A}\right) z_{\mathrm{disk}} = \frac{\kappa_{\mathrm{T}}\dot{M}}{4\pi c} = \frac{\sqrt{2}R_0}{6\epsilon}\frac{\dot{m}m}{\beta^{1/2}}, \tag{24}$$

where $\Omega/\mathrm{A} = 4/3$ for the Keplarian disk. Note that this value is a constant independent to r. Here, $V_{\mathrm{A,disk}}$ is the Alfven velocity in the disk:

$$V_{\mathrm{A,disk}} = \frac{B_{\mathrm{disk}}}{\sqrt{4\pi\rho_{\mathrm{disk}}}} = \frac{c}{8\sqrt{3}\epsilon}\frac{\dot{m}}{\beta^{1/2}r^{3/2}}, \tag{25}$$

and v_{s} is the sound velocity:

$$v_{\mathrm{s}} = \left(\frac{\varepsilon_{\mathrm{disk}}}{3\rho_{\mathrm{disk}}}\right)^{\frac{1}{2}} = \frac{c}{8\sqrt{6}\epsilon}, \tag{26}$$

The typical angular frequency the waves in the burst, which propagate in the light velocity c is calculated as:

$$\omega = \frac{2\pi c}{\lambda} = \frac{12\pi\epsilon c}{\sqrt{2}R_0}\frac{\beta^{1/2}}{\dot{m}m}. \tag{27}$$

The frequency of electro-magnetic wave bursts is given from the value of the ISCO ($r = 1$):

$$\nu = \frac{V_{\mathrm{A,disk}}}{z_{\mathrm{disk}}} = \frac{B_{\mathrm{disk}}}{z_{\mathrm{disk}}\sqrt{4\pi\rho_{\mathrm{disk}}}} = \frac{c}{\sqrt{3}R_0}\frac{1}{\beta^{1/2}mr^{3/2}}, \tag{28}$$

where $V_{\mathrm{A,disk}}$ is the Alfven velocity of the quiet phase. Since the energy released in the waves are dominated by the innermost region of the disk, the rising timescale, τ_{rise} and the periodic recurrence time, τ_{rec} can be calculated from the value of the ISCO ($r = 1$) as:

$$\tau_{\mathrm{rise}} = \frac{2\pi}{\omega} = \frac{\sqrt{2}R_0}{6\epsilon c}\frac{\dot{m}\,m}{\beta^{1/2}}, \tag{29}$$

and

$$\tau_{\mathrm{rec}} = \frac{1}{\nu} = \frac{\sqrt{3}R_0}{c}\beta^{1/2}m, \tag{30}$$

Therefore,

$$\frac{\tau_{\mathrm{rec}}}{\tau_{\mathrm{rise}}} = \frac{6\sqrt{6}\epsilon\beta^{3/2}}{\dot{m}}, \tag{31}$$

The strongest waves are emitted around ISCO ($r = 1$) in the burst state, this maximum flux of electromagnetic burst (Figure 11), is estimated as:

$$\Phi_{\mathrm{w}}(r = 1) = \frac{V_{\mathrm{A,disk}}{B_{\mathrm{disk}}}^2}{4\pi} = \frac{\Omega^2\dot{M}}{\sqrt{2}\pi} = \frac{c^3}{9\sqrt{2}\epsilon\kappa_{\mathrm{T}}R_0}\frac{\dot{m}}{\alpha\beta^{3/2}mr^3}. \tag{32}$$

The waves propagate along the perpendicular (jets) to the accretion disk. Wave flux $\Phi_{\rm w}(D = 3R_{\rm g} = R_0 m)$ is given by $\Phi_{\rm w}(r = 1)$. Since the Alfven velocity in the jets is close to the speed of light, electric field $E_{\rm w}$ of the wave is calculated as:

$$\Phi_{\rm w,jet}(D = R_0 m) = \Phi_{\rm w}(r = 1) = \frac{c{E_{\rm w}}^2}{4\pi}, \tag{33}$$

where D is the distance from the blackhole along the jet. Therefore, we obtain

$$E_{\rm w} = \left[\frac{4\pi}{c}\Phi_{\rm w}(r = 1)\right]^{1/2} = \frac{2c}{3}\left(\frac{\sqrt{2}\pi}{\epsilon\kappa_{\rm T} R_0}\right)^{1/2} \frac{\dot{m}^{1/2}}{\alpha^{\frac{1}{2}}\beta^{\frac{3}{4}}m^{1/2}}. \tag{34}$$

The dimensionless vector potential a_0 at the bottom of the jet is given by

$$a_0 = \frac{eE_{\rm w}}{m_{\rm e}\omega c} = \frac{e}{18 m_{\rm e} c}\left(\frac{\sqrt{2}R_0}{\pi\epsilon^3\kappa_{\rm T}}\right)^{1/2} \frac{\dot{m}^{3/2}m^{1/2}}{\alpha^{1/2}\beta^{5/4}}. \tag{35}$$

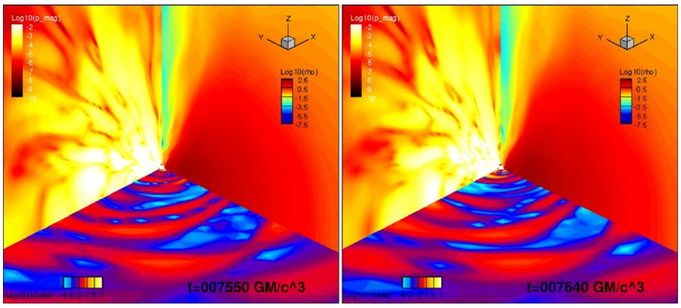

Figure 11. A numerical simulation of the innermost part of the accretion disk around a blackhole. Magnetic fields are amplified in the disk, while these turn into the jets and their episodic disruptive dynamics. After Mizuta et al.[14]

On the other hand, the time-averaged luminosity, $L_{\rm w}$, integrated over the entire disk is calculated as:

$$L_{\rm w} = \int_{mR_0}^{\infty} 2z_{\rm disk}\frac{{B_{\rm disk}}^2}{4\pi} v 2\pi R dR = \frac{4\pi c^3 R_0}{9\sqrt{2}\epsilon\kappa_{\rm T}}\frac{\dot{m}m}{\alpha\beta^{3/2}} = \left(\frac{\sqrt{2}}{3\alpha\beta^{3/2}}\right)\dot{M}_{\rm c}c^2. \tag{36}$$

The ratio $L_{\rm w}/L_{\rm rad}$ of the wave luminosity to radiation luminosity,

$$\frac{L_{\mathrm{w}}}{L_{\mathrm{rad}}} = \frac{\sqrt{2}}{3\epsilon\alpha\beta^{3/2}}, \tag{37}$$

is larger than unity and as large as 10, in other words, the Alfvenic pulses emitted by the repeated magnetic eruptions of the disk are strong enough to maintain the relativistic flow of the jets emanating from the accreting blackhole system, as Shibata and Uchida pioneered.[4-7] The jets, backboned by the relativistic flow and the longitudinal magnetic field, extend long distances of Mega parsec ($\sim 10^{24}$ cm) scales for the case of cosmological quasars and parsec scales $\sim 10^{18}$ cm for the case of galactic microquasars, far beyond the size of their accretion disks.

2.3. Propagation of Alfvenic pulses along the jets

The Alfvenic pulses are propagates in the jets for long distance. Although their typical frequencies are lower than the plasma frequency at the bottom of the jets, they can propagate with the restoring force of cyclotron resonance of electrons and ions. As distance from the blackhole increases, the magnetic field decreases, so that the ratio of the angular frequency of the wave to the cyclotron frequencies (both for electrons and ions) increases. The waves are converted into the higher order of resonances keeping their frequencies constant through the channels near the light cone: the Alfven velocity is close to the light velocity in the jets. As the plasma density also decreases, the frequencies become eventually larger than the local plasma frequency. Afterwards, the waves can propagate as plasma waves, which will be connected to the branch of the electro-magnetic mode.

This subsection examines the dependence of physical parameters in the jet on distance from the bottom and discusses how the waves propagate through it. First, the magnetic field B_{jet} in the jet can be calculated assuming that the magnetic field flux is conserved in the jet.

$$B_{\mathrm{jet}} = [B_{\mathrm{disk}}(r=1)](b/mR_0)^{-2} = [B_{\mathrm{disk}}(r=1)]\left(\frac{D}{mR_0}\right)^{-1} =$$

$$\left(\frac{32\pi c^2}{3\sqrt{6}\kappa_{\mathrm{T}}R_0}\right)^{1/2} \frac{1}{\alpha^{1/2}\beta^{1/2}m^{1/2}} \left(\frac{D}{mR_0}\right)^{-1}. \tag{38}$$

Next, we assume as

$$\gamma = a_0, \tag{39}$$

within the jet, a_0 can be calculated, assuming that the wave intensity within the jet is conserved, i.e., the flux $\Phi_{\mathrm{w,jet}}$ is inversely proportional to the cross-sectional area πb^2 of the jet.

$$a_0(D) = a_0(D = R_0)\left(\frac{b(D)}{R_0 m}\right)^{-1}, \tag{40}$$

where D is the distance from the bottom of the jet, and $b(D)$ is the radius of the jet, which is assumed to $b(0) = 3R_{\mathrm{g}} = R_0 m$. In addition, Figure 13 shows the ratio of plasma frequency $\omega_{\mathrm{p}}'/\omega$ are plotted against the distance $D/(R_0 m)$ from the bottom of the jet for the typical cases ($\Gamma = 10, \alpha = 0.1, \xi = 10^{-2}, \dot{m} = 0.1$ for $m = 1, 10^4,\ 10^8$). Here we assume that

$$b(D) = R_0 m (D/R_0 m)^{1/2}. \tag{41}$$

This relation is consistent with the observation of the jet of M87, the closest active galactic nuclei M87[38] and other AGN jet observation.[39] Therefore, we get

$$a_0(D) = \frac{e}{18 m_{\mathrm{e}} c}\left(\frac{\sqrt{2}R_0}{\pi\epsilon^3\kappa_{\mathrm{T}}}\right)^{\frac{1}{2}} \frac{\dot{m}^{3/2} m^{1/2}}{\alpha^{1/2}\beta^{5/4}}\left(\frac{D}{R_0 m}\right)^{-1/2}. \tag{42}$$

The plasma frequency ω_{p}' corrected for relativistic effects is given by

$$\omega_{\mathrm{p}}' = \left(\frac{4\pi n_{\mathrm{jet}} e^2}{m_e \gamma}\right)^{1/2}. \tag{43}$$

The plasma density n_{jet} in the jet can be calculated from as follows, if we assume the kinetic luminosity of the jet:

$$L_{\mathrm{jet}} = n_{\mathrm{jet}} \mu m_{\mathrm{H}} c^3 \Gamma^2 \pi b^2 = \xi L_{\mathrm{rad}}, \tag{44}$$

is conserved through the jet. Therefore,

$$n_{\mathrm{jet}} = \frac{2}{3\mu m_{\mathrm{H}} \kappa_{\mathrm{T}} R_0} \frac{\xi \dot{m}}{\Gamma^2 m}\left(\frac{D}{R_0 m}\right)^{-1}. \tag{45}$$

Here, ξ_2 is the ratio of the kinetic luminosity of the jet to the radiation luminosity, Γ the bulk Lorentz factor, and $\mu = 1.29$ is the mean molecular weight of the accreting gas. Substituting equations 44, 39, and 42 into equation 43, we get:

$$\omega_{\mathrm{p}}' = \left(\frac{4\pi n_{\mathrm{jet}} e^2}{m_e \gamma}\right)^{1/2} = 4\left(\frac{9\pi^3 e^2 c^2 \epsilon^3}{\sqrt{2}\mu^2 m_{\mathrm{H}}{}^2 \kappa_{\mathrm{T}} R_0{}^3}\right)^{1/4} \frac{\xi^{1/2}\alpha^{1/4}\beta^{5/8}}{\Gamma \dot{m}^{1/4} m^{3/4}} \left(\frac{D}{R_0 m}\right)^{-1/4}. \tag{46}$$

In Figure 13, we plot ω_{c}',, ω_{p}' and ω at the bottom of the jet ($D = R_0$) against the blackhole mass m for the typical case ($\Gamma = 10$, $\alpha = 0.1$, $\xi = 10^{-2}$, $\dot{m} = 0.1$). For most of the interesting cases, the relationship of $\omega_{\mathrm{p}}' > \omega$ holds; In other words, at the bottom of the jets, the plasma in the overdense state ($\omega_{\mathrm{p}}' > \omega$), where plasma waves and electromagnetic waves cannot propagate. On the other hand, Alfven wave or whistler wave can propagate, the Alfven velocity $V_{\mathrm{A,jet}}$ at the bottom of the jet are given by

$$V_{\mathrm{A,jet}} = \frac{B_{\mathrm{jet}}}{\sqrt{4\pi m_{\mathrm{H}} n_{\mathrm{jet}}}} = \frac{2}{\sqrt{6}} \frac{\Gamma c}{\alpha^{1/2}\beta^{1/2}\dot{m}^{1/2}}. \tag{47}$$

In other words, the nominal values of the Alfven velocity

$$V_{\mathrm{A,jet}} \sim 10^{12} [\mathrm{cm\ s^{-1}}] \left(\frac{\Gamma}{10}\right) \left(\frac{\xi}{10^{-2}}\right)^{-1/2} \left(\frac{\dot{m}}{0.1}\right)^{-1/2}. \tag{48}$$

This can approach the speed of light, when the approximation breaks down. Then the wave becomes that of EM waves in magnetized plasma. On the other hand, $\omega_{\mathrm{p}}' = \omega$ at the distance D_0 given by:

$$\left(\frac{D_0}{R_0 m}\right) = \frac{4 e^2 R_0}{9\sqrt{2}\pi \mu^2 m_{\mathrm{H}}{}^2 c^2 \kappa_{\mathrm{T}} \epsilon} \frac{\xi^2 \alpha \beta^{1/2} \dot{m}^3 m}{\Gamma^4}. \tag{49}$$

$$n_{\mathrm{jet}}(D_0) = \frac{3\sqrt{2}\pi c^2 \mu m_{\mathrm{H}} \epsilon}{e^2 R_0{}^2} \frac{\Gamma^2}{\xi \alpha \beta^{1/2} \dot{m}^2 m^2}$$

On the outside of the point D_1 ($D > D_1$), $\omega > \omega_{\mathrm{p}}'$ so that the plasma wave (electromagnetic wave) allows to propagate. The electromagnetic waves propagated as Alfven wave and whistler wave are converted into plasma waves (electromagnetic waves) by nonlinear mode-conversion. This $D > D_2$ leads to the bow wakefield acceleration as described in the next subsection.

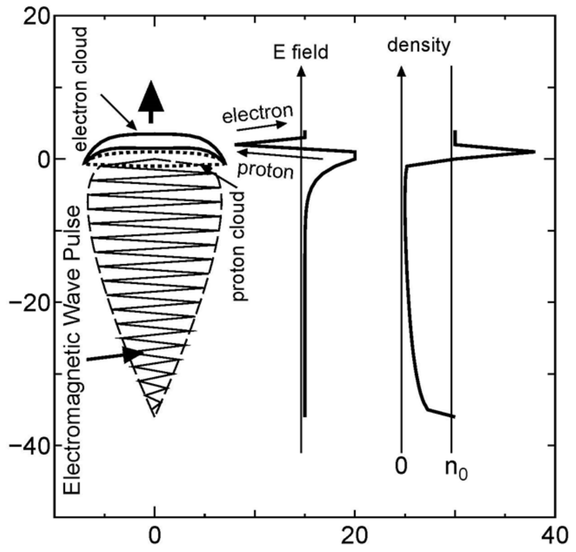

Figure 12. The strong Alfvenic pulse (discussed in Figure 11) can mode-convert itself into an intense electromagnetic pulse (shown on the left of this picture) through the propagation in the jet plasma. The acceleration structure produced by this intense electromagnetic pulse. An electron cloud is formed in front of the pulse due to the pondermotive force of the electromagnetic wave. The electrons are accelerated in front of the slope of the electron cloud, while protons in the backside. This structure is stable and propagates at the velocity very close to the light velocity.[28]

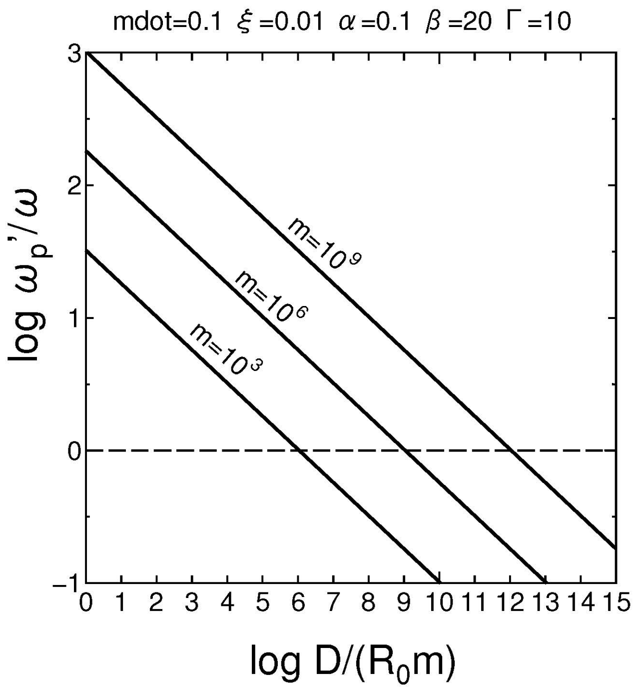

Figure 13. The ratio of the eigenmode frequency of the jet plasma to the excited electromagtntic pulse frequency $\omega_{\mathrm{p}}' /\omega$ is larger than unity at the bottom of the jets ($D/R_0 m$), which means the mode is in overdense plasma.. The overdense disturbances propagate as the Alfven or whistler modes, which use the magnetic field as restoring force, though they are highly relativistic and non-linear. The ratio $\omega_{\mathrm{p}}' /\omega$ decreases as D increases and eventually become oscillations in underdense plasma $\omega_{\mathrm{p}}' /\omega < 1$, beyond where Alfvenic waves turn itself as a propagating electromagnetic wave. Alfven/whistler waves are nonlinearly as well as linearly converted to electromagnetic waves to produce the acceleration structure shown in Figure 12.

2.4. Wakfefield acceleration

We have seen that the rotating accretion disk accompanied by the magnetic fields emanates a well-collimated extended jets that are wrapped around by the netting magnetic fields. These astrophysical jets are one of the largest (if not the largest) and long-standing eminent structure of the Universe (see e.g. Figure 6). This structure, we have observed in many astrophysical objects, also accompanies additional structured entities on it. That was the formation of wakefields that are created upon the jets. First, the presence of the magnetic fields in the jets allow the disturbances from the accretion disk (such as the Alfven shocks) to be propagating in the plasma due to the physical properties of the electromagnetic waves in magnetized plasma (see. e.g. Ichimaru, 1973[31]). This allows the EM disturbances created at or near the accretion disk can propagate through the (otherwise evanescent ($\omega < \omega_{\mathrm{p}}'$) plasma to the propagating regime of plasma ($\omega > \omega_{\mathrm{p}}'$). Thus the presence of the magnetic field in the jets acts as a conduit of these intense EM disturbances that may be created by the accretion disk.

The created intense EM waves (due in part its highly relativistic dynamics) have often highly relativistic group velocity. As has been discussed above, the EM waves with high group velocity is capable of creating an intense longitudinal plasma wave structure (Figure 12), whose phase velocity is also relativistic (close to c) (called wakefields.[40,30] It has been shown and demonstrated (experimentally and theoretically) that these wakefields generated with high phase velocity are robust. The robustness arises from the fact that (1) the phase velocity close to the speed of light, by far, different from the thermal velocities of plasma bulk, so that plasma remains quite stable and the excited waves remain robust. In other words, by the time the plasma electrons respond to the wakefield electric fields, with the electron speed less than c, the waves have escaped away from the responding electrons, thus keeping this high amplitude plasma waves intact.

It remains also robust due to the fact that (2) electrons in this regime, even if the electrons respond to the high phase velocity, all the electrons can move at (or near) the speed of light, which is in fact what the wakfields are moving. so that these electrons, in fact, reinforce the movement of the wakefields. This is called the relativistic coherence[41,42] and is the reason why the wakefields themselves are stable and robust, in addition to the robustness of the observed astrophysical jets.

We see that astrophysical jets only eventually begin to form lobes at their ends when the particles that propagate through the jets are now expended their energies to become low enough to interact with the bulk plasma strongly where a variety of plasma instabilities with the bulk plasma particles may take place.

As discussed above, the conditions for the strong acceleration by wakefield are:[32]

(a) the acceleration structure (wave) is very close to the relativistic propagation velocity (phase velocity), i.e. the speed of light; and

(b) the wave has a relativistic amplitude (i.e. the particles in the wave have a relativistic momentum $e_j E/\omega > m_j c$ in one photon cycle). Where e_j and m_j are the charge and the mass of the particle j, and E and ω are the electric field and angular frequency of the wave.

The condition (b) came from the fact that the significant acceleration by a ponderomotive force of the electromagnetic wave takes place only in the relativistic case: This term becomes significant only if the amplitudes of the electromagnetic waves become relativistic.[32] If these two conditions are satisfied, as shown by a number of ground experimental demonstrations and considerations,[43-47] this acceleration mechanism is more robust to Fermi acceleration,[48] in which charged particles gradually gain energy as they are scattered many times by magnetic clouds. Here, it is worth noting that the coherence in the driver is not necessary in the acceleration. What is important is the focusing energy in a pulse to achieve the condition (a). In the case of photons, the coherence in photons is necessary to concentrate energy, which automatically and naturally creates accelerating structure.

As the pulse of the electromagnetic wave is highly relativistic in the sense that the magnitude, $a_0 = eE_{\mathrm{w}}/(m_e \omega c)$ of the normalized vector potential is much larger than unity and the propagation velocity is nearly equal to the light velocity, the two conditions (a) and (b) for the strong wakefield acceleration are well satisfied. Figure 12 shows the acceleration structure (wake) produced by an electromagnetic pulse. An electron cloud is formed in front of the pulse due to the ponderomotive force of electromagnetic wave. The electrons are accelerated in the front slope of the electron cloud, while protons in the slope of the backside (between two clouds). This acceleration structure is stable and propagates at the velocity very close to the light velocity.

The pondermotive force, F_{pm}, for the electrons of the electromagnetic wave is a force generated from the Lorentz force, $(v/c) \times B$, in the propagation direction of the electromagnetic wave. If the motion of the electrons by the wave is not relativistic ($a_0 < 1$), it can be calculated as the force resulting from the average of the profiles of the electromagnetic pulses. In the relative regime ($a_0 > 1$), this force is more simplified. Since the particle velocity approaches to the light velocity and the plasma satisfies the underdense ($\omega > \omega_{\mathrm{p}}'$) condition as well.

Since to the particle velocity asymptotically approaches to the light velocity and that the plasma satisfies the underdense ($\omega > \omega_{\mathrm{p}}'$) condition as well, B is equal to E ($B = E$). In this case, F_{pm}, is given by

$$F_{\mathrm{pm}} = \Gamma^2 m_{\mathrm{e}} c a_0 \omega_{\mathrm{p}}' . \tag{50}$$

The accelerated electrons emit high energy gamma rays with the energies ranging GeV-PeV due to the collision with the magnetic perturbations. On the other hand, protons and ions are released into interstellar or intergalactic space to be cosmic rays. The highest energy charged particles with $10^{19} - 10^{20}$ eV are observed as Ultra High Energy Cosmic Rays (UHECRs). The cosmic ray protons may lose their energy through the p-p interaction in the interstellar medium in the galaxy, the resultant pions produce neutrinos through their decays.

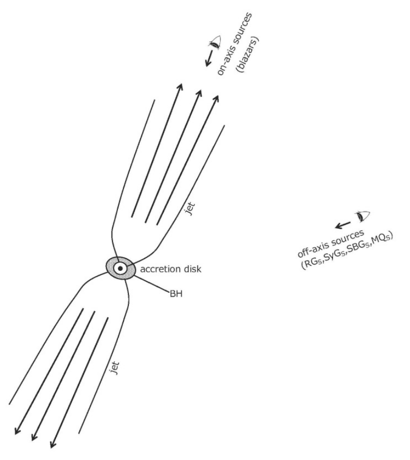

Figure 14. The emitted radiations from such collimated jets can be highly collimated in the direction of the jets as its inherent genealogical mechanism. Luminosity would be larger for on-axis observed

objects (blazars) and smaller for off-axis sources (other sources).

2.4.1. Electrons and gamma-ray emissions

The energies of electrons, which are accelerated in the front side of the bow wake (Figure 12) are transferred to gamma-rays through the collisions of electrons with magnetic fields. In other words,

$$L_{\gamma} = L_{\mathrm{TCR}} = \sigma L_{\mathrm{w}}. \tag{51}$$

This assumption in electron spectrum is consistent with the typical blazer SED (spectrum energy distribution) and variability.[35]

The gamma-ray is most likely beamed along the jets, which is consistent with the correlation observed in gamma-ray flux and apparent opening angle of the jets of AGNs.[43] When the emission is beamed, the isotropic luminosities are overestimated for on-axis sources (blazars) but underestimated off-axis sources (other AGNs and microquasars; Figure 14).

2.4.2. Protons and ions

Protons and ions are accelerated by an electric field (back side: Figure 12) generated by bow wakefield (longitudinal polarization of electronic distributions). The acceleration force F_{acc} is given by

$$F_{\mathrm{acc}} = zF_{\mathrm{pm}} = \frac{2e}{9}\left(\frac{9\sqrt{2}\pi e^2 c^2}{\mu^2 m_{\mathrm{H}}{}^2 \kappa_{\mathrm{T}}{}^3 R_0 \epsilon^3}\right)^{1/4} \frac{z\Gamma^2 \xi^{1/2} \dot{m}^{4/5}}{\alpha^{1/4}\beta^{5/8} m^{1/4}} \left(\frac{D}{R_0 m}\right)^{-3/4}. \tag{52}$$

Here, z is the charge of the particle. Charged particles are repeatedly accelerated by this acceleration structure. The acceleration distance. l_{acc}, of one acceleration event is determined by dephasing of the accelerating particles and estimated as

$$l_{\mathrm{acc}} = 2\gamma_{\mathrm{p}}{}^2 \frac{c}{\omega'_{\mathrm{p}}}. \tag{53}$$

where $\gamma_{\mathrm{p}} = \omega/\omega'_{\mathrm{p}}$.[40] Please note that l_{acc} can be larger than the wavelength ($\sim c/\omega'_{\mathrm{p}}$) of electromagnetic disturbances in the acceleration region, where $\omega'_{\mathrm{p}} < \omega$. This makes the wakefiled acceleration much more efficient compared with the conventional Fermi acceleration, in which the acceleration distance is much smaller than the wavelength of the electro-magnetic disturbance. In such a strong acceleration case, the energy spectrum $f(W)$ of the charged particles has a power law function of the exponent -2,[49,50] in other words, $f(W) = A(W/W_{\rm min})^{-2}$.

The maximum energy, $W_{\rm max}$, of the spectrum of the accelerated particles is assumed to be determined by integrating $F_{\rm acc}$ from D_0 through D_1 as:

$$W_{\rm max} = \int_{D_0}^{D_1} F_{\rm acc} dD'/\Gamma = \frac{2e}{9}\left(\frac{9\sqrt{2}\pi e^2 c^2}{\mu^2 m_{\rm H}{}^2 \kappa_{\rm T}{}^3 R_0 \epsilon^3}\right)^{1/4} \frac{z\Gamma\xi^{1/2}\dot{m}^{4/5}}{\alpha^{1/4}\beta^{5/8}m^{1/4}} \int_{D_0}^{D_1}\left(\frac{D'}{R_0 m}\right)^{-3/4} dD'$$

$$= \frac{8e}{9}\left(\frac{9\sqrt{2}\pi e^2 c^2 R_0{}^3}{\mu^2 m_{\rm H}{}^2 \kappa_{\rm T}{}^3 \epsilon^3}\right)^{1/4} \frac{z\xi^{1/2}\dot{m}^{4/5}m^{3/4}}{\alpha^{1/4}\beta^{5/8}}\left[\left(\frac{D_1}{R_0 m}\right)^{1/4} - \left(\frac{D_0}{R_0 m}\right)^{1/4}\right]$$

$$= \frac{8\sqrt{2}e^2 R_0(\delta^{1/4}-1)}{9\mu m_{\rm H}\kappa_{\rm T}\epsilon}\frac{z\xi\dot{m}^2 m}{\Gamma\,\beta^{1/2}}. \tag{54}$$

where, $D_1 = \delta D_0$ is the distance at which acceleration is finished by the depletion of the driving photon field. Here, we can eliminate $\dot{m}$ using equation 22 as

$$W_{\rm max} = \frac{2\sqrt{2}e^2\kappa_{\rm T}}{\pi^2\mu m_{\rm H} c^6 R_0 \epsilon}\frac{z\xi(\delta^{1/4}-1)}{\Gamma\beta^{1/2}m} L_{\rm rad}{}^2. \tag{55}$$

Figure 15, the accreting blackholes of $1 - 10^{10} M_\odot$ can produce UHECRs with the energy above 5.7×10^{19} eV by the wakefield acceleration.

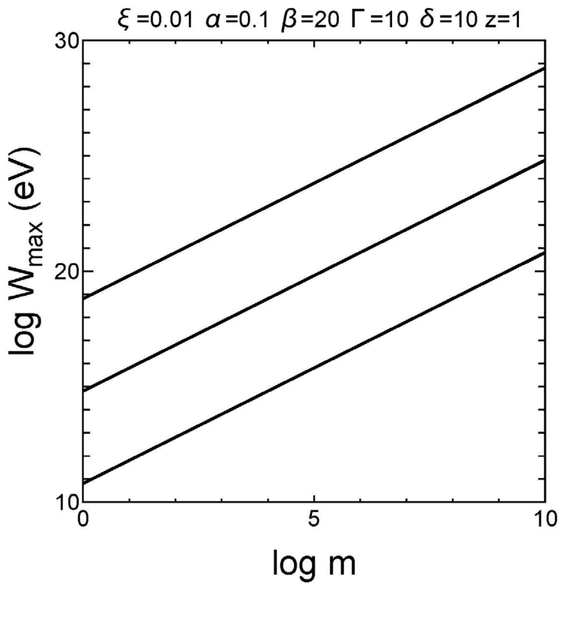

Figure 15. The maximum attainable energies of accelerated particles by the mechanism of wakefield acceleration, $W_{\max}$ are plotted against the mass of the central AGN m for and its time derivative $\dot{m} = 10^{-1}$, 10^{-3}, and 10^{-5}. Accreting blackholes can produce ultrahigh energy cosmic rays UHECRs (above 5.4×10^{19} eV), if accretion rates are high enough.

Given the energy efficiency, σ, of charged-particle acceleration, including the conversion of Alfven wave into electromagnetic waves, the total cosmic ray luminosity, L_{TCR}, is given by

$$L_{\mathrm{TCR}} = \sigma L_{\mathrm{w}} = \int_{W_{\min}}^{W_{\max}} W_{\mathrm{CR}} f(W_{\mathrm{CR}}) dW_{\mathrm{CR}} = A {W_{\min}}^2 \int_{W_{\min}}^{W_{\max}} {W_{\mathrm{CR}}}^{-1} dW_{\mathrm{CR}}$$
$$= A {W_{\min}}^2 \ln(W_{\max}/W_{\min}). \tag{56}$$

In other words,

$$A = \frac{\sigma}{{W_{\min}}^2 \ln(W_{\max}/W_{\min})} L_{\mathrm{w}}. \tag{57}$$

The cosmic-ray number spectrum is represented by:

$$n_{\mathrm{CR}} = \frac{\sigma L_{\mathrm{w}}}{\ln(W_{\max}/W_{\min})} {W_{\mathrm{CR}}}^{-2}, \tag{58}$$

where W_{CR} is the energy of a cosmic-ray particle. The UHECR luminosity is given by:

$$L_{\mathrm{UHECR,th}} = \int_{W_0}^{W_{\max}} W_{\mathrm{CR}} f(W_{\mathrm{CR}}) dW_{\mathrm{CR}} = \frac{\sigma}{\ln\left(\frac{W_{\max}}{W_{\min}}\right)} L_{\mathrm{w}} \int_{W_0}^{W_{\max}} {W_{\mathrm{CR}}}^{-1} dW_{\mathrm{CR}}$$
$$= \frac{\ln(W_{\max}/W_0)}{\ln(W_{\max}/W_{\min})} \sigma L_{\mathrm{w}} = \sigma \zeta L_{\mathrm{w}}. \tag{59}$$

Here,

$$\zeta = \frac{\ln(W_{\max}/W_0)}{\ln(W_{\max}/W_{\min})}. \tag{60}$$

Since the hotspots in northern sky are seen for the events above 5.7×10^{19} eV,[51] we set $W_0 = 0.57 \times 10^{20}$ eV.

Cosmic-ray particles are originally beamed toward the direction of the jets. After released from the jets into the interstellar space, they may be deflected by the interstellar magnetic field. The Larmor radius, D_{L}, of a cosmic ray particle is calculated as:

$$D_L = \frac{W_{\mathrm{CR}}}{ZecB} = 1.1 \times 10^3\ [\mathrm{pc}]\ Z \left(\frac{B}{100\ \mu\mathrm{G}}\right)^{-1} \left(\frac{W}{10^{20}\ \mathrm{eV}}\right). \tag{61}$$

Even UHECRs above 10^{20} eV be significantly lose their orientation toward the jets because of the magnetic field of ~ 100 μG in the starburst regions of the galaxies.[52,53] For the objects with prominent jets, such as AGNs or microquasars, UHECRs are likely beamed toward the direction of the jets. The isotropic luminosities are overestimated for on-axis sources (blazars) but underestimated off-axis sources (other AGNs and microquasars; Figure 16a). However, the objects without prominent jets such as Seyfert galaxies and intermediate mass black holes in the starburst galaxies, the UHECRs are ejected in the starburst region, in which many supernova remnants and molecular locate, the directions of the UHECRs even above 10^{20} eV are likely to be randomized (Figure 16b). UHECRs are deflected by magnetic field in the intergalactic/interstellar space between their source and the Earth. The deflection angles are estimated as:

$$\theta = 0.5° z \left(\frac{d}{\mathrm{Mpc}}\right) \left(\frac{B}{\mathrm{nG}}\right) \left(\frac{W}{10^{20}\ \mathrm{eV}}\right)^{-1}. \tag{62}$$

Since the magnetic field in the intergalactic/interstellar space is turbulent, the spot of UHECR from a point source is likely to be spread by the same magnitude.

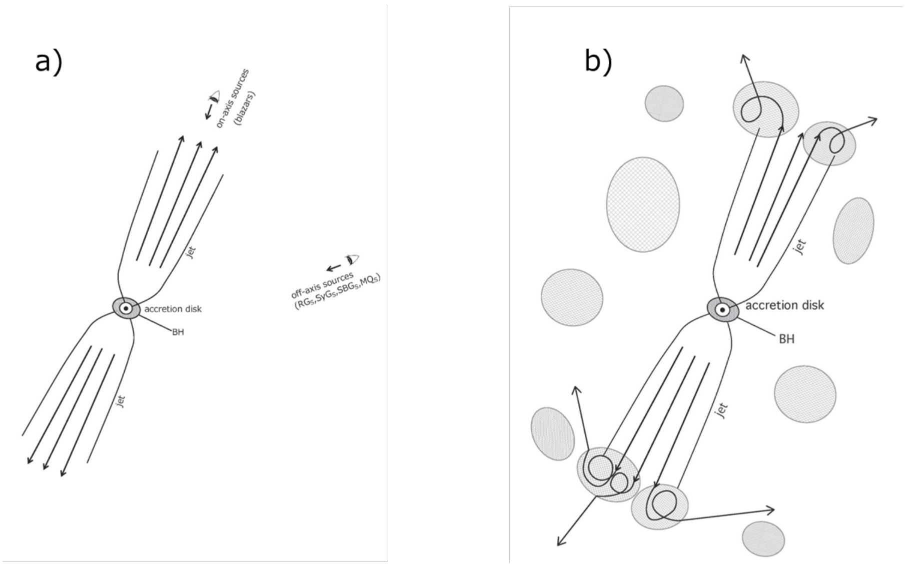

Figure 16. The emission of the protons and ions is originally beamed as shown in (a). But could be deflected by interstellar plasma and magnetic fields of the star burst region when the momentum of the jet is decelerated and thereby strongly interacting with the interstellar plasma and generated plasma turbulence, to form the jet lobes (b).

2.4.3. Neutrino emissions

The cosmic ray protons, accelerated by the wakefield, may lose their energy through the p-p interaction in the interstellar medium in the galaxy, the resultant pions produce neutrinos and gamma-ray photons through their decays. The mean free path, $D_{\rm pp}$ for this process is calculated as:

$$D_{\rm pp} = \frac{1}{n_0 \sigma_{\rm pp}} = 1.2 \times 10^4 \ [\rm pc] \left(\frac{\sigma_{\rm pp}}{2.7 \times 10^{-26}\ \rm cm^2}\right)^{-1} \left(\frac{n_0}{10^3\ \rm cm^{-3}}\right)^{-1}, \tag{63}$$

where we use $\sigma_{\rm pp}$ is the cross section of the p-p interaction and n_0 is the proton density of interstellar space in the galaxy.

The resultant pions produce neutrinos through their decays. The number spectrum n_ν of the neutrinos is calculated as:

$$n_\nu(W_\nu) = n_{CR}(W) \frac{dW_{\rm p}}{dW_\nu} = \frac{f_{\rm pp} \sigma \sigma_\nu L_{\rm w}}{\ln(W_{\rm max}/W_{\rm min})} {W_\nu}^{-2} \tag{64}$$

where $\sigma_\nu = \frac{W_\nu}{W_{\rm P}} \sim 0.05$ and $f_{\rm pp} = \frac{D}{D_{\rm pp}}$ is the probability of the p-p interaction. Here, W_ν, and W_p are the energies of the neutrino and the proton, respectively. The neutrino luminosity can be calculated as:

$$L_{\nu,\mathrm{th}} = \int_{W_{\min,\nu}}^{W_{\max,\nu}} n_\nu W_\nu dW_\nu = f_{\mathrm{pp}}\sigma\sigma_\nu L_{\mathrm{w}} = \frac{f_{\mathrm{pp}}\sigma\sigma_\nu}{6\epsilon\alpha\beta^{3/2}} L_{\mathrm{rad}}. \tag{65}$$

For the objects with prominent jets, such as AGNs or microquasars, neutrinos are likely beamed toward the direction of the jets. The isotropic luminosities are overestimated for on-axis sources (blazars) but underestimated off-axis sources (other AGNs and microquasars: Figure 17 (a)). On the other hand, the objects without prominent jets such as Seyfert galaxies[54] and intermediate mass black holes in the starburst galaxies,[55,56] the direction of the protons are significantly randomized (Figure 17 (b)). In such a case, neutrino emissions can be also isotropic rather than beamed.

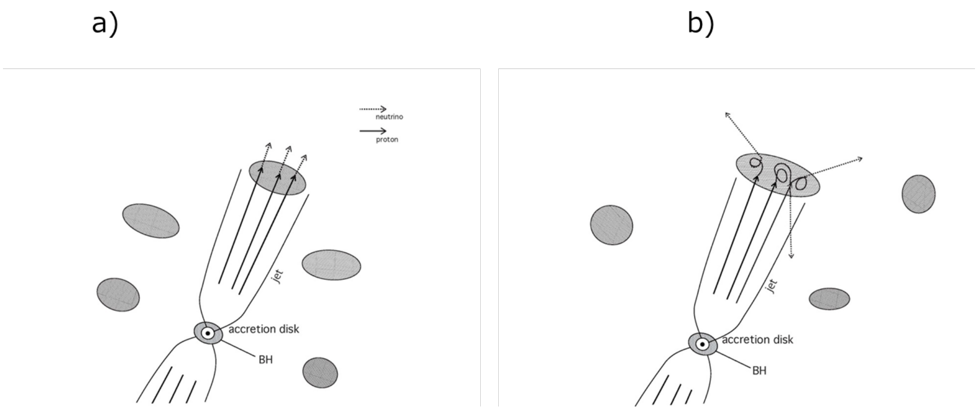

Figure 17. The neutrinos ($\sim 10^{15}$ eV) are produced from the high energy protons ($10^{16} - 10^{17}$ eV) through p-p interaction (a). They are beamed if the original protons are beamed but could be isotropized, since protons with the energy of 10^{17} eV could be defused in the interstellar plasma and magnetic fields of the star burst region (b). Such transition of the jets with its collimated narrow waist into slowdown jets with strongly interacting jets with the interstellar medium corresponds to the typical picture shown in Figure 6.

2.5. Summary

The scaling law for the times scales, maximum energy and luminosities are shown in Table 1. We can summarize the results of the bow wake acceleration theory in the jets emanating from an accreting blackhole as follows:

The bow wakefield accelerates protons and nuclei well above the 10^{20} eV with the wide range of parameters to produce UHECRs (and Table 1).

1) The electrons are also accelerated by the bow wakefield exactly the same way as protons. They emit gamma-ray photons through the interaction with electromagnetic perturbations (Table 1).
2) The accretion of charged particles and emission of gamma-rays show prominent variabilities with the various time scales shown in Table 1 due to the accretion instabilities.
3) The bow wake acceleration theory can provide the luminosity estimates in UHECRs, gamma-rays, and neutrinos. The comparisons of them with the observed isotropic luminosities are not straightforward, if the emissions are strongly beamed.

3. High-Energy Astronomy of blackholes with Multi-Messengers

Blackholes are first recognized as observable objects, when Greenstein and Schmidt in 1964 reported the emission lines of radio stars 3C273 and 3C48 suffer from significant red-shifts, which show that they locate rather far in cosmological distances and therefore much brighter than normal stars, though they look compact, like stars.[57] They named them quasi-stellar objects, or "quasars", in short. The following observations showed that they are active galactic nuclei. Their high luminosities suggested that their central engines are blackholes swallowing (accreting) surrounding gas. The gravitational energy released by mass accretion onto a blackhole is assumed to be converted into the relativistic bulk motion of the jets, though the details were unknown. The jets are found to emit non-thermal emission in almost all frequencies of photons, i.e., radio, infrared, optical, UV, X-ray, and gamma-rays. They also exhibit violent variations in time scales in hours to years. The direct imaging of the supermassive blackhole in the center of M87 was done by the Event Horizon Telescope (Figure 7).[17,58,59]

The discovery of X-ray stars by Giacconi et al. in 1962[60] opened a new window to study stellar-mass blackholes. In fact, a significant fraction of galactic X-ray sources are considered to be blackholes with $\sim 10 M_{\odot}$ in close binaries, where mass is accreting from optical components (normal stars) to the blackholes. They appeared to have jets with non-thermal emissions in addition to the thermal X-ray emission from the accretion disk surrounding the blackhole. They also exhibit time variations in milli-seconds to years.[61] Since these features suggest they are million times smaller version of the quasars, astronomers are calling them now as microquasars.[62]

Now, we have a full set of accreting blackholes from stellar mass ($\sim 10 M_{\odot}$: galactic microquasars), intermediate (100-1000$M_{\odot}$: ultra-luminous X-ray sources in the starburst galaxies), and supermassive ($10^6 - 10^{10} M_{\odot}$: active galactic nuclei). They share the common features, 1) relativistic jets, 2) non-thermal emissions of the full range of photon spectra from radio to high energy gamma-rays ($> 10^{12}$ eV), and 3) violent time variabilities. Although their natures were so far explained by phenomenological models in the framework of the Fermi acceleration mechanism,[48] they are a kind of patch works with many parameters. A compact theory of the accreting blackhole/jet systems was long waited for to unify three common features (relativistic jets, non-thermal emissions, and violent time variabilities) of accreting blackhole systems. The acceleration mechanism seems to be the key.

The accreting blackhole objects has been important targets of multi-messenger astronomy, including cosmic rays (charged particles), high energy gammas, neutrinos, and gravitational waves, as also mentioned above. First, there is growing evidence that the nearby starburst and Seyfert galaxies are the sources of ultra-high energy cosmic rays (UHECRs). For the first place, the Telescope Array (TA) team suggested that there is a hotspot in the northern sky where the directions of arrival of the UHECRs above 57 EeV.[51] He et al. in 2016[63] pointed that starburst galaxy, M82, may contribute to the hot spot. In addition, Pierre Auger Observatory (PAO) team reported that a hotspot in the southern sky above 57 EeV, although it is less statistically significant compared with that in the northern sky.[64] PAO team recently re-analyze the data in a bit lower energy and found additional enhancements of 4σ above 39 EeV toward two starburst galaxies (NGC253 and NGC4945) in the southern sky, too.[65]

These starburst (and Seyfert) galaxies with only less massive blackholes, $10^3 - 10^6\ M_\odot$ but not supermassive ($> 10^7\ M_\odot$), however, have a difficulty to accelerate up $\sim 10^{20}$ eV in the framework of Fermi acceleration. For example, Anchordoqui and Soriano[66] found that acceleration is limited to at most 10^{19} eV for proton even in M82 even if they took into account of extensive shock and strong magnetic field in the nuclear region of starburst galaxies. It is not enough for northern hot spot, in which proton dominant composition was obtained by TA team.[67]

Second, the high energy phenomena associated with accreting blackholes has been observed with gamma-ray emission. First, the Fermi Gamma-ray Space Telescope, formerly GLAST (Gamma-ray Large Area Space Telescope) launched in 2008[68] observed accreting blackholes such as active galactic nuclei (AGN) and binary blackholes in the GeV-100 GeV region.[69-71] In addition, air Cherenkov telescopes, such as MAGIC,[72] H.E.S.S.,[73] or VERITAS[74] and water Cherenkov detector such as High Altitude Water Cherenkov (HAWC) observatory[75] observed accreting blackholes in TeV and multi TeV gamma rays.

In this section, we investigate various blackhole objects with the multi-messenger approach, backboned by the wakefield acceleration (WFA) theory. We selected ten astronomical objects, i.e., one blazars (BL: TXS0506+056), three radio galaxies (RG: Cen A, M87, and For A), three Seyfert galaxies (SyG: NGC1068, NGC4995, NGC6814), two starburst galaxies (SB: M82 and NGC0253), and one microquasars (MQ: SS433). The loci of these ten objects are shown in $m - L_{\rm rad}$ diagram (Figure 18) and in skymap (Figure 19). The theoretical predictions of the WFA theory are compared with the observations at source by source in the rest of the section 3.Although gamma-ray, proton, and neutrino emissions are likely to be beamed, as discussed in section 2, we will discuss energetics of the objects in terms of the isotropic luminosities because of the uncertainty of the degree of the beaming of the emissions. Not that this assumption makes the observational luminosities overestimated in Blazers and underestimated in other sources, as we will discuss for the individual objects.

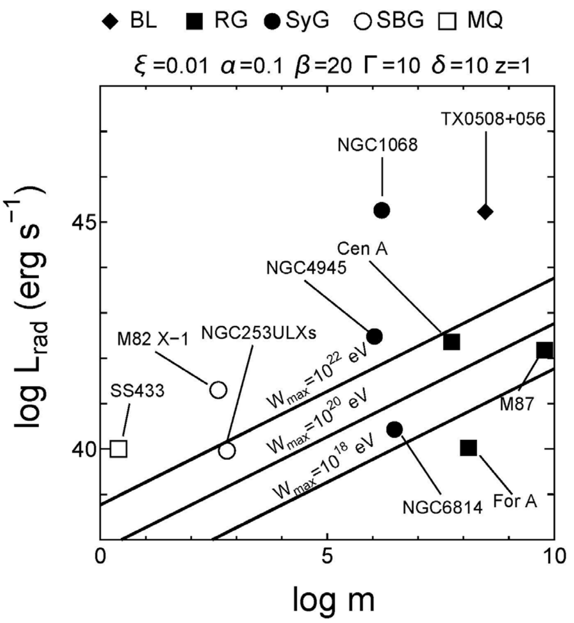

Figure 18. Ten blackhole objects: one blazars (BL: TXS0506+056), three radio galaxies (RG: Cen A, M87, and For A), three Seyfert galaxies (NGC1068, NGC4995, NGC6814), two starburst galaxies (SB: M82 and NGC0253), and one microquasars (MQ: SS433) are plotted in mass (m)-radiation luminosity (L_{rad}) diagram. The solid line represents the locus of $W_{max} = 10^{20}$ eV. Seven objects are well above the solid line, so that they can accelerate UHECRs. Dashed lines denote $\dot{m} = 10^{-5}$, 10^{-3}, and 10^{-1}, respectively.

Table 1. Comparison of the theoretical prediction by the WFA theory with the

observations.

Parameter	TX0506 +056	Cen A	M87	For A	NGC1068	NGC4945	NGC6814	M82	NGC0253	SS433
Type*	BL	RG	RG	RG	SyG	SyG	SyG	SBG	SBG	MQ
$\log d_{\rm obs}$ (pc)	9.26	6.53	7.23	7.28	7.15	6.56	7.36	6.56	6.59	3.54
$\log M_{\rm BH,obs}$ ($M_\odot$)	8.48	7.74	9.79	8.11	7.20	6.04	6.48	2.60	2.78	0.40
$\log L_{\rm rad,obs}$ (erg s^{-1})	45.23	42.36	42.18	40.23	45.26	42.48	40.43	41.30	40.00	40.00
$\log L_{\rm w}$ (erg s^{-1})	45.17	42.30	42.12	40.17	45.20	42.42	40.37	41.24	39.90	39.94
$\log W_{\rm max,th}$ (eV)	26.66	21.66	19.25	17.02	28.00	23.60	19.06	24.68	21.90	24.28
$\theta_{\rm th}$ (degree)	-	14	85	92	70	18	115	18	18	-
$\log L_{\rm UHECR,th}$ (erg s^{-1})	-	39.83	-	-	-	39.95	-	38.77	37.47	37.47
$\log L_{\rm UHECR,obs}$ (erg s^{-1})	-	37.80	-	-	-	37.86	-	38.26	37.83	-
$\log \tau_{\rm rise,th}$ (s)	2.48	-0.395	-0.575	-2.53	2.51	-0.275	-2.325	-1.46	-2.76	-2.76
$\log \tau_{\rm rise,obs}$ (s)	<4.68	-	<5.90	-	-	-	<2.30	-	-	-
$\log \tau_{\rm rec,th}$ (s)	4.84	4.10	6.15	4.47	3.56	2.40	2.84	-1.04	-0.86	-3.24
$\log \tau_{\rm rec,obs}$ (s)	<6.38	4.18	<7.47	-	-	-	-	-0.70	<2.0	<1.0
$\log L_{\gamma,\rm th}$ (erg s^{-1})	44.17	41.30	41.12	39.17	44.20	41.42	39.37	40.24	38.94	38.94
$\log L_{\gamma,\rm obs,GeV}$ (erg s^{-1})	47.08	40.15	41.81	40.57	41.31	40.08	40.84	39.55	39.78	35.01
$\log L_{\gamma,\rm obs,TeV}$ (erg s^{-1})	45.65	38.04	40.48	-	<45.53		-	39.30	39.45	30.03
$\log L_{\nu,\rm th}$ (erg s^{-1})	42.87	40.00	39.82	37.87	42.90	40.12	38.07	38.94	37.64	37.64
$\log L_{\nu,\rm obs}$ (erg s^{-1})	46.18	-	-	-	40.25	-	-	-	-	-

*BL: Blazar, RG: Radio Galaxy, SyG: Seyfert Galaxy, SBG: Starburst Galaxy, MQ: Microquasar

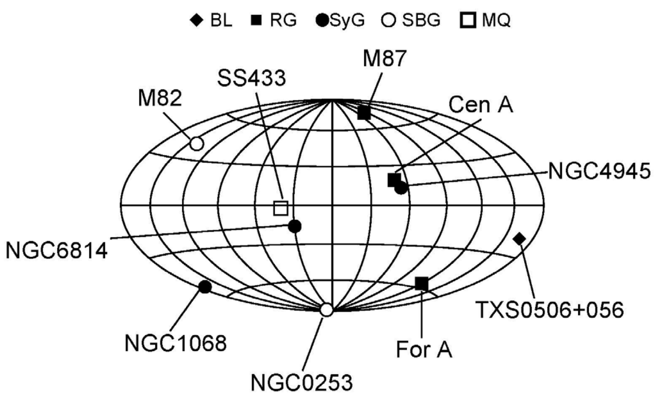

Figure 19. The skymap of the ten blackhole object examples that we consider in the present paper. BL: blazar; RG: Radio Galaxy SyG: Seyfert Galaxy; SBG: Starbusrt Galaxy; MQ: Microquasar.

3.1. Blazars

3.1.1. TXS 0506+056

TXS 0506+056 in constellation Orion is a blazar, a quasar with a relativistic jet pointing directly towards Earth, with a redshift of 0.3365 ± 0.0010,[76] which corresponds to about 1.8 Gpc from the Earth. TXS 0506+056 was first cataloged as a radio source in 1983,[77] and then confirmed as a blazar.[78] Gamma rays were detected by the EGRET and Fermi-LAT missions.[79-81] In addition, radio observations have shown apparent superluminal motion in the jet.[82]

Furthermore, on 22 September 2017, the cubic-kilometer IceCube Neutrino Observatory detected a high-energy neutrino emission from a direction consistent with this flaring gamma-ray blazar TXS 0506+056.[83] The most probable energy for the observed neutrino is around 190 TeV with a 90% confidence level (CL) lower limit of 183 TeV, depending only weakly on the assumed astrophysical energy spectrum. Such observation may imply the existence of extremely high energy protons or nuclei with tens of PeV generated in the jet of the Blazar. The clear emission direction with high energy particles may suggest a different acceleration mechanism for the ultrahigh energy cosmic rays other than the Fermi's stochastic acceleration.[48]

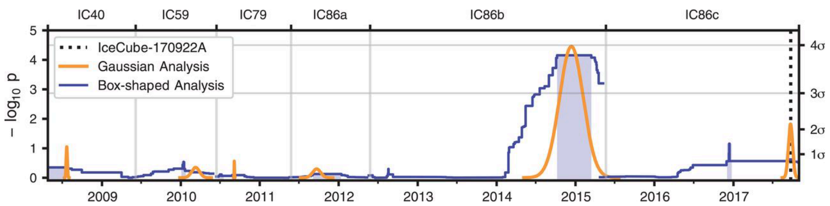

Figure 20. The gamma ray blazar TXS 0506+056 shows quasi-periodic burst pattern in gamma-rays with the energy between 0.1 GeV and 100 GeV.[84] This quasi-periodic burst pattern may be explained by the MRI instability of the accretion disk.[37] After IceCube Collaboration 2018.[84]

During ± 2 weeks of the neutrino observation, a peak flux of gamma ray emission around $5.3 \times 10^{-7}\ \mathrm{cm}^{-2}\ \mathrm{s}^{-1}$ is also reported by Fermi-LAT, with an energy range between $0.1 \sim 10$ GeV.[81] The associated isotropic luminosity during the period reaches as high as $1.2 \times 10^{47}\mathrm{erg\ s}^{-1}$.[84] Analyzing the data prior to the event, a long-term isotropic gamma ray luminosity between 0.1 GeV and 100 GeV is derived with an averaged value of $0.28 \times 10^{47}\mathrm{erg\ s}^{-1}$over 9.5 years of Fermi-LAT observations of TXS 0506+056.[84] According to their study, the Gaussian-shaped time profile of the neutrino emission shows a quasi-periodic burst pattern as shown in Figure 20, which is similar to MRI instability relaxation depicted by Canac et al.[37]

According to the WFA theory, the relativistic ponderomotive acceleration in the jet can boost particles to an energy over ZeV.[28-30,32] Also, because the particles are accelerated linearly, the corresponding signal detected can be highly localized around the location of the blazar. In the rest of the subsection, we will estimate physical parameters using the wakefield theory and compare them with their observational values.

Mass estimation is difficult in general for blazars. Padovani et al.[85], however, estimated the central black hole mass to be $3 \times 10^8\ M_{\odot}$ using the relations of black holes mass and R-band bulge magnitude $M(R) \sim -2.9$,[86] assuming the host galaxy to be a giant elliptical. We adopt 1.7×10^{45} erg s^{-1} as the bolometric luminosity ($\simeq L_{\rm rad}$), taking into account of the overestimation due to jet-induced component using the bolometric luminosity derived from the the OII and OIII lines ($L_{\rm OII} = 9 \times 10^{45}$ erg s^{-1} and $L_{\rm OIII} = 3 \times 10^{45}$ erg s^{-1}. Substituting $m = 3 \times 10^{8}$ and $L_{\rm rad} = 1.7 \times 10^{45}$ erg s^{-1} into equations 29, 30, 51, and 54, we derived $\tau_{\rm rise,th} = 3.0 \times 10^{2}$, $\tau_{\rm rec,th} = 6.9 \times 10^{4}$ s, $L_{\gamma,\rm th} = 1.5 \times 10^{44}$ erg s^{-1}, and $W_{\max} = 4.6 \times 10^{26}$ eV, as shown in Figure 15 and Table 1.

Although the maximum proton energy, $W_{\max}$ for protons is well above 10^{20} eV, UHECR protons propagate only 100 Mpc and cannot reach to the Earth because of the GZK mechanism,[87,88] in which protons undergo inelastic collisions with photons in the cosmic microwave background to their loose energy.

According to the MAGIC observation,[89] very high energy (VHE) gamma rays, above 90 GeV, from TXS 0506+056 varied, increasing by a factor of 6 within a day to 8.7×10^{-11} erg cm^{-2} s^{-1}, which corresponding to the isotropic luminosity of $L_{\gamma,\rm obs,TeV} = 4.6 \times 10^{45}$ erg s^{-1}. We may set $\tau_{\rm rise,obs} = 4.8 \times 10^{4}$ s or shorter as an e-raising time. There are two periods (2017 October 3-4, and 2017 October 31) of enhanced gamma-ray emission. We may set $\tau_{\rm rec,obs}$ as 2.4×10^{6}s or shorter, taking into account the incomplete observation in TeV gamma rays. Both $\tau_{\rm rise,obs}$ and $\tau_{\rm rec,obs}$ are consistent with the theoretical prediction as shown in Table 1.

The theoretical gamma-ray luminosity is calculated as $L_{\gamma,\rm th} = 1.5 \times 10^{44}$ erg s^{-1} (see equation 51), which is much less than the observed isotropic gamma-ray luminosity $L_{\gamma,\rm obs,GeV} = 1.2 \times 10^{47}$erg s^{-1} observed by FERMI-LAT.[84] This is probably due to the concentration of the radiation being axially aligned with the jets. Since jets are close parallel to the line of site in the case of blazars and the actual emission is strongly beamed to the direction of the jets, such isotropic assumption will overestimate the luminosity by integrating the whole sphere by a large factor. If we assume a diameter of 3° for the beam, the corrected estimation of the Fermi-LAT luminosity will be 2 orders magnitudes lower than their reported value. That is, $L_{\gamma,\rm obs}(3°) = \sim 3 \times 10^{44}$erg s^{-1}, which is consistent with the theoretical luminosity.

Substituting $f_{\rm pp} = 1.0$, $L_{\rm rad} = 1.7 \times 10^{45}$ erg s^{-1}, $d = 1.8$ Gpc, $\sigma = 0.1$, $\alpha = 0.1$, $\epsilon = 0.06$, $\sigma_{\nu} = 0.05$ into equation 65, we obtain $L_{\nu,\rm th} = 6.7 \times 10^{42}$ erg s^{-1}. On the other hand, the observation by IceCube suggested isotropic neutrino luminosity of $L_{\nu,\rm obs} = 1.5 \times 10^{46}$ erg s^{-1} at 100 TeV,[84] which is much higher than theoretical expectation, probably due to the beaming, described above.

3.2. Nearby radio galaxies in the Local Super-cluster

Radio galaxies in the local supercluster, such as M87, For A, and Cen A can be considered possible source of UHECRs.

3.2.1. Cen A

Centaurus A (also known as NGC 5128) in constellation Centaurus, is a radio galaxy with kilo-parsec size jets, and at a distance of 3.4 Mpc from the Earth.[90-92] The mass of the central blackhole is well defined by stellar dynamics[93] as $M_{\mathrm{BH}} = 5.5 \times 10^7\ M_{\odot}$. X-ray observations determined $L_{\mathrm{rad}} = 2.3 \times 10^{42}$ erg s^{-1}.[94] As the distance of Cen A is estimated as 3.4 Mpc,[95-97] Cen A, as well as NGC4945 can contribute to the excess flux. In fact, the Pierre Auger Observatory reported that there may be excessive fluxes towards the Centaurus region (Figure 21).[64,65]

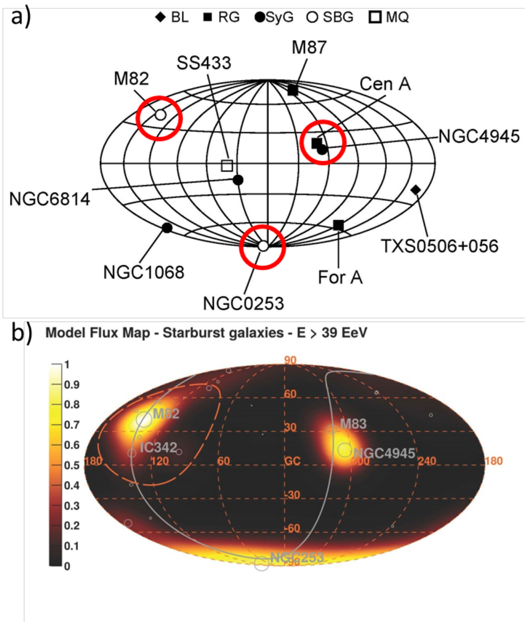

Figure 21. Wakefield acceleration theory suggests three hot spots in the arrival direction of UHECRs. They are consisted of the contributions from four galaxies: M82, NGC0253, Cen A, and NGC4945 (a). The UHECRs from Cen A and NGC4945 cannot be distinguished. The arrival direction analysis of UHECRs above 39 EeV suggested three hot spots (b). After Aab et al. 2018.[65]

Substituting $m = 5.5 \times 10^7$ and $L_{\mathrm{rad}} = 2.3 \times 10^{42}$ erg s^{-1} into equations 29, 30, 51, 55, and 59, we derived $\tau_{\mathrm{rise,th}} = 4.0 \times 10^{-1}$, $\tau_{\mathrm{rec,th}} = 1.3 \times 10^4$ s, and $L_{\gamma,\mathrm{th}} = 2.0 \times 10^{41}$ erg s^{-1}, $W_{\mathrm{max}} = 4.6 \times 10^{21}$ eV, and $L_{\mathrm{UHECR,th}} = 6.7 \times 10^{39}$ erg s^{-1},

The WFA theory predicts that Cen A is capable of accelerating protons to energies above 10^{20} eV (see Table 1). The deflection angle of UHECRs due to intergalactic magnetic field is estimated as small as 14 degrees, using equation 62 and shown in Table 1. The UHECR luminosity is predicted to 6.7×10^{39} erg s^{-1}. On the other hand, Aab et al.[63] suggested UHECR flux of 0.016 event/(100 km^2)/yr, which corresponds to the isotropic luminosity of 6.4×10^{37} erg s^{-1}(see Table 1). The difference between the theoretical prediction and the observation may be explained by the beaming toward jets: in the radio galaxies, jets are not parallel to the line of sight unlike blasars, so that the isotropic assumption leads an underestimate by a large factor.

The episodic recurrence time, $\tau_{\mathrm{rec,th}}$,predicted by WFA theory is consistent with the observation of Fukazawa et al.[98] and Rothschild,[99] who showed 50% time variability in the time scale of 10-20 ks.

The theoretical gamma-ray luminosity for Cen A is calculated as $L_\gamma = 2.0 \times 10^{41}$erg s^{-1}. On the other hand, Cen A has been known to emit gamma rays in the range of GeV and TeV energy, First, Fermi LAT detect gamma-ray flux of 3.0×10^{-9} erg cm^{-2} s^{-1} and photon index of 2.763, which corresponds to the GeV luminosity of 1.7×10^{40} erg s^{-1}.[66] Second, the H.E.S.S. telescope determined the gamma-ray flux of $0.45 \pm 0.07\ 10^{-13}$ ph cm^{-2} s^{-1} TeV^{-1} at 1 TeV. The corresponding gamma-ray luminosity calculated as 1.1×10^{38} erg s^{-1}.[100] The difference between the theoretical and observational values of L_γ is most likely due to the fact that the axis of the jets is at a large angle to our line of sight, and gamma-ray emissions are strongly beamed in the axially direction of the jets.

3.2.2. M87

M87 is an elliptical galaxy in the constellation Virgo with the distance of 17 Mpc.[101] It the nearest radio galaxy with the central blackhole of 6.2×10^{9} [102] has the core luminosity of 7×10^{40} erg s^{-1} in normal phase[103] and 1.5×10^{42} erg s^{-1} in flaring phase.[102] Substituting $m = 6.2 \times 10^{9}$ and $L_{\mathrm{rad}} = 1.5 \times 10^{42}$ erg s^{-1} into equations 29, 30, 51, and 55, we derived $\tau_{\mathrm{rise,th}} = 0.27$, $\tau_{\mathrm{rec,th}} = 1.4 \times 10^{6}$ s , $L_{\gamma,\mathrm{th}} = 1.3 \times 10^{41}$ erg s^{-1}, and $W_{\max} = 1.7 \times 10^{19}$ eV as shown in Table 1.

The Event Horizon telescope[17,58,59] first observed the ring structure of the radius of 21 μas, corresponds to the linear diameter of 5.3×10^{15} cm at the distance of 16.9 Mpc by the VLBI observation at 230 GHz. Since the size of the ring is just consistent with the radius of the innermost circular stable orbit (5.5×10^{15} cm) of the accretion disk of a non-rotating blackhole with the mass of $6.2 \times 10^{9}\ M_\odot$, this structure corresponds to the inner edge of the accretion disk.[17,58,59] obtained the average electron density of $n_{\mathrm{e}} \sim 10^{4-7}$ cm^{-3} , magnetic field strength of 1-30 G, and electron temperature of $(1-12)\times 10^{10}$ K. These values are consistent with the radiatively-inefficient and geometrically-thick accretion flow inside the ISCO of the radiatively-efficient and geometrically-thin accretion disk, which we described in section 2.

It is difficult of M87 to accelerate UHECRs, since $W_{\rm max}$ is less than 1.9×10^{19} eV even in the flaring phase (Table 1). Furthermore, a branch of the local-supercluster filaments different from that toward M82 extends towards M87 from the Milky Way Galaxy (Figure 22). Therefore, the path of UHECR from M87 to our galaxy is also considered to be within the filament structure. In fact, galaxies in this direction, and our galaxy, is "falling" towards M87.[105] The distance to M87 is as large as 17 Mpc,[101] which is about four times larger than that of M82, the deflection due to the magnetic field would exceed 80 degrees and the spot would spread at least several tens of degrees (Table 1). Thus, any excess flux from M 87, even if it exists, is difficult to detect with current ground-based detectors.

According to Ackermann et al.,[70] the GeV gamma-ray flux of 1.7×10^{-9} $\rm cm^{-2}$ $\rm s^{-1}$ and photon index of 2.17, which corresponds to the isotropic GeV gamma-ray luminosity of 6.5×10^{41} erg $\rm s^{-1}$. On the other hand, the WFA theory predicts the gamma-ray luminosity of 1.3×10^{41} erg $\rm s^{-1}$, which is consistent within a factor of two (Table 1). According to Aharonian et al.,[106] M87 nucleus emit TeV gamma-ray radiation of 3×10^{40} erg $\rm s^{-1}$ and showed the variability of one day ($\sim 8\times 10^5$ s) as well as one year ($\sim 3\times 10^7$s). We may set the upper limit of the times scales as $\tau_{\rm rise,obs} < 8\times 10^5$ s, $\tau_{\rm rec,obs} < 3\times 10^7$s, taking into account of the incompleteness of the observations.

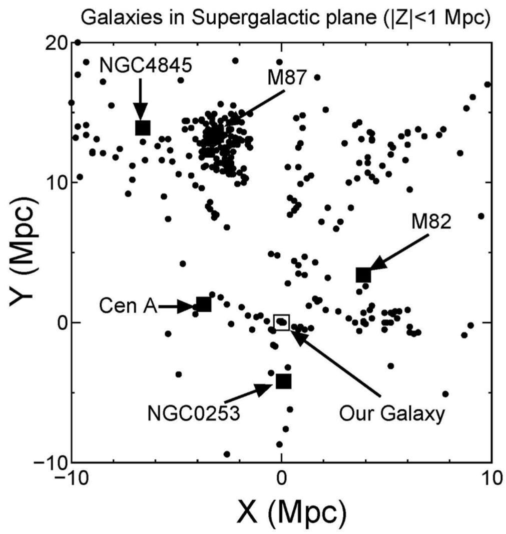

Figure 22. Galaxies in the supergalactic plane. The filament structure of the local supergalaxy can be seen.

3.2.3. For A (NGC1316)

Fornax A (NGC1316) is a radio galaxy locates in the constellation Fornax with the distance of 19 Mpc[107-109] and harbors the central blackhole of $1.3 \times 10^8\ M_\odot$[110] with the luminosity of 1.7×10^{40} erg s^{-1}.[111] The maximum acceleration energy W_{max} is as low as 1.7×10^{17}eV.

Substituting $m = 1.3 \times 10^8$ and $L_{\mathrm{rad}} = 1.7 \times 10^{40}$ erg s^{-1} into equations 29, 30, 51, and 55, we derived $\tau_{\mathrm{rise,th}} = 3.0 \times 10^{-3}$, $\tau_{\mathrm{rec,th}} = 3.0 \times 10^4$ s, and $L_{\gamma,\mathrm{th}} = 91.5 \times 10^{38}$ erg s^{-1}, and $W_{\mathrm{max}} = 1.1 \times 10^{17}$ eV, as shown in Table 1. It does not have an ability to produce UHECRs.

On the other hand, Ackerman et al.[112] detected the extended emission of 5.38×10^{-12} erg cm^{-2} s^{-1} and photon index of 2.08, which corresponds to the isotropic luminosity of 3.7×10^{40} erg s^{-1}. The WFA theory predicts the gamma-ray luminosity of 9.1×10^{38} erg s^{-1}, which is roughly consistent with the observation within factor of five.

3.3. Nearby Seyfert galaxies

Seyfert galaxies harbor profound nuclear activities with non-thermal emissions. They are believed to be due to the jets emanated from the accretion disk around a with supermassive blackhole with a mass of $10^{6-7} M_\odot$ (Table 1).[54] The nuclear regions are covered by Compton thick clouds, ionized by the interaction with the jets and excessive star formation activities, including numerous numbers of supernovae; Many Seyfert galaxies still exhibits the surplus starburst activities and are often difficult to distinguish from starburst galaxies.

3.3.1. NGC1068

NGC1068 is a Seyfert galaxy which has a bright nucleus with the central blackhole of $1.6 \times 10^7\ M_\odot$.[111] It locates at the distance of 14 Mpc[114] in the constellation Cetus. The bolometric luminosity of the nucleus of 1.8×10^{45} erg s^{-1} was obtained from OIV line.[106] It is surrounded by a Compton thick cloud with $N_{\mathrm{H}} > 10^{25}$ cm^{-2}.[115,116] It can accelerate UHECR but the deflection by intergalactic magnetic field is too large (70 degree) to form a hotspot.

Substituting $m = 1.6 \times 10^6$ and $L_{\mathrm{rad}} = 1.8 \times 10^{45}$ erg s^{-1} into equations 29, 30, 51, and 55 we derived $\tau_{\mathrm{rise,th}} = 3.2 \times 10^2$, $\tau_{\mathrm{rec,th}} = 3.6 \times 10^3$ s, $L_{\gamma,\mathrm{th}} = 1.6 \times 10^{44}$ erg s^{-1}, and $W_{\mathrm{max}} = 1.0 \times 10^{28}$ eV, as shown in Table 1. The nucleus of NGC 1068 cannot accelerate UHECRs.

There is no significant luminosity change in the intrinsic luminosity from the accretion disk of the nucleus of NGC 1068. Although Zaino et al.[117] reported the time variability in the time scale of 1-6 months, the detailed spectral analysis revealed that the variability is not due to the change in the intrinsic accretion rate but due to the change in obscuring Compton thick cloud ($N_H > 10^{25}$ cm^{-2}),[114] which surrounds the nucleus. This view is consistent with the infrared and optical observations.[118,119]

Ackermann et al.[71] observed isotropic gamma-ray luminosity of 1.5×10^{41} erg s^{-1}. GeV gamma rays are generally believed to be from supernova remnants in the galaxy as the result of intense starburst activity.

On the other hand, Acciari et al.[120] set an upper limit of NGC 1068 in gamma-ray above 200 GeV at 5.1×10^{-13} erg cm^{-2} s^{-1}. It corresponds to the isotropic luminosity of 3.5×10^{45}erg s^{-1}, which is one order of magnitude large compared with the theoretical prediction. On the other hand, the WFA theory predicts the gamma-ray luminosity of 1.6×10^{44} erg s^{-1}

The IceCube collaboration[121] reported the positive detection of neutrinos at 1 TeV of 3×10^{-13} TeV^{-1} cm^{-2} s^{-1} from NGC 1068 (Figure 23). It corresponds to the isotropic luminosity of $L_{\nu,\mathrm{obs}} = 1.8 \times 10^{40}$ erg s^{-1}. Substituting $L_{\mathrm{rad}} = 1.8 \times 10^{45}$ erg s^{-1}, $f_{\mathrm{pp}} = 1.0$, $\sigma = 0.1$, $\sigma_\nu = 0.05$, α=0.1, and $\beta = 20$ into equation 65, we obtain the isotropic theoretical neutrino luminosity of $L_{\nu,\mathrm{th}} = 8.0 \times 10^{42}$ erg s^{-1}.

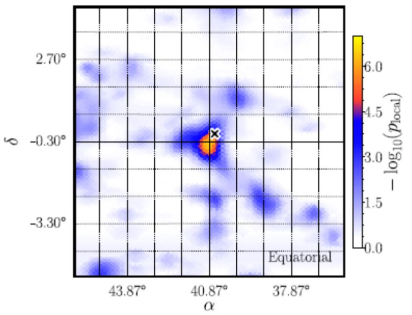

Figure 23. Seyfert galaxy example in the skymap. Local pre-trial p-value map around the Seyfert galaxy NGC1068. The most significant point in the Northern hemisphere coincides with NGC1068 (black cross). After IceCube Collaboration (2020).[121]

3.3.2. NGC4945

NGC4945 is a Seyfert galaxy with an enhanced star forming activity. It is located at the distance of 3.6 Mpc[96] from the Earth. It harbors the central supermassive blackhole with the mass of $1.1 \times 10^6\ M_\odot$.[113] The X-ray emission from the core is heavily obscured by Compton thick cloud with $N_H > 10^{24}$cm^{-2}, like other type 2 Seyfert galaxies [115,122] and the unabsorbed luminosity is estimated as 3×10^{42} erg s^{-1}.[122]

Substituting $m = 1.1 \times 10^6$ and $L_{\rm rad} = 3 \times 10^{42}$ erg s^{-1} into equations 29, 30, 51, 55, and 59, we derived $\tau_{\rm rise,th} = 5.3 \times 10^{-1}$, $\tau_{\rm rec,th} = 2.5 \times 10^2$ s , $L_{\gamma,\rm th} = 1.3 \times 10^{41}$ erg s^{-1}, $W_{\rm max} = 4.0 \times 10^{23}$ eV, and $L_{\rm UHECR,th} = 8.9 \times 10^{39}$ erg s^{-1}, as shown in Table 1.

On the other hand, Aab et al.[65] suggested UHECR flux of 0.016 event/(100 km^2)/yr, which corresponds to luminosity of 7.2×10^{37} erg s^{-1} assuming isotropic emission (Table 1). The difference between theoretical prediction and the observed isotropic luminosity can be explained by the beaming of UHECRs. Note that the arrival direction analysis of UHECRs cannot distinguish the contribution of NGC4945 from that of Cen A (Table 1 and Figure 21).

According to Ackerman et al.[71] the GeV gamma-ray isotropic luminosity of 1.2×10^{40} erg s^{-1}. On the other hand, the WFA theory predicts the gamma-ray luminosity of 2.6×10^{42} erg s^{-1}

3.3.3. NGC6814

Seyfert galaxy NGC6814 locates at the distance of 23 Mpc[114] and harbor the central blackhole of $\sim 3 \times 10^6\ M_\odot$.[114,123] The luminosity of the nucleus source is as high as 2.7×10^{40} erg s^{-1}.[124] Substituting $m = 3.0 \times 10^6$ and $L_{\rm rad} = 2.7 \times 10^{40}$ erg s^{-1} into equations 29, 30, 51, and 55, we derived $\tau_{\rm rise,th} = 4.7 \times 10^{-3}$, $\tau_{\rm rec,th} = 6.9 \times 10^2$ s, $L_{\gamma,\rm th} = 2.4 \times 10^{39}$ erg s^{-1}, $W_{\rm max} = 1.1 \times 10^{39}$ eV. As shown in Table 1, it cannot accelerate UHECRs. According to Ackermann et al.,[70] the GeV gamma-ray flux of 6.8×10^{-10} cm^{-2} s^{-1} and photon index of 2.54, which corresponds to the GeV gamma-ray isotropic luminosity of 6.9×10^{40} erg s^{-1}. Tennant et al.[125] observed the three fold variability within 200 seconds. On the other hand, the WFA theory predicts the gamma-ray luminosity of 2.4×10^{39} erg s^{-1}.

3.4. Intermediate mass blackholes in starburst galaxies

Starburst galaxy has an enhanced star forming activity, which often caused by strong disturbances due to the interaction with other galaxies. The starburst region sometimes covers the entire galaxy ($\sim$10kpc) or is constrained to a part of the galaxy across typically$\sim$1kpc. Thick molecular clouds with the proton density higher than 100 cm^{-2} are pervaded in the starburst region. As a result of this starburst, many young supernova remnants as well as compact young star clusters are embedded in the molecular cloud complex. Ultra-Luminous X-ray Sources (ULXs), which are believed to be intermediate mass blackholes (IMBHs) with mass ranging $10^2 - 10^4$ M$_\odot$. They have been discovered in the starburst galaxies and are likely to be formed in young compact star clusters through runaway merging:[126-128] The blackhholes heavier than 10^2 $M_\odot$ are impossible to be produced by stellar evolution, directly. Ebisuzaki et al.[129] however suggested intermediate mass blackholes with $100 - 1000$ $M_\odot$ can be formed through runaway merging of massive stars at the center of dense stellar cluster[126-128] to be ultra-luminous X-ray (ULX) sources in the starburst galaxies.

In a starburst galaxies, UHECR protons can be randomized significantly, because of the enhanced magnetic field (~ 100 μG) due to high concentration of supernova remnants, since the magnetic field in the starburst region is estimated as high as $100 - 1000$ μG.[52,53] Even UHECRs, which are originally beamed, can be significantly randomized in direction because of the magnetic field in the starburst regions.

3.4.1. M82

M82 is a starburst galaxy of the distance of 3.6 Mpc[130] in the constellation Ursa Major. The starburst activity takes place in a relatively small central region, radius of ~ 200 pc[131] from the dynamic center of the galaxy.

Ultra-luminous X-ray (ULX) sources of luminosity $\geq 10^{40}$ $\mathrm{erg\ s^{-1}}$ inside M82 have been observed (see Xu (2015)[132] and the references therein). Among them, M82 X-1 is the brightest ULX in M82, located about 200 pc away from the dynamic center of the galaxy.[133-138] In general, the maximum luminosity of a star bound by gravity is limited by the Eddington luminosity, defined by:

$$L_{\mathrm{Edd}} = 1.26 \times 10^{38}\ [\mathrm{erg\ s^{-1}}]m. \tag{66}$$

Thus, it can be concluded that M82 X-1 with an X-ray flux of 2×10^{41} erg/s or more [133-135] must have a mass of at least around $10^3 M_\odot$. In addition, the mass of the M82 X-1 estimated from the frequency of the Quasi Periodic Oscillation (QPO) observed in the X-ray luminous intensity as to be 100-1300 $M_\odot$.[139-141] Such a blackhole with mass of $10^2 - 10^5$ $M_\odot$ is called an intermediate mass blackhole,[129] and is considered to be an important key for solving the mystery of formation of the central blackholes by connecting a stellar mass blackhole ($\sim 10^3 M_\odot$) and a supermassive blackhole ($\gg 10^6 M_\odot$) in galactic centers.[131] Here, we adopted the mass of $400 M_\odot$ of Pasham et al., who used QPO frequency to a mass value.[141]

Substituting $m = 4 \times 10^2$ and $L_{\mathrm{rad}} = 2 \times 10^{41}$ $\mathrm{erg\ s^{-1}}$ into equations 29, 30, 51, 55, and 59, we derived $\tau_{\mathrm{rise,th}} = 3.5 \times 10^{-2}$, $\tau_{\mathrm{rec,th}} = 9.1 \times 10^{-2}$ s , $L_{\gamma,\mathrm{th}} = 1.8 \times 10^{40}$ $\mathrm{erg\ s^{-1}}$, $W_{\max} = 4.8 \times 10^{24}$ eV, and $L_{\mathrm{UHECR,th}} = 5.8 \times 10^{38}$ $\mathrm{erg\ s^{-1}}$, as shown in Table 1.

Applying WFA theory to the M82 X-1, it has been shown that acceleration to 10^{20} eV is well feasible (Figure 15, Figure 21, and Table 1) in the accreting blackhole system. On the other hand, the TA team acquired 72 cosmic rays of 57 EeV in 5 years, and observed 19 events (4.5 events of which were expected from uniform arrival) within the hotspot.[51] Since the effective area of TA is 700 km^2, the observed excess flux in the hot spot direction is about 0.4 UHECRs/(100km^2/yr), which correspond to the isotropic luminosity of 1.8×10^{38} erg s^{-1}, which is roughly consistent with the theoretical prediction (Table 1).

If the hot spot in the northern sky comes from M82, the deflecting angle by intergalactic magnetic field is 17.4 degrees.[63] Using equation 62, M 82 ($d = 3.6$ Mpc) is the source of a proton (z=1), each requires a magnetic field of the order of $B = 9.7$ nG. In ordinal intergalactic space, the magnetic field strength is expected as low as 0.1 nG.[142] Therefore, this large deflection angle given by observation could not be explained.

However, Ryu et al.[143] carried out the simulation of the local large-scale structure of the universe and found that the magnetic field of about 10 nG can be expected in the filament structure. Figure 22 shows the distribution of galaxies close to the supergalactic plain (within ± 1 Mpc). The distribution of galaxies represents the network (filament structure) of the local supergalaxy to which our galaxies belong. It can be seen that our Milky Way Galaxy and M82 are in the same filament structure. Therefore, the magnetic field of the UHECR propagating path from M82 to the Milky Way Galaxy can be expected to be about 10 nG, which is higher than that of the ordinary intergalactic space. It is expected that the UHECR propagating through at distances of 3.6 Mpc is deflected by nearly about 18 degrees, as shown in Table 1.

He et al. [61] divided the events belonging to the northern hot spot into two by energy, and found that there was a systematic deviation between them. Assuming that this is due to the deflection by the magnetic field,[144] the position of the true source was estimated. While the estimated position, though extended to 10 degrees, included several high-energy celestial objects such as M82 and Mrk 180, only M82 was located within the GZK-horizon (~100 Mpc) that the UHECRs could reach.

The Telescope Array (TA) team detected 72 cosmic rays of 57 EeV in 5 years. Among them, 19 events are within the hot spot,[51] while 4.5 events were expected from uniform arrival. Since the effective area of TA is $700\ \mathrm{km}^2$, the observed excess flux in the hot spot direction is about 0.016 event/(100 km^2)/yr, which is consistent with the expected isotropic flux from equation $L_{\mathrm{UHECR,obs}} = 1.8 \times 10^{38} \mathrm{erg\ s}^{-1}$ as shown in Table 1. The direction of UHECRs may be randomized, due to the strong magnetic field inside M82.

The QPO period of M82 X-1 is observed in X-ray band to be 0.2 s.[141] The theoretical recurrence time is $\tau_{\text{rec,obs}} = 9.1 \times 10^{-2}$ s (Table 1). This predicted value is well consistent with the QPO period within a factor of 2.

In the WFA theory, electrons are also accelerated in the similar way with protons. The high energy electrons, accelerated by the wakefield in the direction of the jet, emit gamma rays by synchrotron process with the interaction with magnetic perturbations in the jets. This gamma-ray luminosity of M82 X-1 can be also calculated as $1.7 \times 10^{40}\,\text{erg s}^{-1}$ (Table 1). The energy spectrum is likely to be expressed by a single power law from GeV to 100 TeV, with a constant index, which is close to 2 in the strongest acceleration case, depending on the magnitudes of the acceleration field and the magnetic field in the jets.[37] Note that this gamma-ray emission is expected to be strongly concentrated in the direction of the jets.

On the other hand, a bright and isolated gamma-ray excess, consistent with the location of the position of M82 of 100 MeV to 700 GeV gamma-rays that are isotropic in luminosity of 6.9×10^{40} erg s^{-1} with FERMI-LAT.[71] This is consistent with the theoretical prediction, though it might be just by chance, taking into account of the non-isotropic nature of WFA theory.

Gamma-ray emission of $3.7 \times 10^{-13}\,\text{cm}^{-2}\,\text{s}^{-1}$ above 700 GeV were detected from M82.[145] The corresponding isotropic luminosity is about $2 \times 10^{39}\,\text{erg s}^{-1}$. The fitted power-law spectrum suggests that a single physical emission mechanism, such as WFA theory, dominates from GeV to TeV energies for M82, though a popular explanation is those from numerous number of supernova remnants in the nucleus region of starburst galaxy M82.

According to Ackerman et al.,[71] time variabilities have not yet been reported from Fermi-LAT observations. If it is the case in future observations, that will be an evidence that gamma-ray emission comes from a compact object, such as M82 X-1, not from the extended sources, like supernova remnants.

3.4.2. NGC0253

NGC0253 is a nearly edge-on starburst galaxy located in the constellation Sculptor at the distance of 3.9 Mpc[146] from the Earth (Figure 22). It harbors at least three ULXs with the luminosities ranging between $(2.4 - 4.1) \times 10^{39}\,\text{erg s}^{-1}$.[147] The sum of the ULXs is $0.91 \times 10^{39}\,\text{erg s}^{-1}$. We adopt $600 M_{\odot}$ as the mass of an ULX of NGC0253 from the argument of the Eddington limit. Substituting $m = 6 \times 10^2$ and $L_{\text{rad}} = 9.1 \times 10^{39}$ erg s^{-1} into equations 29, 30, 51, 55, and 59, we derived $\tau_{\text{rise,th}} = 1.8 \times 10^{-3}$, $\tau_{\text{rec,th}} = 1.4 \times 10^{-1}$ s, and $L_{\gamma,\text{th}} = 8.8 \times 10^{38}$ erg s^{-1}, $W_{\max} = 7.9 \times 10^{21}$ eV, and $L_{\text{UHECR,th}} = 5.4 \times 10^{37}$ erg s^{-1}, as shown in Table 1.

Gutierrez et al.[148] proposed two candidates for the source of UHECRs, one is TH2[149] and the other is NGC253 X-1. Although TH2 was presumed the brightest radio source nearly coincident to the center of the galaxy, the recent observation by ALMA revealed that the position of TH2 exactly coincides to one of the knots in the central region of NGC 0253, which are most likely HII regions excited by young compact star clusters. The mass of the clusters are estimated as $\sim 10^6\ M_\odot$ and are not likely to have any blackholes, since there are no X-ray emissions. Although one may still assume a hidden non-accreting black hole in the cluster, any blackhole without accretion cannot emit any energy.

Gutierrez et al.[148] assumed a strong magnetic field of 10^4 G around the blackhole to produce jet luminosity through the Blandford-Znajek effect.[148] However, this magnetic field will decay rapidly if no accretion on the blackhole. The luminosity in equation 3 of Gutierrez et al.[148] can not sustain without a certain amount of accretion. In conclusion, TH2 is unlikely to be a source of UHECRs.

Ultra-Luminous X-ray Sources (ULXs), on the other hand, are promising as UHECR sources, such as NGC 0253 X-1, if we take into account wakefield acceleration. NGC 0253 harbors at least three ULXs with the luminosity ranging between $(2.4 - 4.1) \times 10^{39} \mathrm{erg\ s^{-1}}$.[147] The sum of the luminosities of the ULXs reaches $9.1 \times 10^{39} \mathrm{erg\ s^{-1}}$ as shown in Table 1. They are considered to be intermediate black holes with masses that range from $10^2 - 10^4\ M_\odot$.

The maximum energy of protons are estimated to be $W_{\max} = 1.2 \times 10^{21}$ eV even less massive black holes ($\sim 600\ M_\odot$) can generate UHECRs by WFA. Aab et al.[65] reanalyzed the data of arrival direction observed by Pierre Auger Observatory (PAO) and found that a significant (4σ level) enhancement in the arrival direction map of UHECRs above 39 EeV with the search radius of 12.9 degree toward NGC0253. This corresponds to the flux of 0.013 UHECRs/(100 km^2 yr), which corresponds to $L_{\mathrm{UHECR,obs}} = 5.4 \times 10^{37}\ \mathrm{rg\ s^{-1}}$. This is consistent with the theoretical isotropic luminosity of $2.7 \times 10^{37}\ \mathrm{rg\ s^{-1}}$ (Table 1 and Figure 21). Taking into account of rather large uncertainty of theoretical prediction, discussed above. The result of Aab et al.[65] is consistent with the data of Telescope Array team, though statistically marginal.[65,151]

The episodic recurrence time is estimated by the WFA theory to be $\tau_{\mathrm{rec,th}} = 1.4 \times 10^{-1}$ s. Barnard et al.[147] reported significant variabilities can be seen in 100 second bin, which are much longer when compared with the theoretical predictions. Since observations for short time variabilities (less than seconds) have unfortunately not been done for the ULXSs in NGC 253, the theory is not constrained by the observations.

The theoretical gamma-ray luminosity is estimated as $L_{\gamma,\mathrm{th}} = 7.9 \times 10^{38} \mathrm{erg\ s^{-1}}$. The observed gamma ray luminosity (isotropic) is $6.0 \times 10^{39} \mathrm{erg\ s^{-1}}$ in 1-100 GeV[71] and

$2.8 \times 10^{39} \mathrm{erg\ s^{-1}}$ above 220 GeV, which is one order of magnitude higher than the expected gamma-ray flux of ULXs by the wakefield acceleration theory. Direct comparison of L_γ luminosity with theory is difficult, however, due to other contributions from other supernova remnants].[152]

3.5. Galactic microquasars

Galactic blackhole binaries, such as SS433, Cyg X-1, Cyg X-3, Sco X-1 exhibit relativistic jets, violent variabilities in time scales ranging from milliseconds to years and emit radiation from radio to high energy gamma rays (~ TeV; Figure 24).[153,154] Because of such non-thermal phenomena, they are considered counterparts of quasars ($\sim 10^{6-9} M_\odot$) in million times smaller scales with masses of $\sim 10\ M_\odot$, in other words, micorquasars, and yet we find they are capable of generating high energy gamma rays and UHECRs.

Our Milky Way Galaxy has a number of maicroqasars, which are X-ray binaries containing stellar mass blackholes ($\sim 10\ M_\odot$),[155] Many of them are brightest sources in the X-ray sky with the luminosity of $10^{37} - 10^{38}$ erg s^{-1},[156,157] such as Sco X-1, Cyg X-1, Cyg X-3, GX5-1, and GX339-4 (Figure 24), exhibiting strong time variabilities all the time scales from milli-second to months.[158,61,159] Most of them have well collimated jets just like those of AGN but million times smaller in their scale and emit gamma-rays and even high energy gamma-rays.[160,161] Those observational facts shows that an efficient mechanism must work at these stellar size blackholes. One of the candidates would the wakefield acceleration, which accelerates charged particles to 10^{18}-10^{20} eV in their jets, as shown in

Figure 15. When they are in dense molecular cloud, the accelerated charged particles may interact with protons in the cloud to produce neutrinos. Figure 24 shows the sky map of such galactic microquasars. They might contribute to the enhancement along the galactic plane and galactic center in the neutrino arrival directions.

In the rest of the section, we will discuss SS433 in detail.

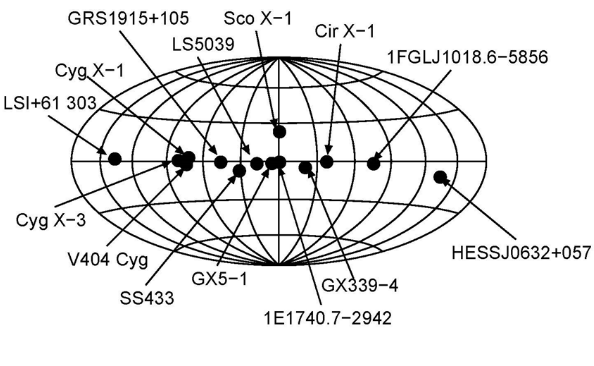

Figure 24 Skymap of microquasas..

3.5.1. SS 433

SS 433 is a galactic binary system consisting of a supergiant star $M = 10 - 30\ M_{\odot}$ and a compact object of $M = 2 - 3\ M_{\odot}$ (commonly considered to be a black hole) in the constellation Aquarius. The distance to the S433 system was estimated as 3.5 kpc[162] and is located inside of the supernova remnant W50, which exploded 20-40 thousands years ago.[163]

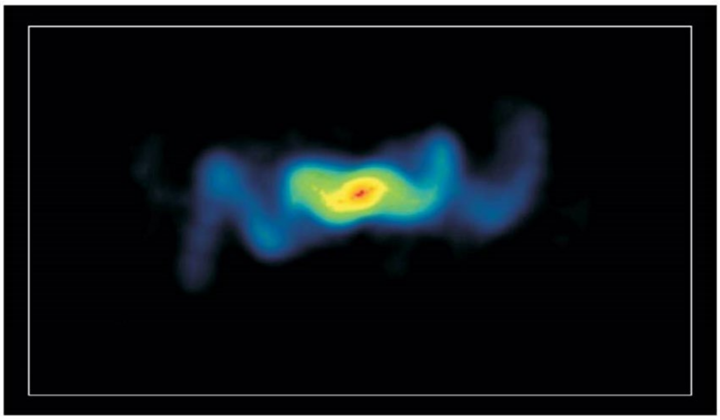

Figure 25. Galactic microquasar SS433. Since the jets are precessing, a pair of cork screw shapes are formed (Credit: B. Saxton from data provided by R.M. Hjellming, K.J. Johnston, NRAO/AUI/NSF).[164]

SS433 emits jets that have an approximate length of 40 pc, and a bulk velocity of 0.26c.[165-166] The two precessing jets model is well established (Figure 25).[167-171]

Kubota et al.[172] determined the mass of the compact object from orbital analyses to be $2.5 M_{\odot}$. According to Cherepashchuk et al.[173] and Abeysekara[174], the jet luminosity is as high as $10^{40}\mathrm{erg\ s^{-1}}$, because of super-critical accretion, in spite o low luminosity ($10^{35-36}\mathrm{erg\ s^{-1}}$) in X-ray band.[175]

Substituting $m = 2.5$ and $L_{\mathrm{rad}} = 10^{40}\ \mathrm{erg\ s^{-1}}$ into equations 29, 30, 51, 55, and 59, we derived $\tau_{\mathrm{rise,th}} = 1.8 \times 10^{-3}$, $\tau_{\mathrm{rec,th}} = 5.8 \times 10^{-4}\ \mathrm{s}$, $L_{\gamma,\mathrm{th}} = 8.8 \times 10^{38}\ \mathrm{erg\ s^{-1}}$, $W_{\max} = 1.9 \times 10^{24}$ eV, and $L_{\mathrm{UHECR,th}} = 2.9 \times 10^{37}\ \mathrm{erg\ s^{-1}}$as shown in Table 1.

According to the WFA theory, SS433 is capable of accelerating protons, and thus UHECRs. The UHECRs produced in SS433, may not be much localized unfortunately, since it is located near the galactic center, where the magnetic field is higher compared with the outer region. It may produce a broad (more than several ten degrees) concentration toward the galactic center, together with other microquasars in the galactic center region.

We can also estimate the theoretical recurrence time as $\tau_{\mathrm{rec,th}} = 5.8 \times 10^{-4}$ s according to wakefield theory (Table 1). Although a significant variation in flux at the time scale of 10 s was observed,[176] there is no information in the millisecond range.

The theoretical gamma-ray luminosity is calculated as $L_{\gamma,\mathrm{th}} = 8.7 \times 10^{39}$ erg s^{-1}. Since gamma rays are strongly beamed in the direction of the jets, they are not necessarily seen from Earth; our line of site is not aligned with the jets. The angle between our line of site and the axis of the jet precession is about 74 degree[177] and the precession angle is about 20 degree.

SS 433 has been observed to emit gamma rays. First, careful analysis of data from the Fermi gamma-ray observatory Large Area Telescope reveals that SS433 system emits extended gamma rays of 2.8×10^{-11} erg cm^{-2} s^{-1} in 500 MeV-10 GeV by Fermi-LAT.[178] The corresponding isotropic luminosity is about 1.0×10^{35} erg s^{-1}. It also showed a modulation of $\sim 10^{-10}$ erg s^{-1} correlation with the precession period.[179] The corresponding isotropic luminosity is 3.6×10^{37} erg s^{-1}. This component may be related to the gamma rays emitted from the electrons accelerated by wakefield in the jets, as suggested by Tajima et al.[30] in 2020, though the observed flux is much less compared with the theoretical prediction for the case of isotropic emission.

At 20 TeV, the HAWC detector in Abeysekara et al.[174] reported the emission is spatially localized in the three lobes (e1, e2, and w1), 40 pc away from the SS433 system.[174] The corresponding isotropic luminosity is 1.1×10^{30} erg s^{-1}. Since the lobes are located where jets interact with the nebula gas, the gamma rays can be explained by the synchrotron emission from high energy electrons accelerated in the wakefiled in the jets, colliding with the magnetic field of $\sim$10μGauss produced by the interaction of jets with nebula clouds.

3.6. Background (isotropic) fluxes of UHECR and neutrinos

The cosmic ray spectrum summing-up the contributions of such numerous numbers of UHECR sources (starburst galaxies and AGNs, distant than 10 Mpc, like NGC1068) over the entire sky is estimated as follows. First, the cosmic-ray flux J_{CR} per unit energy, area, time, and solid angle of cosmic-ray particles is calculated as:

$$J_{\mathrm{CR}} = \frac{c l_\gamma \tau_{\mathrm{CR}}}{4\pi} W^{-2}$$

$$= 1.8 \times 10^{-28}\ [\mathrm{particles/(GeV\ cm^2\ s\ sr)}] \left(\frac{W}{10^{19}\ \mathrm{eV}}\right)^{-2} \left(\frac{l_\gamma}{10^{38}\ \mathrm{erg\ s^{-1}\ (Mpc)^{-3}}}\right) \left(\frac{\tau_{\mathrm{CR}}}{3.4\times 10^9\ \mathrm{yr}}\right),$$

(67)

where l_γ is the local gamma-ray luminosity function of blazars, estimated as $10^{37} - 10^{38}\ \mathrm{erg\,s^{-1}\,(Mpc)^{-3}}$, taking into account of the beaming effect of the relativistic jets[180,181] and $\tau_{\rm CR}$ the lifetime of the cosmic-ray particles.[182] The expected spectrum of cosmic-rays is consistent with the observational flux of UHECR.

If a fraction f of the cosmic rays lose their energies through p-p interaction in the galaxies, resultant pions produce neutrinos through their decays. According to Waxman and Bahcall,[183] the total background accumulated flux of neutrinos through the entire history of the universe can be calculated as:

$$W_\nu^2 J_\nu = 1.1 \times 10^{-8}\ [\ \mathrm{GeV}\ /(\mathrm{cm^2\ s\ sr})] \left(\frac{\bar{f}}{0.02}\right) \left(\frac{l_\gamma}{10^{38}\ \mathrm{erg\,s^{-1}\,(Mpc)^{-3}}}\right) \left(\frac{\tau_\nu}{1.5\times 10^{10}\ \mathrm{yr}}\right) \quad (68)$$

where τ_ν is the neutrino accumulation time, which is the order of Hubble time ($\sim 10^{10}$ yr). Here, we assumed neutrinos are produced with the average energy of $W_\nu = 0.05 W_{\rm p}$ by one p-p collision. The best-fit single power-law parametarization for the astrophysical energy spectrum results in a normalization of 1.44×10^{-18} $[\mathrm{GeV\ cm^{-1}\ s^{-1}\ sr^{-1}}]$ at 100 TeV and the spectral index of 2.37 from 15 TeV to 5 PeV,[184] which is consistent with equation 68 for $W_\nu = 100\ \mathrm{TeV} = 10^5\mathrm{GeV}$.

3.7. Summary

1) The time scales ($\tau_{\rm rise}$ and $\tau_{\rm rec}$) of variabilities are clues to clarify how the WFA theory works in the astronomical objects, though the observation intervals are too sparse to constrain the theory in the current stage.
2) The theoretical luminosities are consistent with the observed isotropic luminosities in the sense that the former is lower than the later in on-axis source (blazars), while the former is higher than the later in off-axis sources (other than blazars), taking into account the beaming effects.
3) UHECR and neutrino emissions could be partially isotropic from the sources with the enhanced star formation (Seyfert and starburst galaxies), because of the randomization of the proton beam be interstellar magnetic field.
4) The observed background components of UHECRs and neutrinos are consistent of those predicted by WFA theory with AGN luminosity functions.

5) Gamm-ray emissions from the jets by the WFA theory likely show time variabilities, by which one can distinguish them from those from the supernova remnants pervading in the star forming regions.

4. Neutron star mergers and core collapse of massive stars

Both neutron star mergers and core collapse of massive stars harbor neutrino dominated accretion flow (NDAF) disk, which emit neutrinos rather than photons.[185] An NDAF disk is present for about 1-3 seconds, until all the mass is sucked into the central black hole of the 2-3 solar masses. If the mechanism similar to bow wake acceleration takes place in NDAF disk, which has $L_{\mathrm{w}} \sim 10^{51-52}$ erg s^{-1}, or about 6-7 orders of magnitude higher than that of photon-cooled accretion disk, the UHECR can be expected to be formed by acceleration from a far stronger wakefield than that of radiation dominant accretion disk.[15] We will discuss wakefield acceleration in NDAF disks in the rest of the section.

4.1. Neutron star mergers (Short gamma-ray bursts)

GW170817 and GRB 170817A mark the discovery of a binary neutron star (BNS) merger detected both as a gravitational wave (GW)[18] and a short-duration gamma-ray burst (SGRB).[186] Detecting GW radiation from the coalescence of BNS and neutron star (NS)– black hole (BH) binary systems has been a major goal of the LIGO[187] and Virgo[188] experiments.

The astrophysical implication of a joint detection of a SGRB and GWs from a BNS merger is the confirmation that binary neutron star mergers are the progenitors of at least some SGRBs. GW170817 has been identified as a GW signal from the in spiral of two low-mass compact objects, interpreted as the first GW observation of a BNS coalescence.[18,189] It was first observed by a low-latency search[190,191] on 2017 August 17 at 12:41:04 UTC by a single-detector trigger in the LIGO-Hanford detector.[189]

GRB 170817A was independently and simultaneously detected in-orbit by the GBM light software known as “triggering.”[192] the signal exceeded 5σ in three (of twelve) GBM NaI detectors. The GBM detection showed two distinct components, the triggering pulse, that lasts about half a second and fell consistent with expectations for SGRBs, followed by a subsequent weaker emission that lasted a few seconds.[192] The GBM light-curves show the two distinct components, as can be seen in the top two panels in Figure 26. The GBM time-tagged event data is binned to match the SPI-ACS temporal resolution (100 msec) and phase (matching bin edges) to allow for an easier comparison between the gamma-ray instruments.

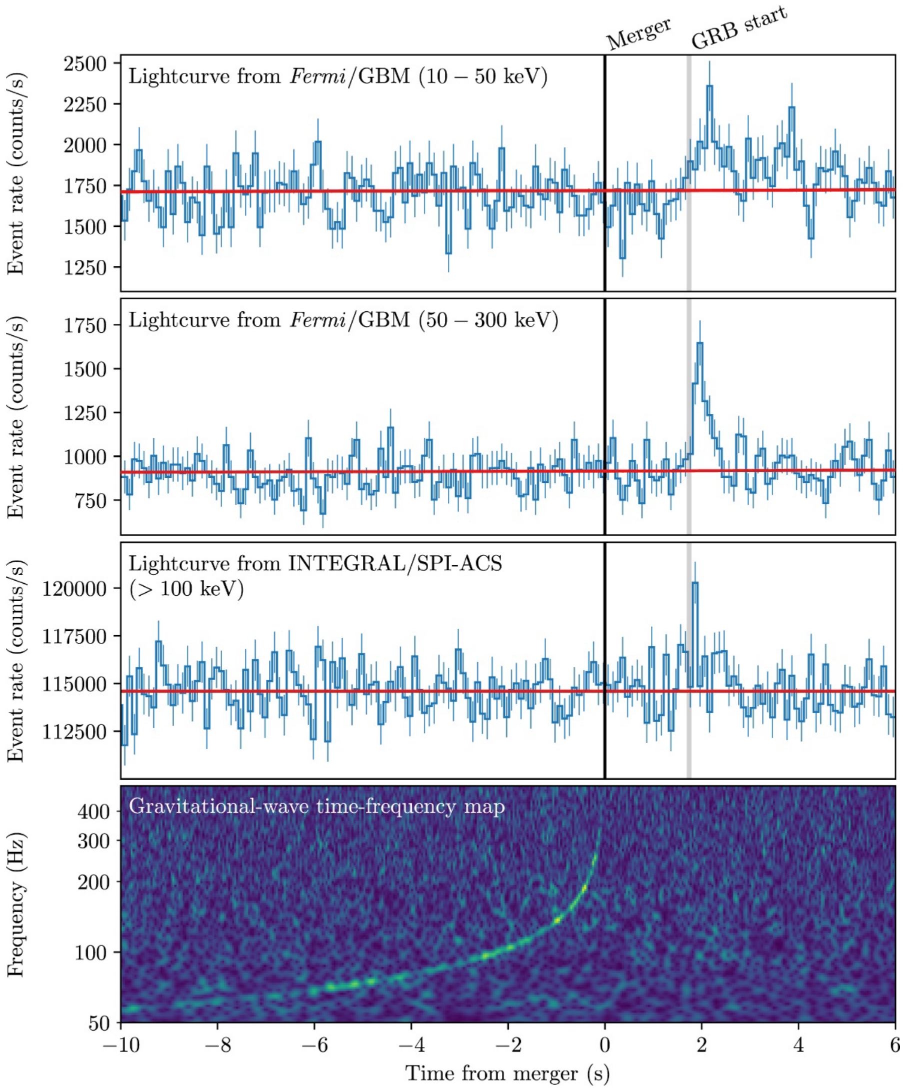

Figure 26. The joint, multi-messenger signal of gravitational wave (GW170817) and gamma-ray burst (GRB 170817A) is shown. GW170817 was followed by GRB 170817A by 1.74 seconds. Top: the summed GBM lightcurve for sodium iodide (NaI) detectors 1, 2, and 5 for GRB 170817A between 10 and 50 keV, matching the 100 msec time bins of the SPI-ACS data. The background estimate from Goldstein et al.[192] is overlaid in red. The middle panel shows the signals in the 50–300 keV energy range. The SPI-ACS lightcurve with energy range beginning at 100 keV and with a high energy limit of least 80 MeV. The bottom frame shows the time-frequency map of GW170817 coherently combining LIGO-Hanford and LIGO- Livingston gravitational wave data. All times here are referenced to the GW170817 trigger time T_0^{GW}.[186]

In one of the early theoretical works on the formation of the binary neutron start merger fireball and subsequent formation of an accretion disk and its associated jet formation may be seen in Figure 27 of Takahashi et al.[193]

We can have a strongly differentially rotating accretion disk from another kind of compact gravitational object such as the merged neutron star and another neutron star.[191] We show the latter case in Figure 27. In this work, Takahashi et al.[193] clearly predicted simultaneous emissions of gamma-ray burst and gravitational waves. In one of the latest multiples of astrophysical observational signals (in this case, in addition to the optical signal), the NS-NS collision was observed by the arrival of the gravitational wave[18] and simultaneous (delayed only by 1.74 second) arrival of gamma burst.[186]

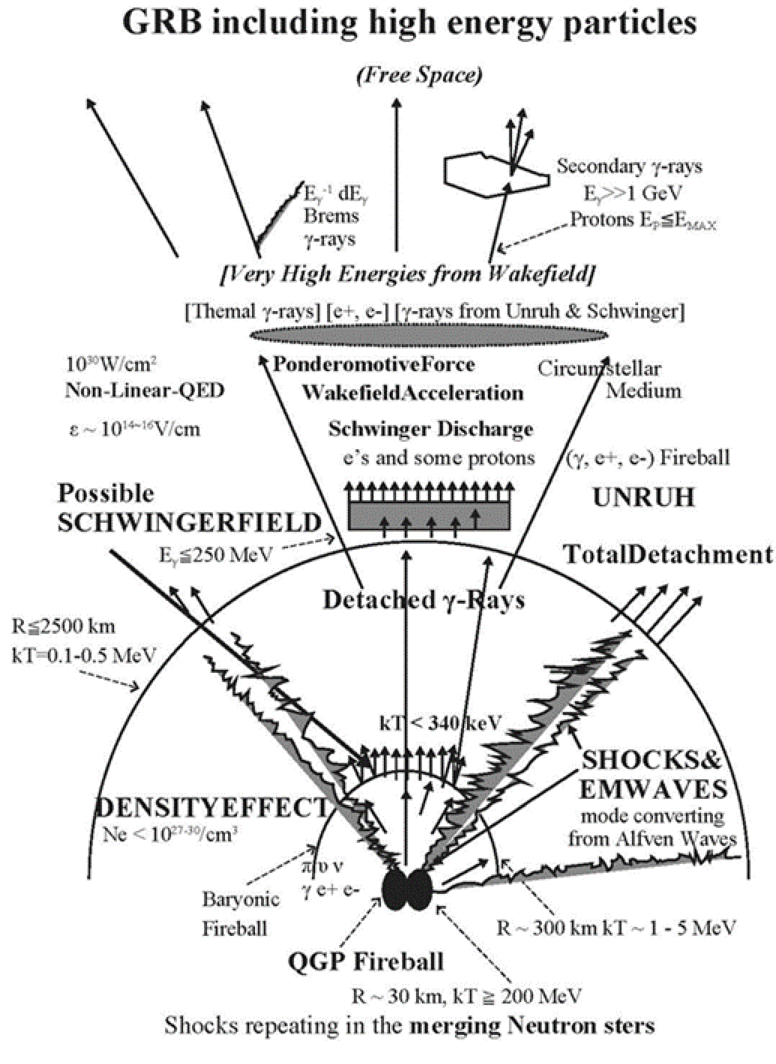

Figure 27. A schematic picture of the model of neutron star coalescence and associated high energy phenomena including gamma-ray burst after Takahashi's model.[193] The NS-NS collision created an accretion disk and its associated jets. While the collision of the compact massed neutron starts may emit gravitational waves, subsequent formation of the accretion disk and jets may give rise to the

electron acceleration and emission of gamma bursts, generating high energy phenomena including gamma-ray burst. After Takahashi et al. (2000).[193]

The neutron stars gradually approach each other with the emission of gravitational waves, and when the lighter star reaches its Roche limit, it is destroyed by the tidal force of the heavier star, to form an accretion disk. This accretion disk becomes a neutrino-cooled accretion disk, NDAF (Neutrino Dominated Accretion Flow),[185] rather than electromagnetic wave, because of the high temperature ($\sim 10^{9-10}$ K) and density (10^{13-15} protons cm^{-3}). Such an accretion disk is present for about 1-3 seconds until all the mass are sucked into the central blackhole of the 2-3 solar mass. If a mechanism similar to the bow wake acceleration does work in $L_{\mathrm{w}} \sim 10^{44-45}$ $\mathrm{erg\ s^{-1}}$, which is 6-7 orders of magnitude higher than that of radiation-cooled accretion disk, the UHECR can be expected to be formed by acceleration by a far stronger wakefield than that of radiation dominant accretion disk, which we discussed mainly in the present paper. On the other hand, the coalescence of neutron star should be accompanied by the dispersal of a large amount of materials processed in the star interior. When a beam of accelerated particles enters the materials, ultra-high energy (10^{20-22} eV) neutrinos can be emitted by the interaction of the beam and the materials. Since most of the energy used to accelerate electrons is emitted as gamma rays, there is also a possibility that a burst of gamma rays is produced. The delay of the gamma rays to the emission of gravitational waves is consistent with the time required for the NDAF disk and jets to form. The formation of the NDAF disk and the formation of the acceleration field due to the coalescence of the neutron stars will be discussed in a separate paper.

Kato et al.[15] investigated such a NDAF disk around a merged neutron star/blackhole with the extremely high accretion rate of 0.01-10 $M_{\odot}/\mathrm{s}$. They concluded that collimated relativistic jets emanated from the NDAF disk. The total expansion energy reaches $10^{51} - 10^{51}$ ergs, depending on the total accretion mass. The expansion energies are comparable to those required for the gamma-ray bursts as well as core-collapsed supernova (Figure 28). The wakefield acceleration in the jets produces ultra-high enegy protons up to 10^{22-24} eV. When a beam of accelerated particles enters the materials, ultra-high energy (10^{20-22} eV) neutrinos can be emitted by the interaction of the beam and the materials. Since most of the energy used to accelerate electrons is emitted as gamma rays, there is also a possibility that a burst of gamma rays is produced. The delay of the gamma rays to the emission of gravitational waves is consistent with the time required for the NDAF disk and jets to form. They also obtained the neutrino spectrum thermally emitted from the NDAF disk (Figure 29).

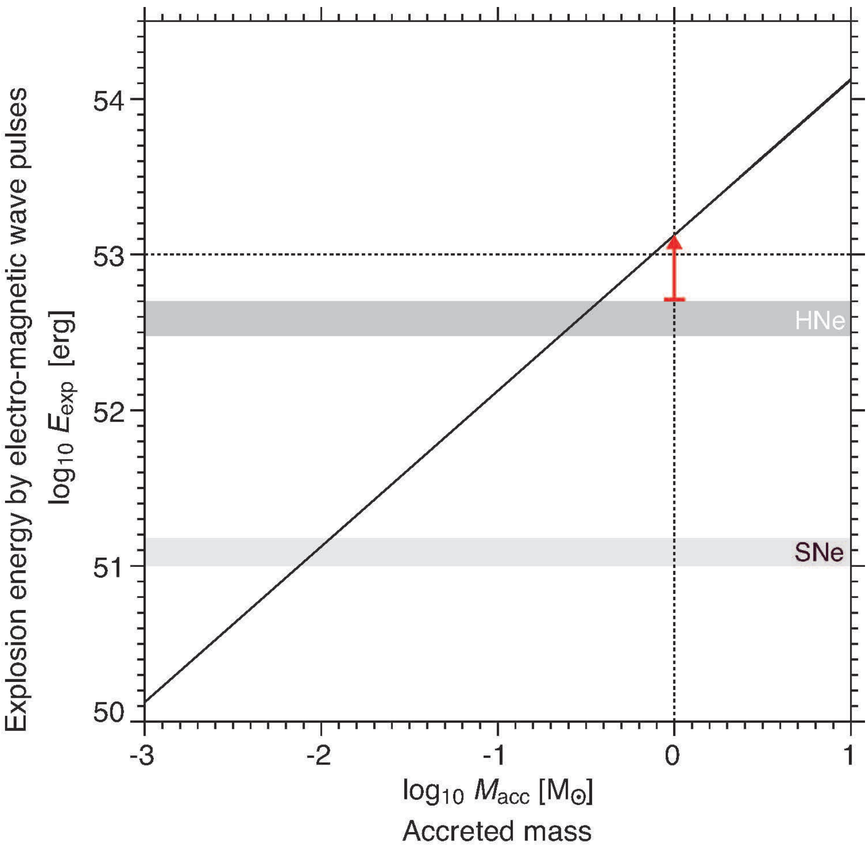

Figure 28. The explosion energy of the jets as a function of the accreted mass, supplied by electromagnetic waves from a neutrino driven accretion flow (NDAF) disk. After Kato, et al., 2022.[15]

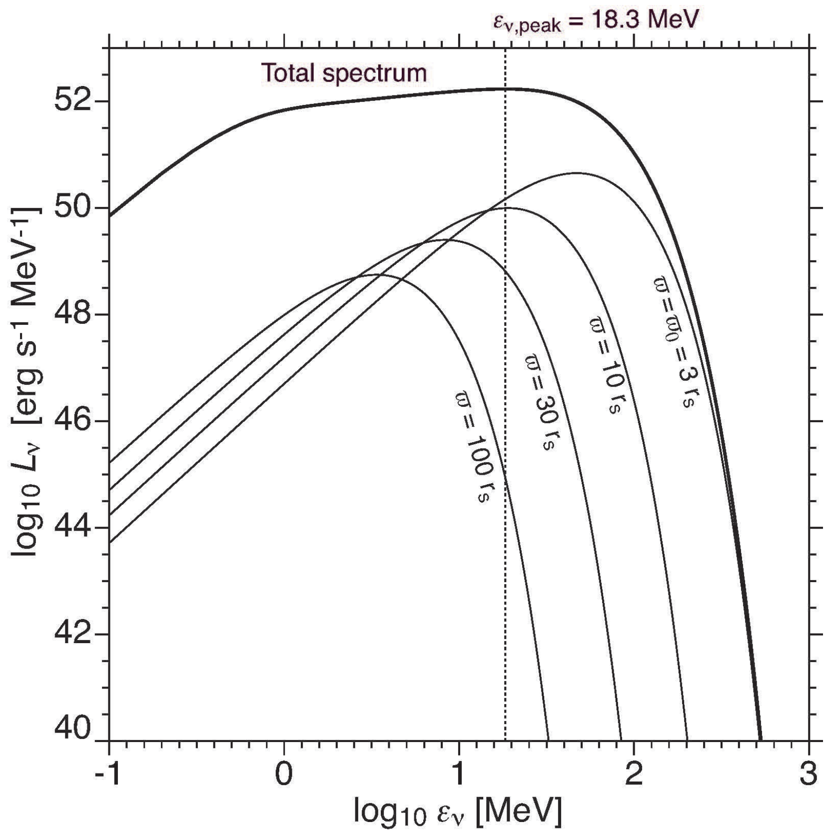

Figure 29. Neutrino luminosity spectrum as a function of the neutrino energy thermally emitted from a neutrino driven accretion flow (NDAF) disk. After Kato et al., 2022.[15]

4.2. Core collapse of massive stars (Long Gamma-ray bursts and Super-/Hyper-novae)

A stellar-mass blackhole is formed in the final stage of massive star's life, when a star implodes on itself.[194] Type Ib/c and Type II supernovae,[195] most hypernovae[196] and long-duration gamma-ray burst[197,198] are believed to be produced by the gravitational energy released when the core of a massive ($\sim 8-10 M_\odot$ or greater) star collapses down to a neutron star or blackhole. If the specific angular momentum of the core is higher than 4.6×10^{16} $[\mathrm{cm}^2\ \mathrm{s}^{-1}](M_{\rm BH}/3M_\odot)$. According to MacFadyen and Woosley,[198] the specific angular momentum is less than this critical value in the most part of the core made by the stellar evolution of a single star. However, the stellar number density in the nucleus of a young compact stellar is so large that massive stars (several ten solar) are sinking down by the dynamical friction among stars to form a binary. The binary continues to shrink through three-body interaction of lighter stars and eventually merge into a massive star before the supernova explosion.[126-129] Suzuki et al.[199] performed the simulation of the merging and found the core of the merging remnants rapidly rotates in the almost break-up rotation: the specific angular momentum of the core is as high as

10^{20} cm^2 s^{-1}. When such a rapidly rotating core of the massive star undergoes the core collapse, the most of the materials cannot fall into the blackhole but to form accretion disk around it.

The connection between long-duration Gamma-Ray Burst (GRN) and a particular class of core-collapse Supernovae (SNe) has been established[200] with the discovery of bright SNe (so called "Hypernovae") in positional and temporal coincidence with the time nearest GRBs.[201,202] The spectra of the SNe are similar to one another, and characterized by P-Cygni lines with broad absorption components, indicative of the presence of material expelled at high velocities. These SNe are thought to be the result of the explosion of the carbon-oxygen core of a massive star, which had lost its outer hydrogen and helium envelopes prior to the collapse of the core. Analysis of the spectra and the light curves of these GRB-SNe suggests that they are all energetic explosions, which ejected large quantities of matter: typically the explosion energy is $E \sim 5 \times 10^{52}$ erg, which is about 50 times larger than in normal core-collapse SNe, and ejected mass is $\sim 10\ M_{\odot}$. Because of the high energy, these have been also called "Hypernovae".

5. Discussions

5.1. WFA in comparison with Fermi mechanism and shock acceleration

The recognition that the magnetic fields play an important role in astrophysics is gaining strength. It is no longer gravitational fields alone that are the engine of the Universe organization and its morphology. The work such as Uchida and Shibata (1984)[4] showed clearly that the magnetic fields are essential that drive the formation of jets emanating from an accretion disk and push the plasma along the jets over the cosmic distance way far greater than the size of the thickness or even the diameter of the accretion disk. Another work that made such recognition stronger is by Balbus-Hawley (1991).[21,22] Yes, there have been classical works preceding these such as Alfven (1981)[1] and Chandrasekhar (1961).[203] The structure forming ability of magnetic fields (in addition to the gravitational fields) and thus associated evolution have been summarized by Tajima and Shibata (1997; TS97).[10] In this review we are making one step beyond the structure formation to recognize that magnetic fields and their active dynamics can serve to generate high energy phenomena of the Universe, such as high energy cosmic rays, bursts of high energy gamma rays and neutrinos.

The magnetic fields emanating from the accretion disk is spiraling out along the axis of the jets (or rather more precisely, the disk-driven spiral magnetic fields and their shear structure drive the emanation of plasma out of the accretion disk to form the jets). Thus the magnetic fields are primarily stretched along the axis of the jets (with some associated poloidal components) by this jet forming mechanism due to the magnetic stress that propels the jet plasma (Figs. 1, 2, 5, and 7). Such a structure may be regarded as shear Alfven waves itself, or a structural foundation of the jets' magnetic fields. This overall magnetic shear structure is in fact the reason why the jet plasma has been emanated from the root of the accretion disk and accelerated along the jest axis. Sometimes these jet motions give rise to even relativistic and highly relativistic jet flows (we codified such by the symbol of Γ in such places as in Eq. 44 in the above). [Sometimes, also, such a dis evolution may happen if and when a couple of compact objects such as neutron star and neutron star collide (as have been considered in Sec. 4.1).]

What we have studied and summarized above in terms of high energy acceleration processes is the additional dynamics on top of this approximately "steady state" structural evolution of the accretion disk-jet systems. As Balbus and Hawley[21,22] demonstrated and furthered by Matsumoto and Tajima in 1995,[24] the accretion disk with magnetic fields can exhibit growing magnetic fields within the disk due to its differential azimuthal motion of the disk, which amplifies the toroidal magnetic fields in a relatively short time (in the scale of the Universe's time). When such outbursts of magnetic fields growth happen in the disk, the originally gravitationally equilibrated disk motion (Keplerian or its relativistic cousin) becomes no long a sustainable dynamically equilibrium of the disk plasma. This outburst can give rise to an additional accretion not shown by the Blandford-Znajek[150] (steady accretion disk rate of plasma accretion) across the radial infall. This phenomenon and quantitative enhanced infall of a large chunk of plasma mass were quantitatively analyzed by Matsumoto and Tajima.[24] This causes, according to Ebisuzaki et al. in 2014,[28,29] large disturbances on the jet forming magnetic fields that emanate from the inner edge of the accretion disk and make huge disturbances on the jet magnetic fields. Since the jets magnetic fields are primarily the axial component (let us call B_z), the infall large accretion of the plasma chunk would cause radial disturbances on the jet magnetic fields primarily. It is important to recognize that this is a large motion of shear magnetic field perturbation, characterized as shear Alfven motions. (This is unlike the compressional squeeze of magnetic flux, which would cause compressional Alfven waves.) Thus we conclude that the evolution of the disk's magnetic fields trigger the large shear bending (and its propagation) along the axial direction of the jets. In other words, these are huge shear Alfvenic pulse propagation along the jets. The shear Alfven pulse propagates along the axial magnetic fields of the jets. Depending on the accretion conditions, disk conditions, and the nonlinear outcome of the Balbus-Hawley disturbance, the generated shear Alfven pulse parameter would vary, but in general it propagates with the group velocity of the Alfven speed v_A (which under certain condition tends to close to be c). As the jet stretches from the root of the disk to away from the disk, the density and magnetic fields etc. decrease and in general the Alfven speed increases, experiencing the mode conversion from shear Alfven waves into ordinary electromagnetic pulse.[28,29]

The shear Alfven wave and its derivative of EM wave pulses are thus generated and propagate along the jet plasma. This shear (or transverse) electromagnetic (EM) fields (that propagates close to the speed of light c) are capable of causing huge wakefields that are primarily composed of the longitudinal electric field visa ponderomotive forces of the EM fields.[40,28,29] Thus, our mainline accelerating process is vis the shear perturbation of magnetic fields and their derived transverse EM fields. The wakfields are their outcome. Although details vary depending upon the parameters and precise astrophysical conditions, the generic dynamics of this mechanism is the transverse EM wave generation with the group velocity close to c. If and when the group velocity of the EM waves is close to c, the wakefields and the accelerated high energy particles whose velocities are close to c) accelerated particles can resonate and ride on the phase with the wakefield for long time, as particles and waves are synchronized (this may be seen by the energy amplification factor of $2\gamma^2$, where γ is the Lorentz factor of the group velocity of the EM pulse.[40] Though probably minority, some particles (such as high energy component of prions (and ions) can stick along the jet for over cosmic distance. Most of other particles may drop out of this synchronicity with the waves, but still enjoy a directed ride over the wakefields. This implies that the generated electrons (and gamma rays subsequently) and ions (such as protons) and their derived neutrinos are directly largely along the jet direction upon their generation and temporarily also synchronized.

E. Fermi[48] in 1951 considered a multitude of particles (such as ions) entering a region of magnetic fields. He showed that the particle bending caused by each encounter of the particle with the magnetic field bends the ion transverse to the magnetic field and superposition of such magnetic bending of the particles stochastically accumulated can gain its overall energies. As we see, the fundamental acceleration of Fermi mechanism is to the transverse to the magnetic field direction. A subsequent derivative of the Fermi stochastic acceleration has been the magnetized shock acceleration. Particle encountering a bursting magnetic shock (with the Mach number M) may see the shock with its propagating speed of $M\sqrt{v_A{}^2 + c_s{}^2}$, which is the propagation speed of shock in a magnetized plasma with s being the sound speed. Fundamentally, the magnetize shock (a compressional Alfven mode) is basically a transverse to the magnetic field lines and a compressional mode.

5.2. Implications for future missions/projects

The current mechanism as described above is inherently coherent process between the excited waves (EM-like waves and their wakefields) and the particles that are to be accelerated (electrons and their derived gammas, positrons, protons and ions, and their derived particles such as neutrinos). Though the presence of intergalactic magnetic fields could deflect ions (and protons) orbits before arriving to the Earth, at least these particles were emanated from a point source (as compared to the size of their traveling distance). Thus one of the derived conclusive characteristics is the point like emission of various species of emissions of particles. Not only spatially correlated, but also can be temporarily correlated.

On the other hand, there are also possibilities that some less coherent process of acceleration along the propagation of the jets, but from the immediate vicinity of the accretion disk via wakefields is possible.[204] Emitted accelerated particles from such a process are less energetic and less aligned in the direction than the that in the jets. Thus, we surmise that these particles comprise lower energy portions of the spectrum.

Following the discussion in Sec. 5.1, we can view that the future observations can begin to separate the mechanisms of emission of radiation of the currently discussed one and the others. We will begin to learn the degree of coherence and lack of it by studying the future missions carefully with the following points of view. First, without the presence of plasma dynamics (i.e. only gravitational dynamics), radiations are mainly stemming from the bright thermonuclear start burning surface and its ensembles (such as galaxies). If and when we have both gravitational objects as well as the presence of magnetic fields in the plasma, while the gravitational interactions make stars and globally condensed objects such as galaxies and their clusters, with plasma the galactic accretion disks evolve in far more dynamically rich and enhanced modes. First, the presence of plasma allows emission of various additional radiations (even in electromagnetic radiations include Cherenkov radiation, synchrotron radiation and Bremsstrahlung under the non-collective (linear) mechanisms.[205] Each of these radiations (not nonlinear ones) is traceable to the emission by a single particle (such an electron). Thus the amount of radiation is proportional to the simple sum of these particles and thus is proportional to the number N of such particles. However, as we have seen in our review, the presence of plasma and magnetic fields in that now open up farm richer behavior of the plasma dynamics and thus the observationally apt phenomena (such as specific and enhanced radiations). If the plasma creates a dynamics that coherently amass a lump of N electron excess (charge of $-Ne$) in the plasma, which would force another clump of charge (now positively) excess with $+Ne$ in the other area. The collective interaction in such a plasma amounts to the strength in proportion to N^2. This squared intensity of the interaction is the origin of the superior intensity of the plasma collective phenomena and their radiation signatures from the collectively interacting phenomena. The wakefields wield is an intense collective phenomena, as they are the relativistic dynamics and this is further strengthened by the relativistic coherence.[41]

On the other hand, consider a chaotic or disorganized ensemble of random N charges. We understand that their average fluctuations of charges are proportional to $\sqrt{N}$. Thus the strength of mutual interactions of such random charge fluctuation is square of the sqrt of N, which is proportional to N. In other words, the random chaotic plasma (non-coherent plasma) exhibit interaction strength (and thus its signature to the emissivity) is proportional linearly to N. This is similar to the simple (non-interactive) linear addition due to the single particle dynamics (such as Cherenkov emission, synchrotron emission) we considered before we considered collective phenomena.

We now understand that plasma's ability of collectively interactive clumps (wakefields included) can emit far stronger radiative signatures than those by linear interactions. This is one of the most important characteristics of collective phenomena of plasma in the Universe, as that means we can either farther objects that contain and emit collective radiation or more intense and detailed patterns if not far away. By employing different bandwidths of radiation, we may thus capture a broader spectrum of plasma nonlinear evolution and dynamics intimately. We also note that since the emitted signals from collective phenomena are brighter as N^2, we can receive those signals far away in deeper places than the linear phenomena. In addition, it reveals the interplay of the astrophysical object's gravitational interaction (or structure) and plasma dynamics. This way, we shall learn more details of the Universe's dynamics and evolution.

One example is the case of a neutron star- neutron star collision, as discussed in Sec. 4.1. If NS and NS did not collide, such a dense compact gravitational object would emit neither gravitational radiation, but nor intense gamma ray emission. However, when NS and NS collide and erupt plasma and its disrupted dynamics (such as jets, disk and other structural features, as discussed in Sec. 4.1) commences, intense plasma waves and wakefields are excited, which are capable of making intense and coinciding gamma emission. We can well imagine in the future that various combinations of emissions from plasma's strong collective interactions, particularly those of wakefields.

6. Conclusions

We have reviewed the astrophysical basis of the wakefield acceleration in the Universe. This mechanism may arise in a variety of circumstances and astrophysical objects.

However, a standard case may be instructive to find the basic understanding, so that we first focus on the typical astrophysical accretion disk and its emanating jets. The major astrophysical energy that drives such an object is the gravitational energy. The central object, the accretion disk, is driven by its central gravitational object (be it a black hole, or other heavy central gravitational object(s) (AGN (active galactic nuclei))) that maintains the rapidly rotating accretion disk (made up with plasma and embedded magnetic fields in it). These combinations are known to form: (1) emanating jets by its magnetic fields (such as by Uchida-Shibata mechanism[4-7]), (2) created and enhanced shearing magnetic fields driven by the magneto-rotational instabilities (such as the Balbus-Hawley instability[21,22] and the Parker instability[23]), which sometimes episodic large inflow of accretion from the disk plasma toward the root of the jets. In this review we have described and clarified how such processes can make up fairly predictive dynamical outlook (not chaotic behaviors, but rather dynamically predictive consequences, as sometimes called the structure forming universe; TS97[10]). These are interesting and fascinating aspects of the predictions of this model of acceleration processes in astrophysical plasma. This is partially due to the fact that our process' definitive drive is directly related to and orchestrated by the well-organized central gravitational object.

We are suggesting this as a potentially relevant physical process and mechanism, which may be an emerging latest theoretical model as a possible alternative to the existing models such as the Fermi acceleration[48] (and its derived or related shock acceleration[204]), magnetic reconnection-driven acceleration,[6,10,205-216] etc. that have been considered for a long period preceding our current scheme. In the Fermi acceleration the stochastic cumulative accumulation of the magnetic field kicks that are randomly moving plasma containing embedded magnetic fields. In a related shock acceleration (again accompanied with magnetic fields embedded in the shocks) the magnetic kicks may be done via the moving plasma shocks (a fast moving supersonic plasma dynamics). In a magnetic reconnection related acceleration the accelerating mechanism may be arising from the snapping plasma flow motion accompanied by the topologically reconnected flux causes fast reconnected flows (again related to the mass motion as its fundamental velocity). These can give rise either cumulatively large energies or some violent motions that may arise. All of this involves the energy conversion from the plasma bulk motion, i.e. ions are moving, which may be called acoustic type (both ions and electrons partake in their motions fundamentally. Not electronic type. On the other hand, the wakefield process (though it may be superposed on the supersonically moving on the jet motion itself) fundamentally is the electronic only process, where magnetic flux is not any more tied with the plasma, but electromagnetic pulses may be of a freely propagating photon nature (This a kind that is freed from the magnetic flux frozen to the plasma (i.e. ionic motion's dictation to the central dynamics)). That is, the photons are driving at the level of the speed of light so that only electrons can keep up with the moving electromagnetic pulse motions. (Though this mechanism is more tightly bound by the original motherhood of the accretion disk and its jets, it also has nature's stochasticity in such aspects as its phase of the wakefields,[49] which determines the power law nature of spectrum accelerated by the wakfield generated in Nature.) This point makes some important manifestations and unique areas of applications in astrophysics as well as unique phenomenology that may not be arising in the past models. We will list some of the interesting aspects.

In contrast to these conventional mechanisms, the wakefield acceleration is based on more organized motions in the Universe (though it may accompany some chaotic natures such as the wakefield phases). The most typical is from the primordial galaxy (i.e. accretion disk and its plasma rotation-driven magnetic fields) assisted organized (often) large scale motion in the Universe.[6,10] Characteristics are such as the well-extended jets (over many kps or even Mps) and their accompanying magneto-rotational propulsion of the jet plasma,[4] accompanied by large magnetic field pulses driven by the magneto-rotational episodic disruption,[20] of the accreting matter onto the jet's magnetic flux. This causes huge and relativistically propagating cosmic electromagnetic wave pulsations,[28-30] which drives the wakefield generation. Even though this is among the largest size phenomena, similar mechanisms can be at work in smaller scales.

As an important special case of such, Takahashi et al.[191] conjectured that a collision of two compact neutron stars that form a rapidly rotating accretion disk and emanating jets from the collision can form a tiny version of wakefield acceleration along its jets and high energy particles (electrons ending up with gamma emissions). This in fact forms a basis of the simultaneous emissions of gravitational waves from the two colliding neutron stars and associated gamma emission.[186] This was discussed in Sec. 4.1. There have been also suggestions and in fact partial realization of observatories in space orbits to use earth's atmosphere as a gigantic scintillation detector such as proposed MASS (Maximum-energy Auger (Air)-Shower Satellite)[211] and EUSO (Extreme Universe Space Observatory).[212-216]

A version smaller than the AGN cosmic scale is the microquasars from the center of our Galaxy. And anything in between, such as starburst galaxies, Seyfert galaxies, etc. are discussed. The characteristics of the conjectured WFA phenomenology includes:

(1) Simultaneous emissions of gammas and (ultra-)high energy cosmic rays (UHECR), and neutrinos.

(2) Near point-like spatial co-incidences of these (UHECR may be bent slightly off by the intervening cosmic magnetic fields).
(3) Possible identification of optical or microwave identification of its sources (unlike the Fermi acceleration).
(4) Multi-messenger astrophysics (including LIGO, James Webb Space telescope, etc.) will tell untold details and nature of the emitting stellar to cosmic objects and their processes.
(5) The time scales and patterns of emitted gamma, optics, microwaves, UHECR, etc. may tell microscopic (relatively speaking as to the global cosmic scales) of the inside of the accelerating process.

Thus the introduction of the wakefield acceleration process to the cosmic acceleration genre will open up not only a rich addition of the physical mechanism to the conventional set of those, but also a new vista and details of the object that emits and its details physical processes in real time in a variety of astrophysical objects as mentioned in this paper. It will enrich astrophysics so much more.

Acknowledgements:

Three of us (TE, TT, and BB) have followed their own path of research to encounter with each other and three of us, which amounted to a joint work of this review. TE and TT ran into a cross point that the late Professor Yoshiyuki Takahashi brought us together by his vision of very active and high energy astrophysical phenomena such as collisions of compact stars and associated emissions of radiation, extreme high energy cosmic rays and their possible origin, and pioneering detection concept of them by space-based observatory of EUSO (Extreme Universe of Space Observatory) in early 2000s. TE joined EUSO projects, led by Professors Yoshi Takahashi, Livio Scarsi, Piergiorgio Picozza, and TE, and got interested in the acceleration of charged particles in the astrophysical jets. Stimulating discussions between TT and TE and other collaborators, such as Professor Etienne Parizot gradually grew into the idea of wakefield acceleration in the universe. TT and BB encountered in the preparation of SSCL (Superconducting Super Collider Laboratory) to try to detect extremely high energy phenomena. After the demise of the SSCL, BB went on to utilize laser to detect never observed Einstein’s gravitational waves and their astrophysical implications, while TT continued to make realization of his earlier wakefield accelerators on Earth. BB and TT again met in the committee of ELI (Extreme Light Infrastructure) SAC (2008), which tried to realize high intensity light phenomena including high energy particle acceleration with laboratory lasers. These encounters and collaborations founded a basis for three of us to investigate and review the Nature’s

acceleration mechanism to extreme high energies, i.e. via wakefield acceleration. BB went on successfully building LIGO and discovered gravitational waves, for which he was recognized for the 2017 Nobel. BB wishes to thank the LIGO Laboratory for their support, the LIGO Scientific Collaboration for their contributions to LIGO data analysis and science, and lastly the National Science Foundation for their long-term support from LIGO conception to the present day.

Along these meanderings and paths, we encountered a huge number of colleagues whose enlightening, collaboration, and encouragements were invaluable. They include: Drs. K. Abazajian, J. Adams, F. Albert, H. Alfven, R. Assmann, S. Barwick, F. Brunel, S. Bulanov, S. Cable, A. Caldwell, P. Chen, S. Corde, J. Dawson, M. Downer, E. Esarey, D. Gilden, C. Haswell, K. Holcomb, W. Horton, G. Huxtable, S. Ichimaru, S. Karsch, Y. Kato, Y. Kishimoto, M. Kivelson, M. Kole, R. Kulsrud, T. Kurki-Suonio, C. Lau, R. Li, J. Leboeuf, R. Lovelace, K. Makishima, R. Matsumoto, K. Mima, S. Mineshige, S. Miyamoto, A. Mizuta, G. Mourou, K. Nakajima, S. Nicks, E. Parizot, F. Perkins, N. Petviashvili, P. Picozza, M. Rosenbluth, N. Rostoker, J.I, Sakai, H. Sato, L. Scarsi, C. Schroeder, K. Shibata, V. Shiltsev, C. Siders, H. Sobel, D. Sugimoto, Y. Takahashi, K. Thorne, S. Weinberg, J. Wheeler, M. Yamada, X. Yan, H. Yu, F. Zimmermann, E. Zweibel. The Rostoker Fund is also acknowledged for its support.

References

1 H. Alfven, Cosmic Plasma (Reidel, Dordrecht, 1981).
2 R.V.E Lovelace, 1976, Dynamo model of double radio sources, Nature, 262, 649-652.
3 R.D. Blandford, 1976, Accretion disc electrodynamics-a model for double radio sources, Mon. Not. Roy. Astron. Soc., 176, 465-481.
4 Uchida, Y. and Shibata, K. 1984, Magnetically buffered accretion to a young star and formation of bipolar flows, Publ. Astron. Soc. Japan, 36, 105-118.
5 Shibata, K. and Uchida Y., 1986, A Magnetodynamic mechanism for The formation of astrophysical jets 1. Dynamical effects of the relaxation of nonlinear magnetic twists, Publ. Astron. Soc. Japan, 37, 31-46.
6 Shibata, K. and Uchida Y., 1986, A Magnetodynamic mechanism for The formation of astrophysical jets 2. dynamic processes in the accretion of magnetized mass in rotation, Publ. Astron. Soc. Japan, 38, 631-660.
7 Shibata, K. and Uchida, Y. 1986, Formation of astrophysical jets by a contractiong magnetic accretion disk, Astrophys. and Space Science, 118, 443-447.
8 Leboeuf, J.N., Tajima, T., Kennel, C.F., and Dawson, J.M., 1978, Global Simulation of the Time-dependent Magnetosphere, Geophys. Res. Lett. 5, 609.
9 Leboeuf, J.N., Tajima, T., Kennel, C.F., and Dawson, J.M., 1981, Global Simulation of the Three-Dimensional Magnetosphere, Geophys. Res. Lett. 8, 257.
10 Tajima, T. and Shibata, K. (TS97), 1997, Plasma Astrophysics, (Addison-Wesley, Reading, MA, 1997). reprinted (Perseus, Boulder, CO, 2002).
11 Mima, K., Tajima, T., and Leboeuf, J.N., 1978, Magnetic Field Generation by the Rayleigh-Taylor Instability, Phys. Rev. Lett. 41, 1715.
12 K. Shibata, T. Tajima, R. Matsumoto, 1990, Magnetic accretion disks fall into 2 types, Astrophys. J. 390, 295-299.
13 Matsumoto, R, Uchida, Y., Hirose, S, Shibata, K, Hayashi, MR, Ferrari, A, Bodo, G., and Norman, C, 1996, Radio jets and the formation of active galaxies: Accretion avalanches on the torus by the effect of a large-scale magnetic field, Astrophys. J., 461, 115-126.
14 A. Mizuta, T. Ebisuzaki, T. Tajima, S. Nagataki, 2018, Mon. Not. Roy. Astrpon. Soc., 479, 2534–2546.
15 Y. Kato, T. Ebisuzaki, and T. Tajima, 2022, Ap. J. 929, 42.
16 J.A. Wheeler, 1990, Journey into Gravity and Spacetime (Scientific American Library), W.H. Freeman&Co.
17 K. Akiyama et al. (The Event Horizon Telescope Collaboration), 2019, First M87

event horizon telescope results. I. The shadow of the supermassive black holes, Astrophys. J. 875, L1.
18 Abbott, B.P.; et al., 2016. Observation of Gravitational Waves from a Binary Blackhole Merger, Phys. Rev. Lett. 116, 061102.
19 Abbott, B. P.; et al. (LIGO Scientific Collaboration & Virgo Collaboration) 2017, "GW170817: Observation of Gravitational Waves from a Binary Neutron Star Inspiral". Physical Review Letters. 119 (16): 161101.
20 R. Matsumoto, et al., 1996, in Basic Physics of Accretion Disks, eds. S. Kato and S. Inagaki.
21 S.A. Balbus, J.F. Hawley, 1991, A powerful local shear instability in weakly magnetized disks. 1. Linear analysis, Astrophys. J. 376 (1991) 214–222.
22 J.F. Hawley,and S.A. Balbus, 1991, A powerful local shear instability in weakly magnetized disks. 2. Nonlinear evolution, Astrophys. J. 376, 223-233.
23 E. N. Parker, 1979, Cosmic Magnetic Field (Clarendon Press, Oxford).
24 R. Matsumoto and T. Tajima, 1995, Magnetic viscosity by localized shear-flow instability in magnetized accretion disk, Astrophys. J. 445, 767–779 .
25 Mineshige, S., Kusunose, M., and Matsumoto, R, 1995, Low-state disks and low-beta disks, Astrophys. J. Lett., 445, L43-L46.
26 M. Kole, 2021, CERN Courier January/February 11, https://cerncourier.com/a/cosmic-plasma-wakefield-acceleration/
27 https://eventhorizontelescope.org/blog/astronomers-image-magnetic-fields-edge-m87s-black-hole
28 Ebisuzaki, T. and Tajima, T., 2014, Astrophysical ZeV acceleration in the relativistic jet from an accreting supermassive blackhole, Astroparticle Physics, 56, 9-15.
29 Ebisuzaki, T. and Tajima, T., 2014, Pondermotive acceleration of charged particles along the relativistic jets of an accreting blackhole, Eur. Phys. J. Special Topics, 223, 1113-1120.
30 T. Tajima, X.Q. Yan, and T. Ebisuzaki, 2020, Wakefield acceleration, Reviews of Modern Plasma Physics, 4, 7-93.
31 S. Ichimaru, 1973, “Basic principles of plasma physics” (Benjamin, Reading, 1973).
32 Ebisuzaki, T. and Tajima, T., 2021, Astrophysical wake acceleration driven by relativistic Alfvenic pulse emitted from bursting accretion disk, Astroparticle Physics, 128, 102567.
33 N.I. Shakura , R.I. Sunyaev , 1973, Black Holes in Binary Systems, Observational Appearance, Astron. Astrophys. 24 (1973) 337 .
34 Tajima, T. and Gilden, D., Reconnection-driven Oscillations on Dwarf Nova Disks,

Ap. J. 320, 741 (1987).

35 C. Haswell, T. Tajima, and J. Sakai, 1992, High energy particle acceleration by explosive electromagnetic interaction in an accretion disk, Astrophys. J., 401, 495-507.

36 Tout, C.A. and Pringle, J.E., 1992, Accretion disk viscosity a simple-model for magnetic dynamo, Monthly Notice of the Royal Society of London, 259, 604-612.

37 N.E. Canac, K.N. Abazajian, T. Tajima, T. Ebisuzaki, S. Horiuchi, 2020, Observational signatures of gamma-rays from bright blazars and wakefield theory, Mon. Not. Roy. Astron. Soc. 493 (2020) 2229-2237.

38 K. Asada , M. Nakamura, 2012, The structure of the M87 jet: a transion from parabolic to conical streamlines, Astrophys. J., 745,L28.

39 A.B. Pushkarev et al. 2012, MOJAVE: Monitoring of Jets in Active galactic nuclei with VLBA Experiments, Mon. Not. Roy. Astron. Soc. 468, 4992 .

40 Tajima, T. and Dawson, J.M., 1979, Laser Electron Accelerator, Phys. Rev. Lett., 43, 267.

41 Tajima, T., 2010, Laser acceleration and its future, Proceedings of the Japan Academy of Series B-physical and Biological Sciences, 86, 147-157.

42 Lau, C.K., Yeh, P.C. Ebisuzaki, T. and Tajima, T., 2015, Ponderomotive acceleration by relativistic waves, Physical Review Special Topics-Accelerators and Beams, 18 024401.

43 K. Nakajima et al., 1995, Observation of Ultrahigh Gradient Electron Acceleration by a Self-Modulated Intense Short Laser Pulse, Phys. Rev. Lett. 74, 4428-4431.

44 G.A. Mourou, T. Tajima, S. Bulanov, 2006, Optics in the Relativistic Regime, Rev. Mod Phys.78, 309-371.

45 E. Esarey, C.B. Schroeder, and W.P. Leemans, 2009, Physics of laser-driven plasma-based electron accelerators, Reviews of Modern Physics, 81, 1229-1285.

46 Tajima, K. Nakajima, and G. Mourou, 2017, Laser Acceleration, Rivista del Nuovo Cimento 40, 33-133.

47 E. Adli et al. (AWAKE Collaboration), 2018, Acceleration of electrons in the plasma wakefield of a proton bunch, Nature 561, 363-367.

48 E. Fermi, 1954, Galactic magnetic fields and the origin of comic radiation, Astrophys. J. 119,1-6.

49 K. Mima, W. Horton, T. Tajima, A. Hasegawa, 1991, in: Nonlinear Dynamics and Particle Acceleration, Y. Ichikawa, T. Tajima, (eds.), (AIP, NY, 1991), p. 27.

50 P.C. Chen , T. Tajima , Y. Takahashi , 2002, Plasma wakefield acceleration for ultrahigh-energy cosmic rays, Phys. Rev. Lett. 89, 161101 .

51 R. U. Abbasi et al., 2014, Indications of intermediate-scale anisotropy of cosmic rays with energy greater than 57EeV in the northern sky measured with the surface detector of the telescope array experiment, Astrophys. J. Lett. 790, L21.
52 T.A. Thompson, et al., 2006, Magnetic fields in starburst galaxies and the origin of the FIR-radio correlation, Astrophys. J. 645, 186-198 .
53 E. Parizot , A. Marcowith, J. Ballet, and Y.A. Gallant, 2006, Observational constraints on energetic particle diffusion in young supernovae remnants: amplified magnetic field and maximum energy, A&A 453, 387–395 .
54 J.F. Gallimore et al. 2006, Survey of kiloparsec-scale radio outflows in radio-quiet galactic nuclei, Astrophys. J., 132, 546-569.
55 A.F.M. Moorwood, 1996, Star burst galaxies, Space Sci. Rev., 77, 303-366.
56 S. Mineo et al., 2011, X-ray emission from star-forming galaxies, -I. High-mass X-ray binaries, Mon. Not. Roy. Astron. Soc., 419, 2095-2115.
57 Greenstein, J.L. and Schmidt, M., 1964, The quasi-stellar radio sources 3C48 and 3C273, Astrophysical Journal, 140, 1-34.
58 K. Akiyama et al. (The Event Horizon Telescope), 2019, First M87 Event Horizon Telescope Results. V, Physical origin of the Asymmetric Ring, Astrophysical Journal, letters, 875, L5.
59 K. Akiyama et al. (The Event Horizon telescope), 2021, First M87 Event Horizon Telescope Results. VIII, Magnetic Field Structure near The Event Horizon, Astrophysicak Journal, Letters, 910, L13.
60 Giacconi, R., Gursky, H., Paolni, F.R., and Rossi, B.B., 1962, Evidence for X-ray from sources outside the solar system, Physical Review Letters, 9, 439-443.
61 S. Miyamoto, 1998, Time variabilities of X-ray binary stars, Advances in Space Research, 22, 943-950.
62 Milabel, I.F. and Rodrigez, L.F., 1999, Sources of relativistic jets in the galaxy, Ann. Rev., Astron. Astrophys, 37, 409-443.
63 H-N He, A. Kusenko, S. Nagataki, 2016, Monte Carlo Baysian search for the plausible source of Telescope Array hot spot. Phys. Rev. D 93, 043011,.
64 J. Abraham, et al. (Pierre Auger Collaboration), 2008, Correlation of the highest-energy cosmic rays with the positions of nearby active galactic nuclei, Astropart. Phys. 29, 188.
65 A Aab et al. (The Pierre Auger Collaboration), 2018, An indication of anisotropy in arrival directions of ultra-high energy cosmic rays through comparison to the flux pattern extragalactic gamma-ray sources, Astrophys. J. Lett. 853. L29.
66 Anchordoqui, L.A. and Soriano, J.F., 2019, Evidence for UHECR origin in star- burst

galaxies, ArXive:1905.13243v1.
67 R.U. Abbasi et al., 2015, Study of ultra-high energy cosmic ray composition using telescope Array's middle drum detector and surface array in hybrid mode, Astroparticle Phys. 64, 49–62.
68 P.F. Michelson, W.B. Atwood and S. Ritz, 2010, Fermi gamma-ray space telescope: High energy results from the first year, Rept. Prog. Phys.73:074901,2010 and arXiv: 1011,0213.
69 A.A. Abdo et al. 2010, The first catalog of active galactic nuclei detected by the FERMI large area telescope, Astrophys. J., 715, 429-457.
70 M. Ackermann et al., 2011, The second catalog of active galactic nuclei detected by the FERMI large area telescope, Astrophys. J., 743, 171.
71 M. Ackermann et al. 2012, GeV observations of star-forming galaxies with the FERMI large area telescope, Astrophys. J., 755, 164.
72 https://magic.mpp.mpg.de/
73 https://www.mpi-hd.mpg.de/
74 K. Ragan (the VERITAS Collaboration), 2012, Some recent highlights from VERITAS, Nuclear Instrument and Methods in Physics Research A, 692, 24-28.
75 T. DeYoung, 2012, The HAWC observatory, Nuclear Instruments and Methods in Physics Research A, 692, 72-76.
76 S. Paiano et al. 2018, The redshift of the BL Lac object TXS 0506+056, Astrophys. J. Letters, 854, L32.
77 C.R. .Lawrence et al. 1983, 5 GHz observations of sources in the Arecibo 611 MHz survey, Astrophys. J., Suppl., 51, 67-114.
78 Massaro et al., 2009, Roma-BZCAT: a multifrequency catalogue of blazars, A&A, 495, 691-696.
79 R.C. Lamb and D.J. Macomb, 1997, Pint source of GeV gamma rays, Astrophys. J., 488, 872-880.
80 J.P. Halpern et al. 2003, Redshifts of candidate gamma-ray blazars, Astrophys. J., 125, 572-579.
81 A.A. Abdo et al. 2010, Gamma-ray light curves and variability of bright FERMI-detected blazars, Astrophys. J., 722, 520-542.
82 J.L. Richards et al. 2011, Blazars in the FERMI era: the OVRO 40 m telescope monitoring program, Astrophys. J. Suppl., 194, 29.
83 Aartsen et al. (IceCube Coillaboration), 2018, neutrino emission from the direction of the blazer TXS0506+056 prior to the IceCube-170922A alert, Science, 361, 147-151

84 Aartsen et al. (IceCube Collabolation, FERMI-LAT, MAGIC, AGILE, ASAS-SN, HAWC, H.E.S.S., KANATA, KISO, KAPTEYN, LIVERPOOL TELESCOPE, SUBARU, SWIFT/NUSTAR, VERITAS, VLA/17B-403 TEAMS), 2018, multimessenger observations of a flaring blazar coincident with high-energy neutrino IceCube-170922A, Science, 361, 146.
85 P. Padvani, F. Oikonomou, M. Petropulou, G. Gimommi, and E.R. Resconi, 2019, TXS 0506+056, the first cosmic neutrino source, is not a BL Lac, Man. Not. Roy. Astron. Soc., 484, L104-L108.
86 S. Paiano et al. 2018, The redshift of the BL Lac object TXS 0506+056, Astrophys. J. Letters, 854, L32.
87 K. Greisen, 1966, End of the comic-ray spectrum?, Phys. Rev. Let., 16, 748-750.
88 G.T. Zatsepin and V.A. Kuzmin, 1966, Upper limit of spectrum of cosmic rays, JETP Letters-USSR, 4, 78.
89 S. Ansoldi et al., 2018, The blazar TXS 0506+056 associated with a high energy neutrino: insight into extragalactic jets and comic-ray acceleration, Astrophys. J. Let., 863, L10.
90 L. Ferrarese, J.R. Mould, P. Stetson, J.H. Tonry, 2007, The discovery of cephieds and distance to NGC5128, Astrophys. J., 654 (2007) 186–218 .
91 D.E. Harris , et al. , Astrophys. J., The outburst of HST-1 in the M87 jet, 640 (2006) 211–218.
92 D. Majaess, 2010, The cepheids of Centaurus A (NGC5128) and implications for H_0, Acta Astronomica, 60, 121–136 .
93 N. Neumayer, 2010, The supermassive black hole at the heart of Centaurus A: Revealed by the kinematics of gas and stars, Pub. Of the Astron. Soc. Aus., 27, 449-456.
94 E. Jourdain et al. 1993, On the hard X-ray variability of Centaurus A, Astrophys. J., 412, 586-592.
95 F.P. Israel, 1998, Centaurus A-NGC 5128, Astron. Astrophys Rev., 8 237-278.
96 I.D. Karachentsev, M.E. Sharina, A.E. Dolphin, E.K. Grebel, et al., New distances to galaxies in the Centaurus A group, 2002, Astron. Astrophys., 385, 21–31. Bibcode:2002A&A...385...21K, doi: 10.1051/0004-6361:20020042 .
97 G.L.H. Harris, M. Rejkuba, W.E. Harris, 2010, The distance to NGC5128 (Centaurus A), Publ. Astron. Soc. Australia, 27, 457–462 .
98 Fukazawa et al., 2011, SUZAKU view of X-ray spectral variability of the radio galaxy Centaurus A: Partial covering absorber reflector, and possible jet component, Astrophys. J. 743, 124.

99 R.E. Rothschild et al. 2011, twelve and a half years of observation of Centaurus A with RXTE, Astrophys. J., 733, 23.
100 H. Abdalla et al. (H.E.S.S. collaboration), 2018, The gamma-ray spectrum of the core of Centaurus A as observed with H.E.S.S. and Fermi-LAT, A&A, 619, A71.
101 S. Bird , W.E. Harris , J.P. Blakeslee , C. Flynn , 2010, The inner halo of M87; a first direct view of the red-giant population, A Ap, 524, A71.
102 Gebhardt, K. et al. 2011, The black hole mass in M87 from GEMINI/NIFS adaptive optics observations, Astrophys, J., 729, 119.
103 T. Di Matteo , et al., 2003, Accretion onto the supermassive black hole in M87, Astrophys. J., 582, 133–140.
104 D.E. Harris et al. 2006, The outburst of HST-1 in the M87 jet, Astrophys. J., 640, 211-218.
105 M. Aaronson, J. Huchra, J. Mould, P.L. Schechter, R.B. Tully, 1982, The velocity field in the local supercluster, Ap.J. 258 , 64 .
106 F. Aharonian et al.. 2006, Fast variability of tera-electron volt gamma-ray from the radio galaxy M87, Science, 314, 1424-1427.
107 B.F. Madore et al. 1999, The Hubble space telescope key project on the extragalactic distance scale XV. A cephid distance to the Fornax cluster and its implications, Astrophys. J. 515, 29-41. .
108 J.B. Jensen, et al., 2003, Measuing distance and probing the unresolved stellar populations of galaxies using infrared surface brightness fluctuations, Astrophys. J., 583, 712-726 .
109 J.J. Feldmeier , et al., 2007, Calibrating Type Ia supernovae using the planetary nebula luminosity function. I. initial results, Astrophys. J. 657, 76.
110 N. Nowak , et al. , 2008, The supermassive black hole of Fornax A, Mon. Not. Roy. Astron. Soc., 391, 1629-1649. .
111 M.S. Tashiro , et al., 2009, Hard x-ray spectrum from west lobe of radio galaxy Fornax A observed with Suzaku, Publ. Astron. Soc. Japan, 61, S327-S335.
112 M. Ackermann et al., 2016, Fermi large area telescope detection of extended gamma-ray emission from the radio galaxy Fornax A, Astrophys. J., 826, 1.
113 A.D. Gouling , et al.,, 2010, Towards a complete census of active galactic nuclei in nearby galaxies: the incidence of growing blackholes, Mon. Not. Roy. Astron. Soc. 406, 597–611.
114 R.B. Tully, J.R. Fisher, Nearby Galaxies Catalogue 1988, Cambridge University press, Cambridge, UK, 1988 .

115 S. Marchesi , et al., 2018, Compton-thick AGNs in the NuSTAR Era, Astrophys. J., 859, 49–65 .
116 Matt, G., Bianchi, S., Guainazzi, M., & Molendi, S. 2004, A&A, 414, 155.
117 A. Zaino et al., 2020, Probing the circumnuclear absorbing medium of the buried AGN in NGC 1068 through NuStar observations, Mon. Not. Roy. Astron. Soc., 492, 3872-3884.
118 O.G. Taranova and V.I, Shenavrin, 2006, Infrered variability of nucleus of Seyfert galaxy NGC1068 in 1998-2004, Astronomy Letters, 32, 439-445.
119 S.F. Honig and M. Kishimoto, 2011, Constraining properties of dusty environments by infrared variability, A&A, 534, A121.
120 V.A. Acciari et al. (MAGIC collaboration), 2019, constraints on gamma-ray and neutrino emission from NGC1068 with the MAGIC telescopes, Astrophys. J., 883, 135.
121 M.G. Aartsen et al. (IceCube Collaboration), 2020, Time-integrated neutrino source searches with 10 years of IceCube data, Phys. Rev. Let., 124. 051103.
122 M. Guainazzi , et al., 2000, A broad-band X-ray view of NGC 4945, A&A, 356, 463–475 .
123 A. Pancoast , et al., 2014, Modelling reverberation mapping data – II. Dynamical modelling of the Lick AGN Monitoring Project 2008 data set, Mon. Not. Roy. Astron. Soc., 445, 3073-3091.
124 G.M. Madejski , et al., 1993, Solving the mystery of the X-ray periodicity in the Seyfert galaxy NGC6814, Nature, 365, 626-628.
125 A.F. Tennant et al., 1981, Rapid x-ray variability in the Seyfert-galaxy NGC-6814, Astrophys. J., 251, 15-25.
126 S. Portegies-Zwart , J. Makino , S.L.W. McMillan , P. Hut, 1999, Star cluster ecology III. Runaway collisions in young compact star clusters, Astron. Astrphys. 348, 117–126.
127 S. S.Portgies-Zwart , S.L.W.McMillan, 2002, The runaway growth of intermediate－mass black holes in dense star clusters, Astrophys.J., 576, 899–907.
128 S. Portgies-Zwart, H. Baumgardt , S.L.W. McMillan, 2006, The ecology of star clusters and intermediate－mass black holes in The GALACTIC BULGE Ap. J. 641, 319–326.
129 T. Ebisuzaki et al., 2001, Missing link found? The“runaway”path to supermassive black holes, Astrophys. J., 562, L19-L22.
130 W.L. Freedman et al., 1984, The Hubble space telescope extragalactic distance scale key project. I. the discovery of cepheids and a new distance to M81, Astrophys., J.,

427, 628-655.
131 H.J. Volk et al., 1996, The nonthermal energy content and gamma ray emission of starburst galaxies and clusters of galaxies, Space Science Reviews, 75, 279-297.
132 Xu X-J, Liu, J., Liu, J. 2015, A likely micro-quasar in the shadow of M82 X-1, Astrophys. J. 799, L28.
133 Matsumoto, H., & Tsuru, T. G. 1999, X-Ray Evidence of an AGN in M82, Publ. Astron. Soc. Japan, 51, 321.
134 Tsuru, T. G., Matsumoto, H., Inui, T., et al. 2004, M82 X-1, the hyper luminous x-ray source, Progress of Theoretical Physics Supplement, 155, 59.
135 Patruno, A., Portegies Zwart, S., Dewi, J., and Hopman, C. 2006, The ultraluminous X-ray source in M82: an intermediate-mass black hole with a giant companion, Mon. Not. Roy. Astron. Soc., 370, L6.
136 Feng, H., & Kaaret, P. 2010, Origin of the x-ray quasi-periodic oscillations and identification of a transient ultraluminous x-ray source in M82, ApJ, 712, L169.
137 Dewangan, G. C., Titarchuk, L., & Griths, R. E., 2006, Black hole mass of the ultraluminous x-ray source M82 X-1, Astrophys. J. Letters, 637, L21.
138 H. Feng and P. Kaaret, Origin of The x-ray quasi-periodic oscillations and identification of a transient ultraluminous x-ray source in M82、Astrophys. J., 668, 941-948.
139 X.L. Zhou et al. 2010, Calibrating the correlation between black hole mass and x-ray variability amplitude: x-ray only black hole mass estimate for active galactic nuclei and ultra-luminous x-ray sources, Astrophys. J. 710, 16-23.
140 P. Casella, G. Ponti, A. Patruno, T. Belloni, G. Miniutti, L. Zampieri, 2008, Weighing the black holes in ultraluminous X-ray sources through timing, Mon. Not. R. Astron. Soc., 387, 1707-1711.
141 D. Pasham, T.E. Strohmayer, R.F. Mushotzky, 2014, A 400-solar-mass black hole in the galaxy M82, Nature, 513, 74-76.
142 K. Dolag et al., 2005, Constrained simulations of the magnetic field in the local Universe and the propagation of ultrahigh energy cosmic rays, J. Cosmology and Astroparticle Physics, 01, 009.
143 D. Ryu, S. Das, S., H. Kang, 2010, Intergalactic magnetic field and arrival direction of ultra-high-energy protons, Astrophys. J., 710, 1422-1431.
144 N. Globus, D. Allard, and E. Parizot, 2008, Propagation of high-energy cosmic rays in extragalactic turbulent magnetic fields: resulting energy spectrum and composition, A&A, 479, 97-110.
145 V.A. Acciari et al., 2009, A connection between star formation activity with cosmic

rays in the starburst galaxy M82, Nature, 462,770-772.
146 R. Rekola et al., 2005, Distance to NGC 253 based on the planetary nebula luminosity function, Mon. Not. R. Astron. Soc., 361, 330-336.
147 R. Barnard, 2010, In-depth studies of NGC253 ULXs with XMM-Newton: remarkable variability in ULX1, and evidence for extended coronae, Mon. Not. Roy. Soc, 404, 42-47.
148 E.M. Gutierrez, G.E, Romeo, and F. L. Vieyro, 2020, Cosmic rays from the nearby starburst galaxy NGC 253: the effect of a low-luminosity active galactic nucleus, Mon. Not. R. Astron. Soc., 494, 2109-2116.
149 J.L. Turner and P.T.P. Ho, 1985, The 1 parsec radio core and possible nuclear ejection in NGC253, Astrophys. J., 293, L77-L81.
150 R.D. Blandford and R.L. Znajek, Electromagnetic extraction of energy from Kerr black holes, Mon. Not. R. Astron. Soc., 179, 433-456.
151 R. Attallah and D. Bouchachi, 2018, Ultrahigh energy cosmic rays from nearby starburst galaxies, Mon. Not. R. Atron. Soc., 478, 800-806.
152 B. Eichmann and J.B. Tjus, 2016, The radio-gamma correlation in starburst galaxies, Astrophys. J. 821, 87.
153 Milabel, I.F. and Rodrigez, L.F., 1999, Sources of relativistic jets in the galaxy, Ann. Rev., Astron. Astrophys, 37, 409-443.
154 I.F. Mirabel, 2007, Microquasars, C.R, Physique, 8, 8-15.
155 J.N. Bachall, 1978, Masses of neutron stars and blackholes, Ann. Rev. Astron. Astrophys., 16, 241-264.
156 R. Gicconi et al., 1978, The UHURU catalogue of X-ray sources, Astrophys. J. 178, 281-308.
157 S. Yamaguchi and K. Koyama, 1990, New x-ray sources near the galactic bulge region, Publ. Astron. Soc. Japan, 42, L83-L91.
158 Agrawal et al., 1971, Rapid variabilities in the high energy x-ray flux from Cyg X-1, Nature, 232, 38-40.
159 T.M. Belloni and L. Stella, 2014, Fast variability from black-hole binaries, Space Sci. Rev. 183, 43-60.
160 G.E. Romeo, 2005, Microquasars and gamma-ray sources, Chin. J. Astron. Astrophys., 5, suppl. 110-120.
161 I.F. Mirabel, 2006, Very energetic ganma-rays from microquasars and binary pulsars, Science, 312, 1759-1760.
162 I.F. Mirabel, 2012, Gamma-ray binaries revealed, Science, 335, 175-176. K.M. Blundel and P. Hirst, Jet population of wind ejecta from a major flare in the black

hole microquaser SS433, Astrophys. J. Lett., 735, L7.
163 P.T. Goodall, K.M. Blurndell. And S.J.B. Burnell, Probing the history of SS 433's jet kinematics via decade-resolution radio observations of W 50, Mon. Not. R. Astron. Soc., 414, 2828-2837.
164 https://public.nrao.edu/gallery/a-wobbling-jet/
165 B. Margon, 1984, Observations of SS 433, Ann. Rev. Astron. Astrophys, 22, 507-536.
166 S. Fabrika, 2004, The jest and supercritical accretion disk in SS433, Astrophys. And Space Physics, Rev., 12, 1-97.
167 A.C. Fabian and M. J. Rees, 1979, SS 433: a doube jet in action?, Mon. Not. R. Astron. Soc., short communication, 13-16.
168 M. Milgrom, 1979, Interpretation of the large variations in the line positions in SS433, A&A, 76, L3-L6.
169 G.O. Abell and B. Margon, 1979, Kinematics model for SS433, Nature, 279, 701-703.
170 R.M.Hjellming and K.J. Johnston, 1981, An analysis of the proper motions of SS433 radio jets, Astrophys. J., 246, L141-L145.
171 J.I. Katz et al. 1982, Nodding motions of accretion rings and disks- a short-term period in S433, Astrophys. J., 260, 780-793.
172 K. Kubota et al., 2010, SUBARU and GEMINI observations of SS 433: New constraint on the mass of the compact object, Astrophys. J., 709, 1374-1386.
173 A.M. Cherepashchuk et al. 2005, INTEGRAL observations of SS433:Results of a coordinated campaign, A&A, 437, 561-573.
174 A.U. Abeysekara et al., 2018, Very-high-energy particle acceleration powered
by the jets of the microquasar SS 433, Nature, 562, 82-85.
175 S. Safi-Harb S., H. Oegelman, 1997, ROSAT and ASCA observations of W50 associated with the peculiar source SS 433, Astrophys. J., 483, 868-881.
176 M. Revnivtsev et al. 2004, First simultaneous X-ray and optical observations of rapid variability of supercritical accretor SS433 A&A, 424, L5-L8.
177 V.V. Davydov et al. 2008, Spectroscopic monitoring of SS 433: A search for long-term variations of kinematic model parameters, Astronomy Reports, 52, 487-506.
178 X.N. Sun et al., 2019, Tentative evidence of spatially extended GeV emission from SS433/W50, A&A, 626, A113.
179 K. Rasul et al., 2019, Gamma-rays from SS433: evidence for periodicity, Mon. Not. R. Astron. Soc., 485, 2970-2975.
180 M. Ajello et al., 2012, The luminosity function of FERMI-detected flat-spectrum radio quasars, Astrophys. J. 751, 108.

181 A.E. Broderick, 2012, The cosmological impact of luminous TeV blazars. I. Implications of plasma instabilities for the intergalactic field and extragalactic gamma-ray background, Astrophys. J. 752, 22.
182 T. Stanev, 2009, Propagation of ultrahigh energy cosmic rays, New Journal of Physics, 11, 065013.
183 E. Waxman and J. Bachall, 1998, High energy neutrinos from astrophysical sources: an upper bound, Physical Rev. D, 59,023002.
184 R. Abbasi et al. (IceCube Collaboration), 2022, Improved characterization of the astrophysical muon-neutrino flux with 9.5 years of IceCube data, Astrophys. J., 985, 50.
185 R. Narayan , et al., 2001, Accretion model of gamma-ray bursts, Astrophys. J., 557, 949–957.
186 B.P. Abbott et al. (LIGO scientific collaboration et al.), 2017, Multi-messenger observations of a binary neutron star merger, Astrophys. J. Lett., 848, L12.
187 Aasi et al. (LIGO Scientific Collaboration), 2015, Advanced LIGO, Classical and Quantaum Gravity, 32, 7
188 Acernese et al. (Virgo collaboration), 2015, Advanced Virgo: a second-generation interferometric gravitational wave detector, Classical and Quantum Gravity 32, 2.
189 B.P. Abbott et al. (LIGO Scientfic Collaboration and Virgo Collaboration), 2017, GW170817: Observation of gravitational waves from a binary neutron star inspiral, Physical Review Letters, 119, 161101.
190 K. Cannon et al., 2012, Toward early-warning detection of gravitational waves from compact binary coalescence, Astrophys. J., 748, 136.
191 C. Messick et al. 2017, Analysis framework for the prompt discovery of compact binary mergers in gravitational-wave data, Phys. Rev. D., 95, 042001.
192 A. Goldstein et al., 2017, An ordinary short gamma-ray burst with extraordinary implications: Fermi-GBM detection of GRB 170817A, Astrophys. J. Lett., 848, 2.
193 Y. Takahashi, L.W. Hillman, and T. Tajima, 2000, Relativistic lasers and High energy Astrophysics, gamma-ray burst and highest energy acceleration, Gamma-ray Burst, 5^{th} Huntsville Symposium, Huntsville Alabama, 1999, pp171-221.
194 C.L. Fryer, 2003, Stellar collapse, International Journal of Modern Physics D, 12, 1795-1835.
195 A.V. Filipenko, 1997, Optical spectral supernovae, Ann. Rev. Astron. Astrophys. 35, 309-355.
196 T. Nakamura et al., 2001, Light curve and spectral models for the hypernova sn 1998bw associated with GRB 980425, Astrophys. J., 550, 991-999.

197 S.E. Woosley, 1993, Gamma-ray bursts from stellar mass accretion disks around black-hokes, Astrophys. J., 405, 273-277.
198 A.I. MacFadyen and S.E. Woosley, 1999, Collapsars: gamma-ray burst and explosions in "failed supernovae", Astrophys. J. 524, 262-289.
199 Susuki, T., Nakasato, N., Baumgardt, H., A. Ibukiyama, J. Makino, and T. Ebisuzaki, 2007, Evolution of collisionally merged massive stars, Astrophysical Journal, 668, 435-448.
200 P.A. Mazzali et al., 2008, The metamorphosis of supernova SN 2008D/XRF 080109: A link between supernovae and GRBs/Hypernovae, Science, 321, 1185-1188.
201 K. Iwamoto et al., 1998, A hypernova model for the supernova associated with the gamma-ray burst of 25 April 1998, Nature, 395, 672-674.
202 P.A. Mazzali et al., 2003, The type Ic hypernova SN 2003dh/GRB 030329, Astrophys. J., 559. L95-L98.
203 S. Chandrasekhar, Hydrodynamic and hydromagnetic stability (Clarendon, Oxford, 1961).
204 K. A. Holcomb and T. Tajima, A Mechanism for Gamma-Ray Bursts by Alfvén-Wave Acceleration in a Non-uniform Atmosphere, Astrophys. J. 378, 682 (1991)
205 J.D. Jackson, 1962, Classical Electrodynamics, John Weiley and Suns Inc.
206 N. Shimada and M. Hoshino, Strong electron acceleration at high Mach number shock waves: Simulation study of electron dynamics, 2000, Astrophys. J. 543, L67-L71.
207 T. Yokoyama and K. Shibata, 1995, Magnetic reconnection as the origin of x-ray
208 Shibata, K and Uchida, Y. 1990, Interaction of molecular bipolar flows with interstellar condensations – sweeping magnetic twist mechanism and the blobs in LYNDS-1551 molecular outflow, Publ. Astron. Soc. Japan, 42, 39-67.
209 E.M.D. Dal Pino et al., 2005, Production of the large scale superluminal ejections of the microquasar GRS 1915+105 by violent magnetic reconnection, A&A, 441, 845-853.
210 C.A. Haswell, T. Tajima, and J.I. Sakai, 1992, High-energy particle-acceleration by explosive electromagnetic-interaction in an accretion disk, Astrophys. J., 401, 495-507.
211 Y. Takahashi, 1995, Maximum-energy Auger (Air)-shower Satellite (MASS) for observing cosmic rays in the energy region $10^{19\text{-}20}$ eV, 24th international Cosmic ray conference, vol. 3, held August 28-September 8, 1995 in Rome, Italy. Edited by N. Iucci and E. Lamanna. International Union of Pure and Applied Physics, 595.
212 L. Scarsi, 2001, The extreme universe of cosmic rays: Observations from space,

Nuovo Cimento Della Societa Italiana di Fiscica C-Geophysics and Space Physics 24, 4-5, 471-482.
213 Y. Takahashi et al. (JEM-EUSO collaboration), 2009, The JEM-EUSO mission, New Journal of Physics, 11, 065009.
214 T. Ebisuzaki et al. (JEM-EUSO collaboration), 2014, The JEM-EUSO mission, Advances in Space Research, 53, 1499-1455.
215 Adams et al. (JEM-EUSO collaboration), 2015, The JEM-EUSO mission: An introduction, Experimental Astronomy, 40, 3-17.
216 Casolino M. et al. (JEM-EUSO collaboration), 2015, The JEM-EUSO instrument, 40, 19-44.